INTEGRATED HYDRAULIC FRACTURE PLACEMENT AND DESIGN OPTIMIZATION IN UNCONVENTIONAL GAS RESERVOIRS

A Dissertation

by

XIAODAN MA

Submitted to the Office of Graduate and Professional Studies of
Texas A&M University
in partial fulfillment of the requirements for the degree of

DOCTOR OF PHILOSOPHY

Chair of Committee,	Eduardo Gildin
Committee Members,	Akhil Datta-Gupta
	Michael King
	Yalchin Efendiev
Head of Department,	A. Daniel Hill

December 2013

Major Subject: Petroleum Engineering

ABSTRACT

Unconventional reservoir such as tight and shale gas reservoirs has the potential of becoming the main source of cleaner energy in the 21th century. Production from these reservoirs is mainly accomplished through engineered hydraulic fracturing to generate fracture networks that provide the gas flow pathways from the rock matrix to the production wells. While hydraulic fracturing technology has progressed considerably in the last thirty years, designing the fracturing system primarily involves judgments from a team of engineers, geoscientists and geophysicists, without taking advantage of computational tools, such as numerical optimization techniques to improve short-term and long-term reservoir production.

This thesis focuses on developing novel optimization algorithms that can be used to improve the design and implementation of hydraulic fracturing in a shale gas reservoir to increase production and the net present value of unconventional assets. In particular, we consider simultaneous perturbation stochastic approximation (SPSA) and Covariance Matrix Adaptation - Evolution Strategy (CMA-ES) algorithms, which are proven very efficient in finding nearly optimal solutions. We show that with a judicious choice of control variables (continuous or discrete) we can obtain efficient algorithms for performing hydraulic fracture optimization in unconventional reservoirs.

To achieve this, the hydraulic fracture production optimization problem is divided into two aspects: fracture stages placement optimization with fix stage numbers and unknown stage numbers. After check the parameters of fracture model that could be used to simulate future reservoir behavior with a higher degree of confidence, the fracture stages optimization is scheduling the fracturing sequence, and adjusting the fracture stages intensity at different

locations, which is similar to well placement problem. In addition to the detailed investigation of the new optimization technique, uncertainty quantification of reservoir properties and its implications on the optimization workflow is also considered in the shale gas reservoir model. Taking into account that shale gas reservoirs are highly heterogeneous systems, stochastic optimization methods are the most suitable framework for hydraulic fracture stages placement.

DEDICATION

To my beloved parents, and my brother for their endless love and support

ACKNOWLEDGEMENTS

I would like to take this opportunity to express my deepest gratitude and appreciation to the people who have given me their assistance throughout my studies and during the preparation of this thesis. I would like to express my deepest gratitude to my advisors, Dr. Eduardo Gildin, for his continuous enlightenment, trust, academic guidance, and financial support. As well, I would like to extend my appreciation to Dr. Datta-Gupta, Dr. King, Dr. Nasrabadi and Dr. Efendiev, for their valuable comments and suggestions that have shaped this dissertation.

Special thanks to my colleagues at Texas A&M University, Mohammadali Tarrahi, Jiang Xie (Now with Chevron), Weirong Li and Changdong Yang, with whom I discussed the research projects, for their constructive discussions over the years.

Thanks also go to my colleagues in our research group: Reza Ghasemi, Gorgonio Fuentes Cruz, and Thorn Ler (Now with PTTEP). I also want to thank my friends and the department faculty and staff for making my time at Texas A&M University a great experience. I would like to acknowledge the financial support the Crisman Institute in the Harold Vance Department of Petroleum Engineering of Texas A&M University.

Finally, thanks to my mother and father for their encouragement and love.

NOMENCLATURE

A = SPSA nonnegative coefficient

a = SPSA nonnegative coefficient

a_k = SPSA gain sequence

b = Discount rate, %/100/year

C = Covariance matrix C in CMA-ES

c = SPSA nonnegative coefficient

c_k = SPSA gain sequence

C_w = Base cost for drilling a horizontal well, $

C_f = HF cost per stage, $

C_p = Penetration cost of per drilled gridblock

H_j = Number of HF stages in well *j*

K = Total number of steps in simulation

g = Gradient of the objective function *J*

$Q_{g,j}{}^{k}$ = Gas production rate, Mscf/day

$Q_{w,j}{}^{k}$ = Water disposal cost, STB/day

Q_j = Operating cost of well *j*, $/day

r_g = Gas price, $/Mscf

t^k = Year period, days

N_{prod} = Production well index

P = Pressure, psi

P_L = Langmuir pressure parameter, psi

u = control variable vector

V = Adsorbed gas content, Mscf/ton

V_L = Langmuir volume parameter, Mscf/ton

Δ_k = SPSA and CMA-ES perturbation parameter

Δt_k = Time step for NPV calculation

α = SPSA nonnegative coefficient

γ = SPSA nonnegative coefficient

λ = Population size of offspring number in CMA-ES

σ = coordinate wise standard deviation (step size) in CMA-ES

TABLE OF CONTENTS

Page

ABSTRACT ii

DEDICATION iv

ACKNOWLEDGEMENTS v

NOMENCLATURE vi

TABLE OF CONTENTS viii

LIST OF FIGURES x

LIST OF TABLES xiv

CHAPTER I INTRODUCTION 1

1.1 Background 1
1.2 Literature Review 4
1.2.1 Optimal Hydraulic Fracture Stages Network Design 4
1.2.2 Optimal Well Location and Hydraulic Fracture Placement Design 7
1.2.3 Uncertainty Quantification and Sensitivity Analysis 11
1.3 Problem Description and Objectives 13
1.3.1 Work Objectives 13
1.3.2 Optimization Problems 15
1.4 Thesis Outline 16

CHAPTER II MODELS OF SHALE GAS RESERVOIR 18

2.1 Introduction 18
2.2 Shale Gas Model and Reservoir Properties 19
2.2.1 Dual Permeability 19
2.2.2 Desorption Model 21
2.2.3 Shale Gas Reservoir Properties 23
2.2.4 LGR and Equilibrium Hydraulic Fracture Permeability 28
2.3 History Match with Real Field Data 30
2.4 Sensitivities Analysis 34
2.5 MATLAB Coupling to the Optimization Process 42

CHAPTER III ALGORITHMS FOR OPTIMIZATIONS 44

3.1 Introduction 44
3.2 Objective Function 44
3.3 Simultaneous Perturbation Stochastic Approximation (SPSA) 47
3.3.1 Methodology of SPSA 47
3.3.2 Numerical Case of SPSA 48
3.4 Covariance Matrix Adaptation Evolution Strategy (CMA-ES) 50
3.4.1 Methodology of CMA-ES 50
3.4.2 Numerical Case of CMA-ES 52
3.5 Finite Difference (FD) Method 54

CHAPTER IV OPTIMIZATIONS WITH FIXED NUMBER OF HYDRAULIC FRACTURE STAGES 55

4.1 Introduction 55
4.2 Well Placement Optimization 57
4.2.1 Case I: Homogenous Reservoir 59
4.2.2 Case II: Heterogeneous Reservoir 62
4.3 HF Stages Placement Optimization 65
4.3.1 Algorithms Applied to a Single Well Case 66
4.3.2 Algorithms Applied to Two Wells Case 69
4.4 Joint Wellbore and HF Stages Placement – Hierarchical Optimization 74
4.4.1 Hierarchical Optimization in Homogeneous Case 75
4.4.2 Hierarchical Optimization in Heterogeneous Case 78
4.5 Discussions 81

CHAPTER V OPTIMIZATIONS WITH UNFIXED NUMBER OF HYDRAULIC FRACTURE STAGES 83

5.1 Introduction 83
5.2 Gradient-based Optimization on HF Stages Placement Problem 84
5.2.1 Algorithms for Gradient-based Optimizations 86
5.2.2 Test Experiments and Case Results 90
5.3 HF Stages Placement Optimization with Realistic Constrains 92
5.3.1 Assumptions and Flowcharts for the Improved Approach 93
5.3.1 Optimization for Non-fixed HF Stages Number on Single Well 96
5.3.2 Optimization of HF Stages Networks with Non-fixed HF Stages Number 100
5.4 Uncertainty Quantification and Discussions 102

CHAPTER VI CONCLUSIONS AND RECOMMENDATIONS 104

6.1 Conclusions 104
6.2 Recommendations 105

REFERENCES 107

APPENDIX A 113

LIST OF FIGURES

Page

Fig. 1.1 Resource triangle for natural oil and gas (From Holditch, 2007)..... 2

Fig. 1.2 Example: find optimize hydraulic fracture stage locations for 2 wells 15

Fig. 2.1 Flow connections in the dual permeability model (From Pruess et al., 1999) 20

Fig. 2.2 A simple structural diagram for absorbed dual permeability model 22

Fig. 2.3 Langmuir isotherm curve and adsorption date of Barnett Shale 22

Fig. 2.4 Fracture network generated by Petrel 2012 (up) and fracture network permeability map after upscaling (down) 26

Fig. 2.5 Relative permeability curves for fracture system 27

Fig. 2.6 Capillary pressure curves for the gas shale reservoir model 27

Fig. 2.7 Rock Compaction table for fracture system 28

Fig. 2.8 LGR and SRV features used in the model. 29

Fig. 2.9 Model of multistage hydraulic fractures distribution along horizontal well 31

Fig. 2.10 Gas production rates of well 314 from Barnett Shale matched by simulation data 32

Fig. 2.11 Cumulative gas production rates of well 314 from Barnett Shale matched by simulation data 33

Fig. 2.12 Pressure distributions of dual-permeability system: Matrix and fracture, after 5 year of gas production 33

Fig. 2.13 Gas production predictions of well 314 from Barnett Shale, 20 years period... 34

Fig. 2.14 Sensitivity diagram of shale gas reservoir, for 20 years production period…....35

Fig. 2.15 Gas price prediction for 20 years with 10%/year escalation rate…….....37

Fig. 2.16 Cumulative NPV curves by different value of HF costs, given HF stage = 12, solid line is gas price with escalation factor 10%/year, dash line has no

factor……..……...38

Fig. 2.17 Cumulative NPV curves by different number of HF stage, solid line is gas price with escalation factor 10%/year, dash line has no factor…….....39

Fig. 2.18 Cumulative NPV curves by different values of HF half-length, given HF stage = 12, solid line is gas price with escalation factor 10%/year, dash line has no factor ……..…...39

Fig. 2.19 Cumulative NPV curves by different values of HF permeability, given HF stage = 12, solid line is gas price with escalation factor 10%/year, dash line has no factor……..…..…..….....40

Fig. 2.20 Cumulative NPV curves by different values of matrix permeability, given HF stage = 12, solid line is gas price with escalation factor 10%/year, dash line has no factor…….……..……...40

Fig. 2.21 Cumulative NPV curves by different natural fracture efficient permeability values, given HF stage = 12, solid line is gas price with escalation factor 10%/year, dash line no factor……...…..41

Fig. 2.22 Cumulative NPV curves by different values of SRV permeability, given HF stage = 12, solid line is gas price with escalation factor 10%/year, dash line has no factor ..……..…….…….....41

Fig. 2.23 Flowchart of code connection between MATLAB and ECLIPSE…….…..43

Fig. 3.1 Example of solving 2-D continuous Rosenbrock function by SPSA…….……...49

Fig. 3.2 Concept of directional optimization in CMA-ES algorithm (From Wikipedia "CMA-ES").....50

Fig. 3.3 Example of solving 2-D continuous Rosenbrock function by CMA-ES.....53

Fig. 4.1 SPSA and CMA-ES flowchart for optimization of fixed HF stage number 57

Fig. 4.2 Conceptual model of wellbore placement optimization.....58

Fig. 4.3 Homogeneous case, one of initial wellbore placement (left) and the optimized result of wellbore locations (right).....59

Fig. 4.4 Pressure distribution after 20 years production in the initial case (up) and the optimized results (down), homogeneous case 60

Fig. 4.5 Wellbore placement optimization approach by the algorithms SPSA (up) and CMA-ES (down), homogeneous case.....61

Fig. 4.6 Pressure distribution after 20 years production in the initial case (up) and the optimized results (down), heterogeneous case 62

Fig. 4.7 Wellbore placement optimization approach by the algorithms SPSA (up) and CMA-ES (down), heterogeneous case 63

Fig. 4.8 The optimization distributions of wellbore placement for four different initial using the known geologic model in heterogeneous case 64

Fig. 4.9 Conceptual model of HF stages placement optimization 66

Fig. 4.10 Initial placement of HF stages (left) and one optimized result (right) on a single well 67

Fig. 4.11 Pressure distribution of initial HF stages placement (left) and one of the optimized result (right) on a single well 67

Fig. 4.12 Optimization approaches by the algorithms SPSA (up) and CMA-ES (down) in the case of single well 68

Fig. 4.13 Homogeneous case, initial HF stages placement on two wells (left) and one optimized result (right) 69

Fig. 4.14 Homogeneous case, optimization approaches of HF stages by the algorithmsSPSA (up) and CMA-ES (down) 70

Fig. 4.15 Pressure distribution of initial HF stages placement (left) and one of the optimized result (right) on two wells 71

Fig. 4.16 Heterogeneous case, optimization approaches by the algorithms SPSA (up) and CMA-ES (down) 72

Fig. 4.17 Initial case (up-left) and three optimization distributions of HF stages placement using the known geologic model in heterogeneous case 73

Fig. 4.18 Conceptual model of the hierarchical optimization framework 74

Fig. 4.19 Homogeneous case, initial condition of hierarchical optimization (left) and one optimized result (right) 76

Fig. 4.20 Homogeneous case, pressure distribution of initial condition before hierarchical optimization (left) and one optimized result (right) 76

Fig. 4.21 Homogeneous case, hierarchical optimization approach by the algorithms SPSA (left) and CMA-ES (right) 77

Fig. 4.22 Heterogeneous case, hierarchical optimization approach by the algorithms SPSA (up) and CMA-ES (down) 79

Fig. 4.23 Initial case (up-left) and three optimization distributions of hierarchical optimization using the known geologic model in heterogeneous case 80

Fig. 5.1 Control vector used for represent HF stages 85

Fig. 5.2 FD flowchart for HF stages optimization 87

Fig. 5.3 Example of FD perturbation at 1st iteration ……...…..87

Fig. 5.4 SPSA flowchart for HF stages optimization..... 89

Fig. 5.5 Example of SPSA perturbation at 1st iteration…….…….……90

Fig. 5.6 Optimization of HF stages placement in homogeneous case by FD…….....91

Fig. 5.7 Optimization of HF stages placement in homogeneous case by SPSA…….…....91

Fig. 5.8 NPV curve of HF stages placement optimization in homogeneous case by FD and SPSA…….…….……..92

Fig. 5.9 Two patterns of HF stages distribution with intervals 100 ft and 160 ft 94

Fig. 5.10 NPV curve corresponding to different number of HF stages 94

Fig. 5.11 Flowchart of the optimization approach with more realistic constrains..... 95

Fig. 5.12 Initial and the optimal number and locations of HF stages for single well 97

Fig 5.13 Optimization to NPV with given 12 HF stages 98

Fig. 5.14 The optimization and elimination process by SPSA and CMA-ES, single well case..... 99

Fig. 5.15 Initial and the optimal number and locations of HF stages for two wells 100

Fig. 5.16 The optimization and elimination process by SPSA and CMA-ES, two Wells case…….……..101

LIST OF TABLES

Page

Table 2.1 Overview of shale gas reservoir properties and literature values 24

Table 2.2 Reservoir properties and hydraulic fracture parameters in history matching... 32

Table 2.3 Reference values of model parameters and changing range..... 36

Table 3.1 Parameter values for the NPV function. (Schweitzer, 2009; Bruner, 2011) 45

Table 3.2 Algorithm description of SPSA 48

Table 3.3 Algorithm description of CMA-ES..... 52

Table 4.1 NPVs of four wellbore placement cases in heterogeneous case in Fig. 4.8 64

Table 4.2 Initial HF stages placement and three optimized results in heterogeneous case shown in Fig. 4.17..... 73

Table 4.3 Initial HF stages placement and three optimized results in heterogeneous case shown in Fig. 4.23..... 80

Table 4.4 Compare computational times between SPSA and CMA-ES with cases tested in Chapter IV……..…….....……..82

Table A.1 Reservoir properties and hydraulic fracture parameters used for wellbore placement optimization in Chapter IV……...……..……...113

Table A.2 Reservoir properties and hydraulic fracture parameters used for HF stages placement optimization on two wellbores in Chapter IV……..113

Table A.3 Reservoir properties and hydraulic fracture parameters test for FD and SPSA optimizations in Chapter V……..…….….....114

Table A.4 Reservoir properties and hydraulic fracture parameters for SPSA and CMA-ES optimizations in Chapter V…….……..…….....114

CHAPTER I

INTRODUCTION

1.1 Background

Unconventional resources, such as tight gas sands and shale gas reservoirs, are reshaping the energy supply structure in the United States and are being established as the main cleaner energy sources in the twenty first century (Curtis, 2002; Jenkins and Boyer, 2008). Shale gas, which has gas production from hydrocarbon rich shale formations, is one of the most rapidly expanding trends in onshore domestic oil and gas exploration and production today (Arthur, 2008). In shale gas reservoirs, it is known that gas is stored in three forms: adsorbed gas on the surface of shale, free gas in matrix bulk pores and in nature fractures. However, shale gas reservoirs have a very low matrix permeability and only a few small natural fractures which make it impossible to drain the reservoirs in a standard way (Gray, 2008; GWPC and ALL Consulting, 2009).

Because of the low productivity of vertical wells in unconventional formation, horizontal well and hydraulic fracturing, the technology to artificially create extra fractures in shale reservoirs which causes sufficient opening up of the tight formation to allow a proper pressure differential to be applied and gas to be produced, has developed substantially ever since it was first widely used in North America in the 1950s (Holditch, 2007). The invention and application of multi-stage hydraulic fracturing in horizontal wells was definitely a game changer and made unconventional reservoirs into potentially exploitable assets (King, 2010). This new technique has been changing the energy future worldwide (Energy Information Administration, 2010).

Although modern hydraulic fracturing jobs have become a standard action in unconventional reservoirs, the optional hydraulic fracturing multi-stage design is still done in a very manual and "ad-hoc" way. This indeed can lead to suboptimal gas production as only certain intervals along the length of the wellborn can be stimulated with non-optimal solutions. To this end, optimization strategies have the potential to enhance the hydraulic fracturing stages design and improve on the decision making process. In the conventional reservoir area, optimization approaches used in production enhancement and history matching has been successfully introduced to learn the reservoir behavior and obtain better recovery factors and yet, the same strategies have not been applied in the unconventional area, leading great space to realize the untapped potential in exploring unconventional reservoir.

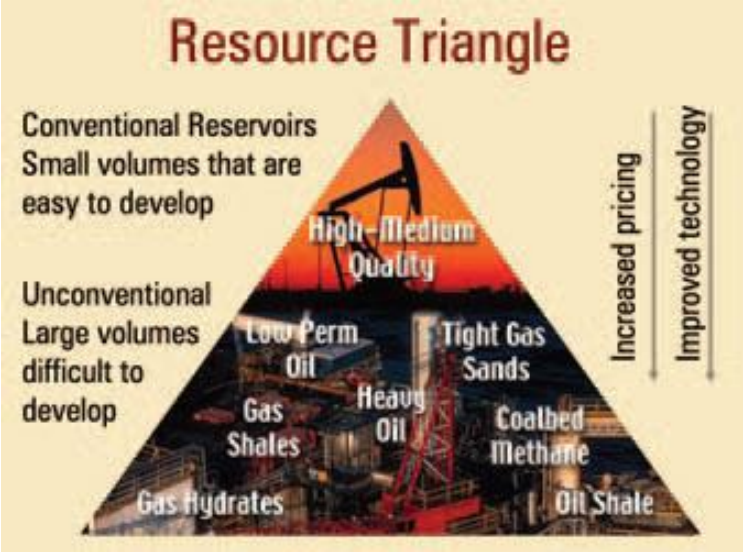

Fig 1.1 Resource triangle for natural oil and gas (From Holditch, 2007)

In general, the production optimization problems in unconventional resources are more complex than the conventional resources (**Fig. 1.1**). After proper assessment of the

properties of unconventional reservoirs, which are distinct from conventional reservoirs, the production scenario influenced by the parameters of hydraulic fractures processes and hydraulic fracture stages topology needs to be identified.

Well placement and production schedule optimization in conventional reservoirs have been introduced to address improvements is closed-loop reservoir management (Wang, Li and Reynolds, 2007; Zandvliet et al., 2008; Zhang et al., 2010). The objective of these optimizations always consider the expense of well drilling and operations as well as profits from production rates, and economical metrics such in the optimization (maximization) framework. Also, the location and drilling schedule of new infill wells must be included in the economic optimization strategies for oil/gas production. In this case, optimization methodologies have been used to develop strategies to identify the optimal locations of new injectors/producers. This same idea can be translated into hydraulic fracture optimization cases, whereby the optimal number and locations of fracture stages can be identified in the well placement problems.

The objective of this research is to develop novel optimization algorithms for the design of hydraulic fractures stages and locations in a shale gas reservoir to increase production and the net present value of unconventional assets. Since the locations of hydraulic fracture (HF) stages in a grid-based simulation framework are discrete numbers, we need optimization strategies that can handle a mixture of continuous and discrete values. Thus, in this thesis we develop optimization approaches that can handle the discrete vector of the hydraulic fracture stages placement at the same time that also optimize the continuous vector of the economics of certain projects -- the Net Present Value (NPV) of the unconventional reservoirs development. In particular, we consider two algorithms,

simultaneous perturbation stochastic approximation (SPSA) and Covariance Matrix Adaptation - Evolution Strategy (CMA-ES) algorithms, which are proven very efficient in finding nearly optimal solutions in continuous and integer optimizations. We investigate how efficient these two algorithms work and compare them by several numerical experiments.

This thesis aims at also making contributions to the analysis of influence to NPV and gas production rate by HF stage locations along wellbore or HF stage networks between multi-wellbore. Different number and location distributions give several HF stage patterns, and yield different range of NPVs. From which pattern of HF stages distribution can produce more gas rate and higher NPV is worth discussing. Beside, even though the framework of optimization process is completely deterministic, there might have some uncertainty in the optimal fracturing process. Therefore, we will take account into uncertainty caused by these two algorithms and will explain their advantages and disadvantages.

1.2 Literature Review

In this literature review, we discuss references selected in this research to describe what has been done in the past and what the major gaps to be addressed are. This section is divided in three main parts, describing the three main aspects of this research: (1) optimal hydraulic fracture stages network design; (2) optimal well placement and hydraulic fracture stages location design; (3) uncertainty quantification and sensitivity study.

1.2.1 Optimal Hydraulic Fracture Stages Network Design

Hydraulic fracturing is most popular technology in the advanced horizontal drilling field. With the optimized network design of hydraulic fracture stages, oil and gas production could

have been largely improved. A significant amount of work has been done towards optimization of hydraulic fracture stages and network by the fracture 2D or 3D models. The fracture stages work has been placed at the initial step of well stimulation.

Hareland et al. (1994) uses a pseudo three-dimensional hydraulic fracturing model with different fracture height growth models, in conjunction with a fractured reservoir production model to optimize hydraulic fracture design. This paper shows that this approach can be used to optimize hydraulic fracture design and that it has strong economic benefits.

Dempsey et al. (2001) shows a case study of hydraulic fracture optimization in tight gas wells with water production in the Wind River Basin, Wyoming. An extensive data set of core analysis, rock mechanics testing, pre- and post-fracture well logs, pressure build up analysis, detailed fracture modeling, and detailed production analysis was compiled in order to better understand and evaluate well performance and stimulation effectiveness in this field.

Holditch et al. (2005) gives the typical figure about flow path of hydraulic fracture stages in different time steps. It also examines the use of hydraulic fracturing technology in different fluid systems and different reservoirs. He (2007) also gives the typical figure about flow path of hydraulic fracture stages in different time steps, and gives a review in past 30 years of hydraulic fracturing.

Warpinski (2009) presents that ultra-low shale permeability require an interconnected fracture network of moderate conductivity with a relatively small spacing between fractures to obtain reasonable recovery factors. Micro-seismic mapping demonstrates that such networks are achievable by both the modeling and the mapping.

Myerhofer (2010) gives clear explanation that what is Stimulated Reservoir Volume (SRV) in fracture network. This paper illustrates how both SRV and fracture spacing for give

conductivity can affect production acceleration and ultimate recovery. And they also talk about the effect of fracture conductivity and how this concept can be used to improve completion design and well spacing and placement strategies.

Moridis et al. (2010), based on a sensitivity analysis of dual permeability gas shale modeling, performed in the work of the authors conclude that non-Darcy flow seems to have a secondary effect and does not seem to justify the substantially larger complexity, conceptual and computational needs.

Gorucu et al. (2011) shows a study at optimizations of the design of hydraulically fractured horizontal well placed in naturally fractured tight gas sand reservoir systems. A commercial reservoir simulator is coupled with artificial neural network (ANN) to create an expert system that can be used to design an efficient stimulation strategy.

Mirzei and Cipolla (2012) develop a new reservoir modeling and simulation technique has been developed for these complex fracture networks that combine discrete fracture network (DFN) modeling and unstructured fracture (UF) modeling to simulate well performance and improve stimulation design. Results from this new model show a gas shale reservoir can be drained more effectively if a complex fracture network can be created by hydraulic fracture stimulation.

Wilson and Durlofsky (2012) present a general workflow for applying optimization to the development of shale gas reservoir. Starting with a detailed full-physics simulation model, the approach generates a much simple and efficient, reduced-physics surrogate model. The reduced-physics model is using a history-matching procedure to prove results in close agreement with the full-physics model.

To sum, hydraulic fracture network design about interval and intensity in shale gas reservoirs is an unfinished work, hydraulic fracture network design at dual permeability model in shale gas reservoirs is a good topic with potential, which could help improve hydraulic fracture design in unconventional reservoirs to maximize production and profit. This thesis proposes to address the optimal network design in unconventional reservoirs.

1.2.2 Optimal Well Location and Hydraulic Fracture Placement Design

The economics of oil and gas filed development can be improved significantly by using computational optimization to guide operations. Several techniques have been developed for optimal well placement in conventional reservoirs. A critical issue, however, is that due to the fact that the placement optimization algorithm deals with a set of discrete parameters (well locations are discrete parameters in the simulation model), gradients of the objective function (NPV) with respect to these parameters are not well defined.

In the conventional reservoir area, Handles et al. (2007) examine the adjoint method used indirectly for the well placement problem. This paper has two main contributions: first to determine the effect of production constraints on optimal well locations, and second to determine optimal well locations using a gradient-based optimization method. After set each well surrounded eight “pseudo-wells” with a very low rate in the neighboring grid blocks in the 2D plane, an adjoint model is then used to calculate the gradient of the objective function (NPV) over the life of the reservoir with respect to the rate at each pseudo-well.

Wang et al. (2007) consider the placement of one or more injection wells in a 2D reservoir to maximize NPV. The paper presents a novel idea to convert the problem of optimizing on discrete variables into an optimization problem on continuous variables for the

optimal well placement. The idea is to initialize the problem by putting a well in every grid block and then optimize NPV. To do so, they have introduced new differentiable continuous variables that control the water injection rate of these individual injector wells and assumed the total water injection rate to be a constant.

B. Güyaguler(2007) introduce an optimization procedure utilizing Mixed Integer Linear Programming (MILP) (Nemhauser and Wolsey, 1998), where by the well rates accounted as system constraints while the maximum for an objective is sought (e.g. field oil rate or cash revenue). The proposed approach is able to efficiently handle the nonlinearities in the system by way of piece-wise linear functions, and the optimization system is examined by synthetic cases and two real field cases.

Zhang et al. (2010) presents a novel idea to convert the discrete optimization problem into an optimization problem with continuous variables. The idea is to initialize the problem by putting a well in every gridblock and maximize the net present value (NPV) with respect to the rates of the hypothesized wells. The NPV includes an additional term to account for the cost of "drilling a well."

In the unconventional reservoir area, hydraulic fracture stages and network design is a popular technology in horizontal drilling applied to improved oil and gas production. There has been some work published in recent years in the cases of optimization at hydraulic fracture stages placement. In what follows, I will describe some of these works.

Hareland er al. (1993) present hydraulic fracture designs by a three-dimensional three stress layer hydraulic fracturing model in conjunction with a fractured reservoir production. The hydraulic fracturing model has varying widths along the fracture and has the option to choose constant, linear or parabolic fracture height growth criterion. The fracturing fluid

rheology is modeled with a non-Newtonian pressure loss model in the fracture, with the special case being the Newtonian model.

Huffman er al. (1996) examine the effect of fracture of fracture half-length on NPV for infinite conductivity fractures. The paper presents a 3D case study that demonstrates how post-treatment evaluations expressed in economic terms can be used to assess the performance of stimulations and to guide future design choices.

Richardson (2000) presents a methodology that optimizes fracture stimulation design for any reservoir type and can be readily applied by practicing stimulation engineers. The analysis includes adjustments to fracture conductivity for closure pressure, temperature, embedment, gel damage, non-Darcy turbulent flow, and non-Darcy multi-phase flow.

Byung Lee et al. (2009) investigate the impact of fracture number, location, spacing and geometry on reservoir drainage efficiency by using a sector model with a multi-segmented horizontal wellbore model. Comparing various types of reservoirs shows how fracturing design can benefit from understanding the interaction between the reservoir and the horizontal wellbore intersected by hydraulically induced fractures.

Fazelipour (2010) presents innovative techniques in his paper, in order to history-match horizontal wellbores by focusing on the mentioned matrix/fracture challenges to sensitize the complex growth and attributes of hydraulic-fractures. SRV and real complex horizontal well model are considered.

Sehbi (2011) presents a fast approach to optimizing well completions in tight gas reservoirs using a rigorous semi-analytic computation of well drainage volumes in the presence of multiple stages of hydraulic fractures. His approach relies on a high frequency asymptotic solution of the diffusivity equation and emulates the propagation of a ‘pressure

front' in the reservoir along gas streamlines, with a field example as application of the approach by optimizing well completions in a horizontal well recently drilled in the Cotton Valley formation.

Sam Holt (2011) describes several numerical optimization algorithms mainly using gradient-based approaches to the hydraulic fracture stage optimize frameworks in shale gas reservoir. He proposes three distinct variable parameterizing placement methods to overcome the inherent continuous to discrete variables conversion issues, and analysis each strengths and weaknesses.

Wei Yu et al. (2013) demonstrates the accuracy of numerical modeling of multistage hydraulic fractures for actual Barnett Shale production data by considering the gas desorption effect. Six uncertain parameters within a reasonable range based on Barnett Shale information, and finally identify the optimum design under conditions of different gas prices based on NPV maximization. This integrated approach can contribute to obtaining the optimal drainage area around the wells by optimizing well placement and hydraulic fracturing treatment design and provide insight into hydraulic fracture interference between single well and neighboring wells.

Based on the review of mentioned references, there is definitely a challenging open area namely, the optimal investigate hydraulic fracture stages placement in unconventional reservoirs. In particular, the problem of continuous/discrete variables in gradient-based optimization is still an open problem to be addressed. To this project, we will pay special attentions to two algorithms (SPSA, CMA-ES) on our optimization approaches. I propose to achieve the objection of this project by investigating the hydraulic fractures optimization by

these two algorithms and ideas borrowed from the well placement ideas in conventional reservoirs.

1.2.3 Uncertainty Quantification and Sensitivity Analysis

Reservoir properties such as porosity, permeability, and geo-mechanical properties, are usually the main sources of uncertain in the determinations of the fracturing dynamics. Also the grid based solution techniques (reservoir simulations) yield problems with a large number of parameters in uncertainty ranges from measured field data. Thus, uncertainty quantification methodologies need be included into our proposed optimization algorithms. In the next paragraphs, I will review some of these methodologies in the case of conventional and unconventional reservoirs.

Bouzarkouna (2011) propose an optimization methodology for determining optimal well locations and trajectories based on the Covariance Matrix Adaptation – Evolution Strategy (CMA-ES) which is recognized as one of the most powerful derivative-free optimizers for continuous optimization. The mean value of NPV (in US dollars) and its corresponding standard deviation for well placement optimization locations using CMA-ES with meta-models of one multi-segment well are discussed.

Orangi et al. (2011) conduct reservoir simulation studies of horizontal wells with 14-stage hydraulic fractures to investigate the impact of rock and fluid properties and the drainage area of hydraulically fractured wells in a standard development pattern. The simulation is conducted in a shale reservoir containing a wide spectrum of rock and fluid types, dry gas to gas-condensate, and oil. A number of cases have been run with a wide

range of fracture, matrix and fluid properties considering condensate banking, fracture patterns, pore volume compressibility, and relative permeability.

Novlesky et al. (2011) discusses a workflow used in developing a numerical shale gas model for Nexen's Horn River shale gas reservoir. Micro-seismic data in construction of the stimulated reservoir volume (SRV) and the network of hydraulic fractures are used in the model. Discussions are given to gain understanding and insight into the uncertainties that have the greatest impact on well performance.

Xie et al. (2011) present a method for history matching and uncertainty quantification for channelized reservoir models using Level Set Method and Markov Chain Monte Carlo. In his approach, the channel field boundary is described by a level set function, then move and evolve the channelized reservoir properties. Markov Chain Monte Carlo method is utilized to perturb the coefficients of principal components of velocity field to update channel reservoir model matching production history. Two stage methods are used to screen out the undesired proposals.

Lianlin Li (2012) consider simultaneous optimization of well locations and dynamic rate allocations under geologic uncertainty using a variant of the simultaneous perturbation and stochastic approximation (SPSA). In addition, by taking advantage of the robustness of SPSA against errors in calculating the cost function, we develop an efficient field development optimization under geologic uncertainty, where an ensemble of models are used to describe important flow and transport reservoir properties.

To this end, new optimization strategies that involve simultaneous improvement of designing hydraulic fracturing stages need to be based on integrating engineering and geologic judgments as with model-based numerical optimization techniques. Uncertainty

quantification should be considered and proposed during these approaches. And sensitivity analysis of reservoir and fracture properties is also our interest.

1.3 Problem Description and Objectives

Project economics is often the decisive element in the feasibility study of any potential hydrocarbon reservoir. To implement this objective, we consider a industry standard called Net Present Value (NPV) calculation which relies on including the time value of the money of the profits and costs associated with the development of a reservoir. Once the objective function is setup, we need to actually solve the discrete optimization problem by means of efficient algorithms. This will be describing in the next sections.

1.3.1 Work Objectives

This research focuses on developing novel optimization algorithms that can be used to improve the design and implementation of hydraulic fracturing in a shale gas reservoir to increase production and the net present value of unconventional assets. To accomplish this, the hydraulic fracturing optimization problem is divided into two aspects: (1) hydraulic fracture stages network design under some given conditions and (2) hydraulic fracture stages and wellbores placement in a dual loop optimization framework.

In particular, we consider the simultaneous perturbation stochastic approximation (SPSA) and Covariance Matrix Adaptation - Evolution Strategy (CMA-ES) algorithms, which are proven very efficient in finding nearly optimal solutions in gradient-based optimization methods. We show that with a judicious choice of control variables (continuous

or discrete) we can obtain efficient algorithms for performing hydraulic fracture optimization in unconventional reservoirs.

Optimization strategies: To improve productivity of shale gas formations, wells that are drilled as horizontal well have multi-stage hydraulic fracturing treatments. Each stage is located dozens meters or even more far apart. To properly place these HF stages in a way that make sense physically and economically, i.e., the additional fracture stage for HF stage network does contributes to increase production rate and NPV, an optimization algorithm need to be developed to compute the optimal locations. **Fig. 1.2** gives an example that given fixed number of HF stages, non-evenly distribute stages could also influence NPV a lot, which also prove the importance of HF stage locations.

Uncertainty and sensitivity: The proposed optimization workflow described in this thesis is based on reliable knowledge of spatial distribution of reservoir properties and hydraulic fracture parameters. Whether these parameters influence the optimization results needs to be pay attentions. The properties that are underground, however, are highly uncertain. How sensitive total gas production is with respect to the model parameters, and the range of optimize value, is the topic we are interested in.

Significance: The significance of the proposed developments for optimization of unconventional reservoirs can be readily appreciated by observing the latest trends and emerging technologies in developing conventional reservoirs and the limitations and challenges of the current practices in producing unconventional resources. We are planning to develop advanced optimization workflows to improve production strategies and economic life-cycle value of unconventional resources. The ultimate goal of the project is to enhance the current industry practices in producing unconventional gas resources.

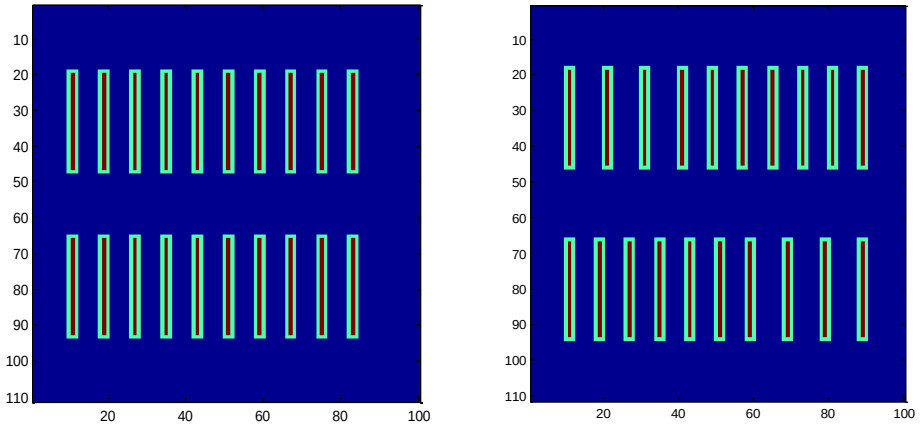

Fig. 1.2 Example: find optimize hydraulic fracture stage locations for 2 wells

1.3.2 Optimization Problems

In a more mathematical framework, the optimization problem can be stated as follows: Find the optimal hydraulic fracture locations u such that

$$u^* = arg \max_{u \in U} J(u) \tag{1.1}$$

where $J(u)$ is the objective function that is related to the economics parameters to calculate NPV in this model. The parameter space for the optimal solutions u^* is the the number and locations of possible hydraulic fracture stages, which are in general named control vector in the simulation.

In general, for most of production optimization problems, we deal with objective functions that are functions of continuous variables. The problem in this thesis is, however, the optimization solution u to be a discretized vector with integer numbers. This is due to the fact that we will be using a grid-based simulator as the framework for computing the optimization solutions. And the locations of HF stages are intrinsically connected with the gridblock indices (discrete values) in the simulator.

We implement two algorithms to solve the discrete optimization problem, the Simultaneous Perturbation Stochastic Approximation (SPSA) and the Covariance Matrix Adaptation Evolution Strategy (CMA-ES). To accomplish the application of these optimization techniques, we set several test cases and apply to homogeneous permeability maps and heterogeneous maps. Also, the optimal results will be compared with NPV of HF stages placed evenly on different types of permeability maps to comment on efficiency of the algorithms.

1.4 Thesis Outline

This thesis is organized as follows. In Chapter II, we discuss several aspects of building up shale gas reservoir models. As the simulation model applied in the optimization problems, we consider the major characteristics of shale gas reservoir, such as ultra-low permeability, gas adsorption and natural fracture influence. To properly evaluate the simulation results, we consider the realistic test cases and real date sets. Thus we show that we matched simulation results with real field gas rates data.

In Chapter III, we present the methologies of two algorithms, SPSA and CMA-ES, with application to optimization problems that have continuous solutions. Flowcharts of each algorithm applied in reservoir models are also listed out.

In Chapter IV, we test these two algorithms on the optimal wellbore placement and HF stages network design with given number of HF stages. Homogeneous and heterogeneous permeability maps are used in several test cases.

In Chapter V, we consider more complex cases that have the unknown number of HF stages, and implement the optimization approaches by these two algorithms. Different permeability maps and test cases are also described.

Finally, in Chapter VI, we present the conclusions from these optimization tests, and make some recommendations for future works.

CHAPTER II

MODELS OF SHALE GAS RESERVOIR

2.1 Introduction

In this thesis, we apply the optimization approaches to unconventional reservoirs and in particular to shale gas reservoirs. Our objective is to find optimized locations of hydraulic fracture stages in these reservoirs; therefore, a realistic, consistent and practical reservoir model is required, in combination with an efficient reservoir simulator.

The shale gas reservoir model in this optimization routine is simulated using a commercial reservoir simulator, namely Schlumberger compositional ECLIPSE™ 300 (E300) reservoir simulator (version 2012.2). E300 has several features for absorption models to simulate gas shale reservoirs based on Coal Bed Methane Model. Base on the factory default model SHALEGAS1.DATA input data file as an initial basic model, we build a completely new model that was suit for the needs of this thesis.

This chapter is structured as: at first, we set several input parameters to simulate the accurate gas shale matrix- and fracture flow and subsequent production of shale gas; we use several published data, model grid and reservoir properties of a gas shale reservoir as documented in this thesis, to represent the practical values used in our model and also to match the real field data used here. Then, a quantitative assessment of the sensitivity of the reservoir model to various reservoir and economic parameters is performed and discussed.

2.2 Shale Gas Model and Reservoir Properties

In order to build shale gas model, one has to pay attention on two features of the reservoir: dual-permeability system and gas adsorption, and generate a table for reservoir properties in each reasonable range. Also, the models consider several options to handle different sizes of grids.

2.2.1 Dual Permeability

In shale gas reservoirs, the natural gas volume can be stored in a local macro-porosity system (fracture porosity) within the shale, and these reservoir rocks have a sizeable fraction and are easily to be fractured. To represent the interaction between matrix and fracture subsystem, we consider a dual permeability model, and the method itself is briefly discussed here. More detail descriptions can be found in Chapter 16 from ECLIPSE Technical description 2012.2.

The dual permeability flow system describes flows from matrix to matrix cell, from fracture cell to fracture cell, and from matrix cell to its corresponding fracture cell and vice versa (**Fig. 2.1**). In this flow system, we are not only considering the flow from matrix to fracture cell and fracture to fracture cells, which is flow in dual porosity system, but also adding one more flow type that is from matrix to matrix cells.

In the dual permeability model, the matrix cell of a matrix-fracture coupled grid block is treated as a source term. The source, upon an applied pressure drawdown, expulses the shale gas into the matrix porosity and subsequently into the fracture network cell, which is linked within the same matrix-fracture coupled grid block. The fracture network cell acts as a sink term in this process.

To represent two cells per matrix-fracture coupled grid block, being one for the matrix properties and the other for the fracture properties, ECLIPSE uses these two grid cells and merges them automatically into one matrix-fracture coupled grid block. Here, we only consider one layer in the z-direction and focus on solving gas flow, with gravitational effects not taken into account in this thesis.

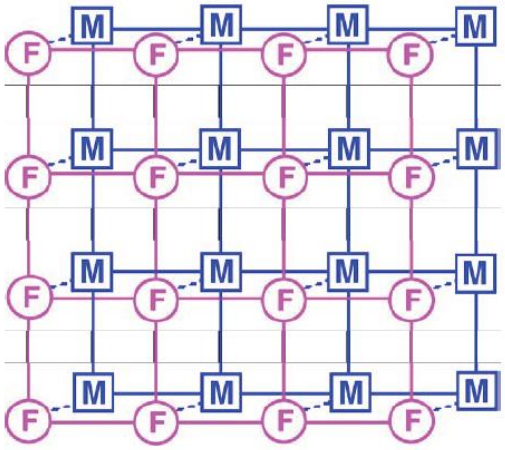

Fig. 2.1 Flow connections in the dual permeability model (From Pruess et al., 1999)

The transmissibility couples matrix-fracture cells that exist between each cell of the matrix grid and the corresponding cell in the fracture grid, which is calculated as proportional to the cell bulk volume. It is defined as:

$$TR = CDARCY \cdot K \cdot V \cdot \sigma_V \tag{2.1}$$

Where TR is the transmissibility $[\text{length}^3]$, $CDARCY$ is Darcy's constant in appropriate units$[\text{length}^2]$, K is the matrix permeability in the X-direction in our cases, V is the volume of the matrix grid block$[\text{length}^3]$, and σ_V is the transmissibility multiplier$[\text{length}^2]$. The formula for σ_V is given as:

$$\sigma_V = 4 \cdot \left(\frac{1}{{L_x}^2} + \frac{1}{{L_y}^2} + \frac{1}{{L_z}^2} \right) \tag{2.2}$$

where L_x, L_y and L_z [m] determine the fracture spacing in the X-, Y- and Z- direction respectively. Since we only have one layer, only fractures in the X- and Y- direction are considered in this model. As an example, we can calculate the transmissibility multiplier value based on the given parameters as listed Table 2-1. This case would yield a value of $\sigma_V = 0.036$.

2.2.2 Desorption Model

In this dual permeability system, the transient behavior in the matrix becomes important (Pruess et al., 1999). Some of the gas might be adsorbed on the surface of the shale and some exists as a free gas in the matrix pore structure (**Fig. 2.2**). In order to model such behavior, the dual/multi porosity/ permeability option can be used together with the Coal Bed Methane Model for adsorbed gas on the rock formation in the chosen reservoir simulator.

The adsorbed concentration on the surface of the coal is assumed to be a function of pressure only, and is described as in the Langmuir Isotherm. The Langmuir Isotherm is inputted as a table of pressure versus adsorbed concentrations. Different isotherms can be used in different regions of the field. To this end, we assume the shale matrix desorbs pure methane gas at a rate determined by the application of the Langmuir Isotherm. The general formula for the Langmuir Isotherm is:

$$V(P) = \frac{V_L \cdot P}{P_L + P} \tag{2.3}$$

where $V(P)$ [MSCF/Ton] is the adsorbed gas content at pressure P[psi], V_L is the Langmuir volume parameter [MSCF/Ton] which gives the storage capacity of adsorbed gas content at

infinite pressure, and P_L the Langmuir pressure parameter [psi]. The specific Langmuir parameters for methane in gas shale reservoirs are scarcely documented and were obtained from collective measurements performed by Ross and Bustin (2009) and Freeman et al. (2009) (**Fig. 2.3**).

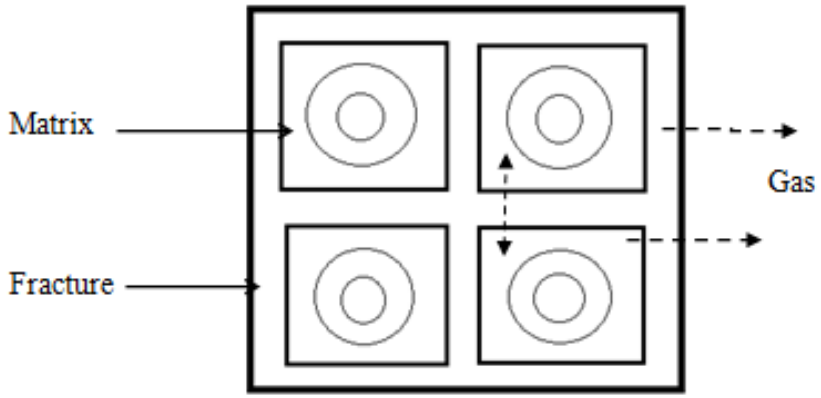

Fig. 2.2 A simple structural diagram for absorbed dual permeability model

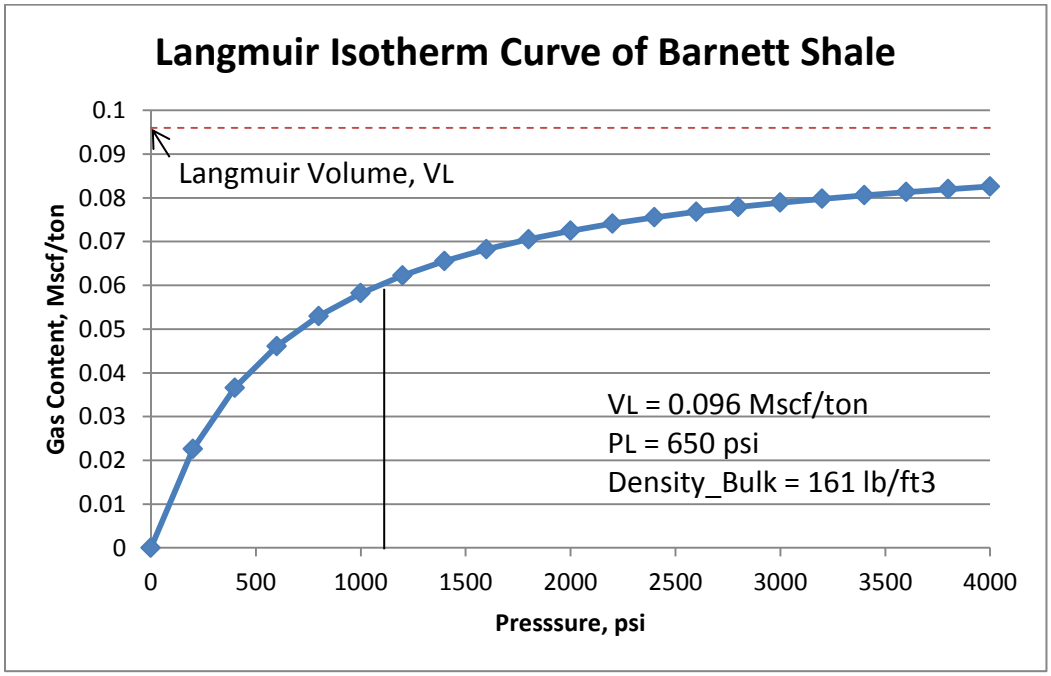

Fig. 2.3 Langmuir isotherm curve and adsorption date of Barnett Shale

The Langmuir isotherm (blue line in **Fig. 2.3**) shows the quantity of adsorbed gas that a saturated sample will contain at a given pressure. Decreasing pressure will cause the methane to desorb in accordance with the behavior prescribed by the blue line. As can be seen, gas desorption increases in a nonlinear manner as the pressure declines. Thus, in this example, a sample at 1000 psi pressure will result about 58 SCF/ton adsorbed gas. In addition, the red line gives us the value of gas volume at infinite pressure situation.

2.2.3 Shale Gas Reservoir Properties

In this section we discuss about the gas shale reservoir properties chosen to populate the model. All the reservoir properties and their corresponding values are all taken from published literature with reasonable ranges. We assume that methane is the single gas component in the reservoir, and thus, we input all parameters for viscosity, density, Z-factor into the model. The range of each property values and numbers chosen in this model are listed in **Table 2.1**.

The value of matrix permeability is from extremely low (sub nanoDarcy scale) to very low (microDarcy scale). We assume that the natural fracture permeability in the shale reservoir can be simulated in two different situations: homogeneous and heterogeneous. Because we define clearly permeability of the matrix and fracture system, in this case the keyword of corresponding net bulk fracture permeability will not be active at the ECLIPSE reservoir simulator.

In the proposed closer to real gas shale model in this thesis, heterogeneities fracture permeability map is also considered. In order to represent natural fracture network and capture the interaction between matrix and fracture subsystems, we apply the dual

permeability model (Pruess, 1999). This shale model assumes that natural gas is stored in a local macro-porosity system (fracture porosity) and that a significant portion of the reservoir rock can be easily fractured. Application of the natural fracture subsystem gives an opportunity to test cases with both homogeneous and complex heterogeneous permeability maps (**Fig. 2.4**).

Table 2.1 Overview of shale gas reservoir properties and literature values

Property	Units (Field)	Value Range	Model Value
Reservoir Thickness	ft	50 – 300	200
Reservoir Depth	ft	5000 – 7500	6500
Reservoir Temperature	F	100– 180	150
Shale Rock Density	lb/ft3	161-162	161
Matrix Permeability	mD	0.001 – 1e-8	0.00015
Matrix Porosity		0.01 – 0.1	0.06
natural Fracture Permeability	mD	0.1-10	0.0002 (Effective)
natural Fracture Porosity		0.001	0.00005 (Effective)
hydraulic Fracture Permeability	mD	1000 – 10000	10000
Adsorbed gas content/ Total gas content	%	20 – 85	70
Langmuir Pressure	psi	650	650
Langmuir Volume	MSCF/Ton	0.096	0.096
Reservoir Life-Span	year	10 - 30	20

In our model, the depth of top layer was chosen from known gas shale formations in Barnett Shale. Values for the porosity of the matrix and the natural fracture (both bulk porosities) need to be set in different value respectively, and the fracture porosity is incredibly lower than the matrix porosity, because it can be treated as no fracture porosity in this shale gas model. For an example, the width of one natural fracture is only 0.0001 meter.

After the bulk volume of the fracture grid block divided the combined volume of these 'pores', the fracture bulk porosity is very small.

In a gas-water gas shale system, the rock is expected to be extremely water-wet, making the gas the non-wetting phase. The relative permeability of each phase decides the ability of a specific phase to flow through the pores of both the matrix and the fracture network. Based on experimental data of very tight sandstones by Maas (2011), several input variables such as minimum and critical saturations, end-point relative permeability and Corey exponents are used to construct the relative permeability curves (**Fig. 2.5**). The capillary pressure curves as well as the depth of the gas-water contact (GWC) can be used to determine the initial saturations (**Fig. 2.6**) of the fluids in the reservoir.

Also, when the reservoir is being depleted due to an applied pressure drawdown, the rock compaction function is introduced (Rubin, 2009; Cipolla et al., 2010), in order to model the effect of reduced fracture conductivity (or closing of the fractures) at lower pressures. This function is used to represent the closing of fractures and results in a steeper production decline. The rock compaction table that was used in this work is shown in **Fig. 2.7**. Its effect on the stress-dependent fracture network conductivity, could explain the steeper production decline and lower ultimate gas recovery that is observed. The matrix compressibility is assumed to be negligible.

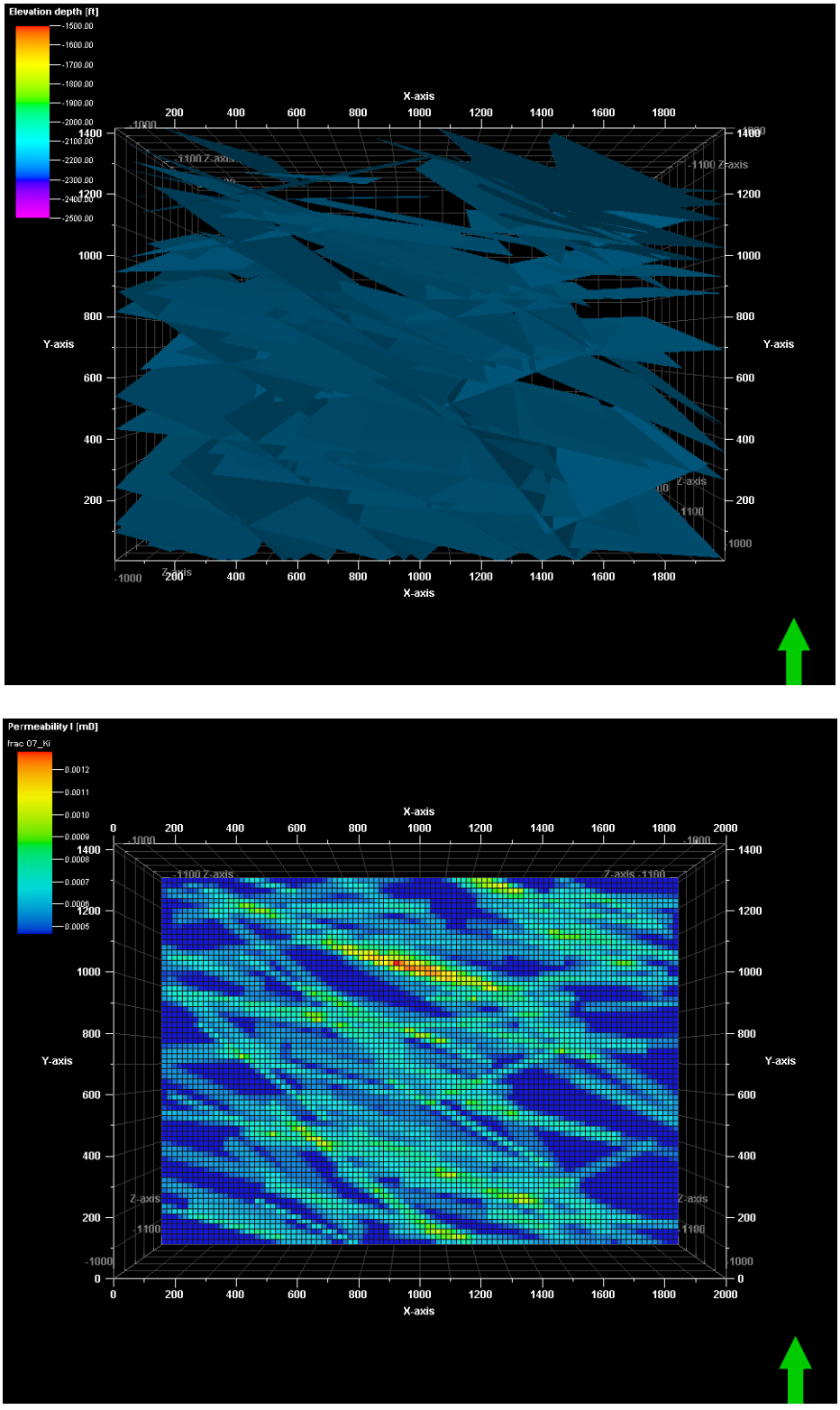

Fig. 2.4 Fracture network generated by Petrel 2012 (up) and fracture network permeability map after upscaling (down)

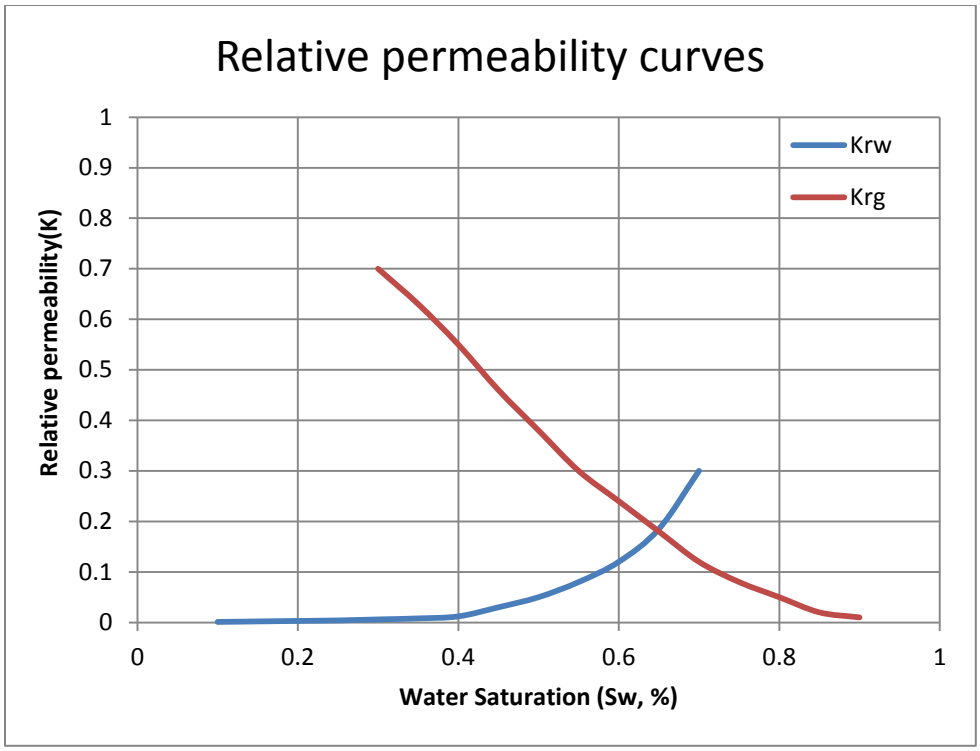

Fig. 2.5 Relative permeability curves for fracture system

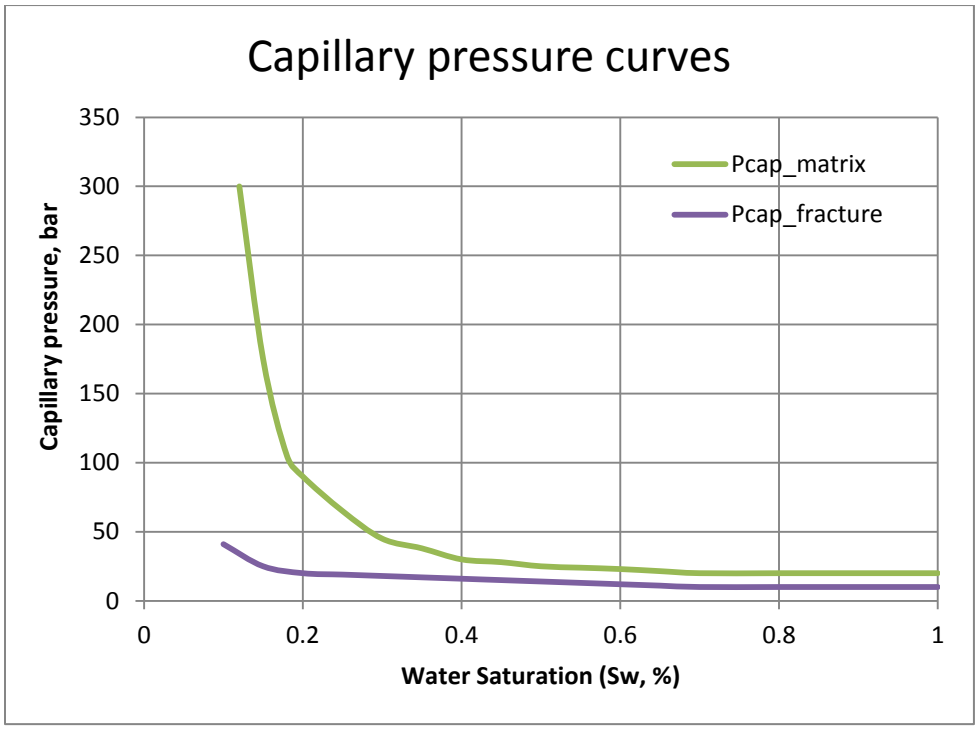

Fig. 2.6 Capillary pressure curves, to serve as input data for the gas shale reservoir model

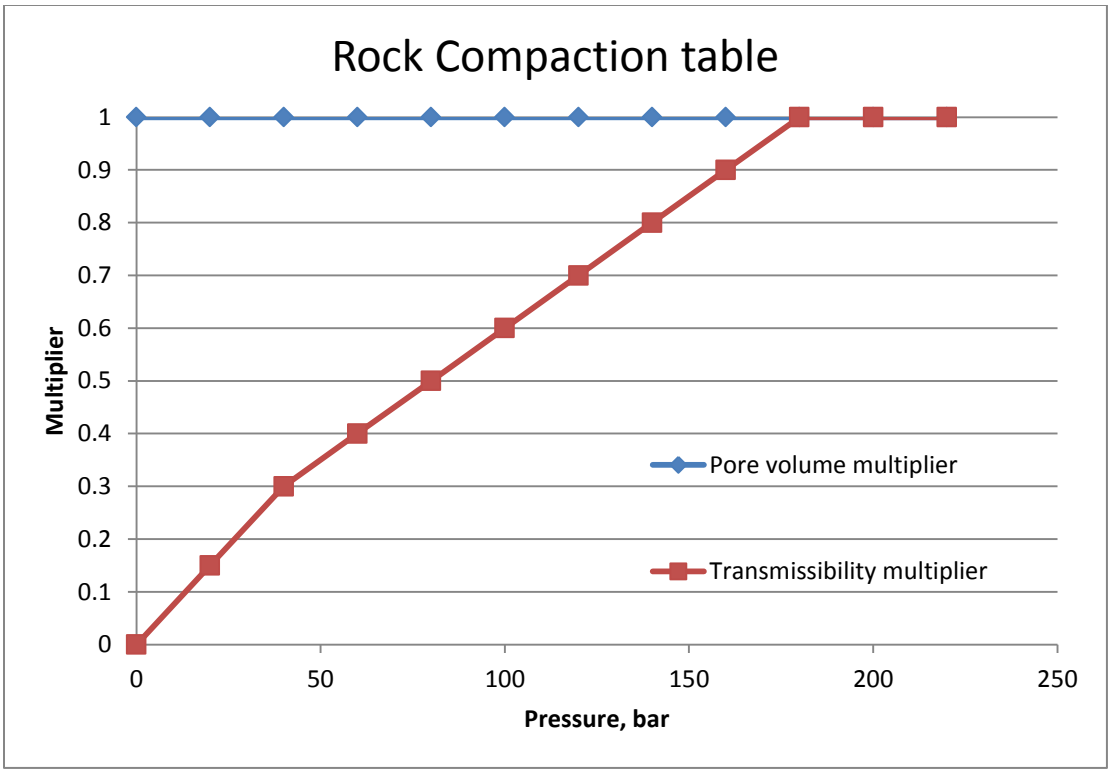

Fig. 2.7 Rock Compaction table for fracture system

2.2.4 LGR and Equilibrium Hydraulic Fracture Permeability

To quantify the stimulation effort of a hydraulic fracture stage, it is common practice to work with the dimensionless fracture conductivity ratio term F_{CD}. This is the ratio of the permeability of the fracture multiplied by its propped fracture width and the permeability of the formation multiplied by the fracture half length (Economides and Martin, 2007). Mathematically the formula is defined as:

$$F_{CD} = \frac{k_f \cdot w_f}{k \cdot X_f} \tag{2.4}$$

where F_{CD} is the dimensionless fracture conductivity, k_f is the fracture conductivity [mD], w_f is the width of the fracture [ft], k is the reservoir permeability [mD] and X_f is the fracture half length [ft]. In general, the width w_f of hydraulic fracture is very narrow, around 0.003 ft

(Moridis, 2011). However, the shale gas model used for optimization approaches has a coarse grid, for example, with cell dimensions of 20×20×200 feet. To represent traverse HF's more accurately within the model, we enable local grid refinement (LGR) feature in particular coarse gridblocks. The LGR's are divided into nine layers (**Fig. 2.8**) with different ratios that have the central layer only 0.4 ft along X-direction with the equivalent permeability of each HF stage. Under this local grid refinement scale, the permeability of HF stage which locates in the central line of grid should also be calculated as the equilibrium value for the forward simulations.

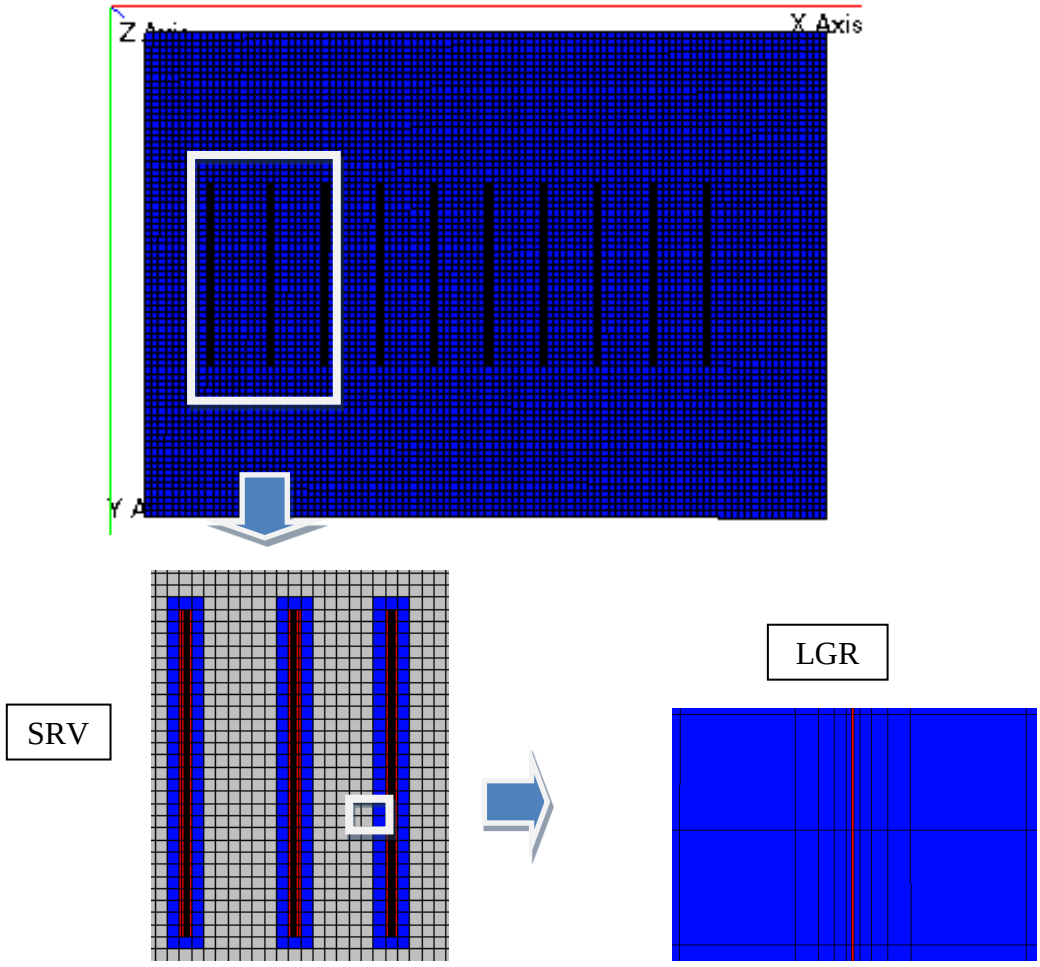

Fig. 2.8 LGR and SRV features used in the model.

In ECLIPSE simulator, there is no direct keyword to define the hydraulic fracture conductivity in the reservoir model. Instead we model the hydraulic fracturing stimulation effort at some grids that enhances the fracture permeability largely in the influenced zone, Stimulated Reservoir Volume (SRV). The transmissibility variable, which includes a permeability term, can also be interpreted as an indirect measure for the enhanced fracture conductivity. A zone representing stimulated reservoir volume (SRV) around each HF is also incorporated into the model (**Fig. 2.8**). LGR's and SRV's change automatically as HF's switch their locations during the optimization process.

2.3 History Match with Real Field Data

In order to exam the simulation model, we compare the production data with real field gas rate of Well 314 from Barnett Shale. Published reservoir properties from Barnett Shale (Al-Ahmadi, 2011), are listed out in **Table 2.2** and is used for this history matching case. In this model, the reservoir is assumed to be homogeneous, containing multistage hydraulic fractures as evenly spaced along the horizontal well with a single perforated interval for each stage (**Fig. 2.9**).

In this thesis, we consider the matrix permeability and the natural fracture effective permeability as the unknown parameters to be matched in the history matching process. We approached this problem from ad-hoc attempts to compute the proper values of these parameters.

The field production data is from well 314, and history matching curves are presented in **Fig. 2.10** and **Fig. 2.11**. After performing history matching, **Fig. 2.10** shows that we get good match between numerical simulation results and the field gas rate data, which also

provide a reasonable simulation model for production prediction and the following optimization approaches. The simulation result can be assessed again with **Fig. 2.11**, which shows the matched cumulative production rates with small misfit between the measured production rate and the simulated result. **Fig. 2.12** shows the pressure drop distributions in matrix and fracture system after 5 years production. It shows the gas flow not only affects the fracture cells, but also happens to the matrix cells.

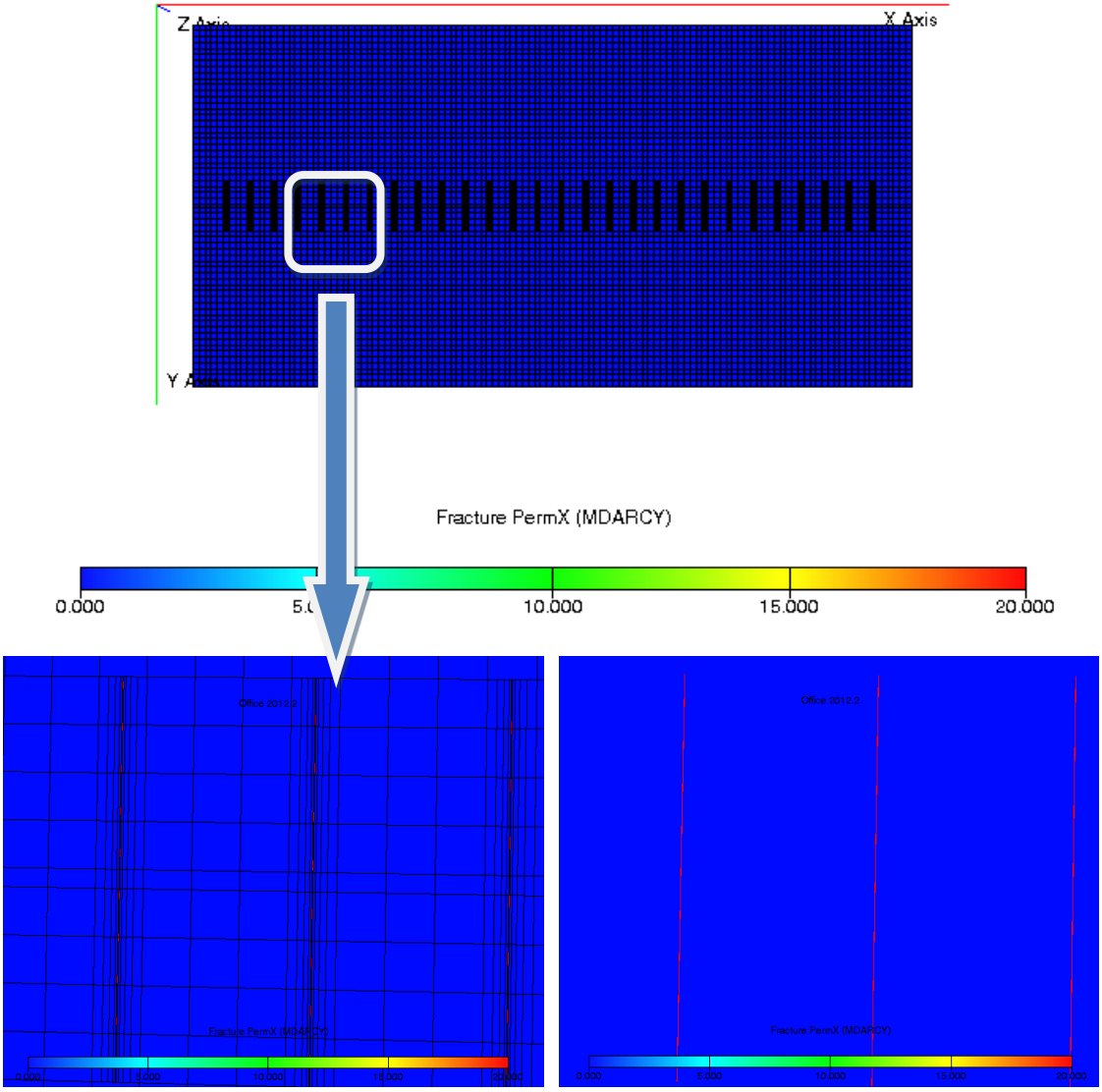

Fig. 2.9 Model of multistage hydraulic fractures distribution along horizontal well

Table 2.2 Reservoir properties and hydraulic fracture parameters in history matching

Parameters	*Values*	*Unit*
Model dimensions	3000 x 1510 x 300	ft
Initial reservoir pressure	2950	psi
Reservoir temperature	150	F
Bulk Density	161	lbs/ft3
Bottom hole pressure	500	psi
Horizontal well length	2968	ft
Production Period	5	years
Matrix permeability	0.00015	md
Matrix porosity	0.06	100%
Natural fracture efficient permeability	0.0001	md
Natural fracture porosity	0.00005	100%
Hydraulic fracture conductivity	1	md-ft
Hydraulic fracture spacing	100	ft
Hydraulic fracture height	300	ft
Hydraulic fracture half-length	105	ft
SRV permeability, Zone 1	0.05	md
SRV permeability, Zone 2	0.0005	md
Number of hydraulic fractures	28	stages

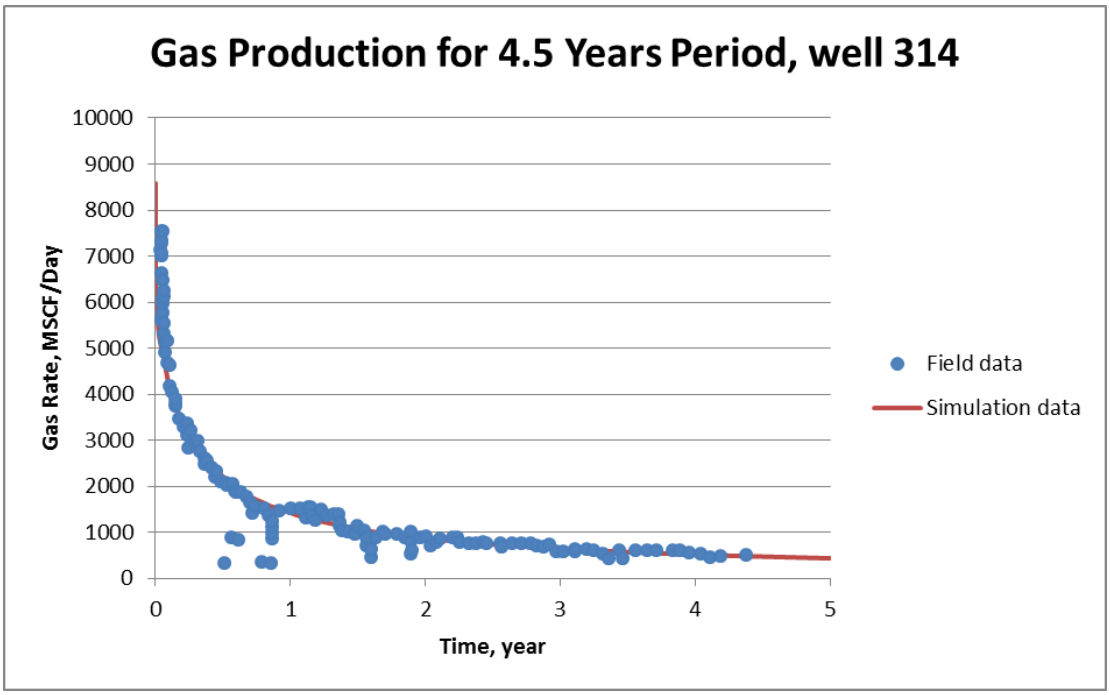

Fig. 2.10 Gas production rates of well 314 from Barnett Shale matched by simulation data

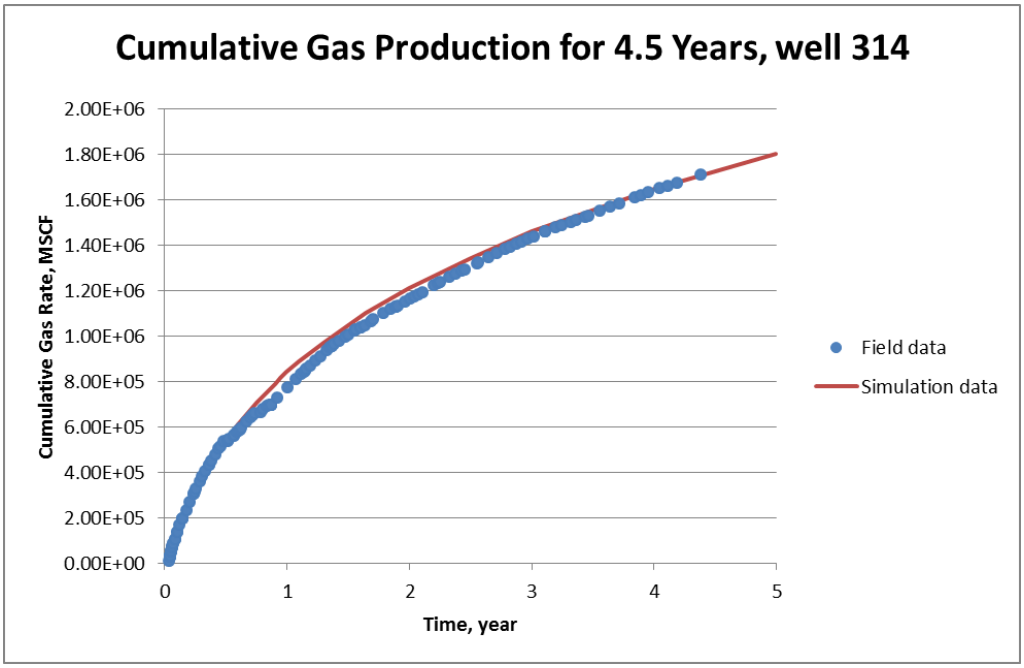

Fig. 2.11 Cumulative gas production rates of well 314 from Barnett Shale matched by simulation data

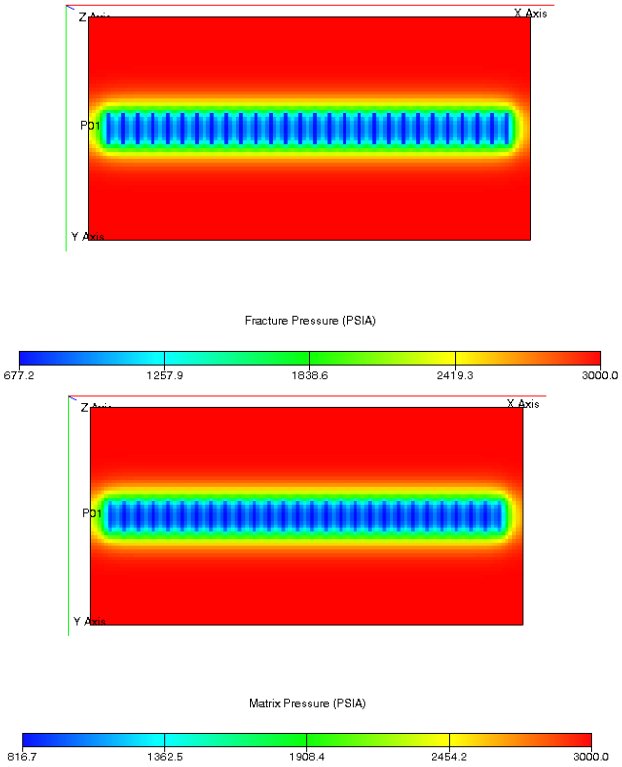

Fig. 2.12 Pressure distributions of dual-permeability system: Matrix and fracture, after 5 year of gas production

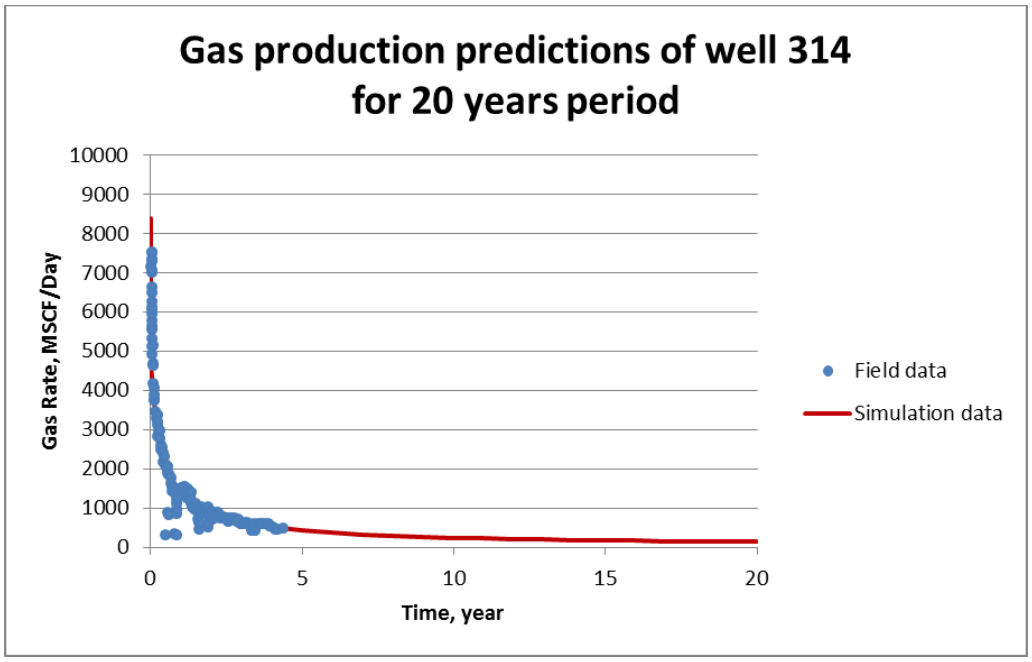

Fig. 2.13 Gas production predictions of well 314 from Barnett Shale, 20 years period

Beside history matching, we also tested the model with production time period as 20 years. **Fig. 2.13** shows the production prediction curve of well 314 for 20 years, which complies with a typical curve of shale gas production rate.

2.4 Sensitivities Analysis

Before we start the optimization problem, we need to perform a sensitivity analysis of the parameters affecting the variability of the NPV, and in particular, the hydraulic fracture stages to be placed and their locations. In this analysis, we put focus on certain reservoir properties and parameters of hydraulic fractures. After manually scheduling the hydraulic fracturing sequence and adjusting the fracturing intensity and parameters at different locations in several steps, we can observe how many of the fracture parameters affect the output of the model. Based the sensitivity analysis process, we can determine which parameters during the optimization approaches we should focus on.

The sensitivity process is as follows. First, we give a list of reference values for the reservoir properties and hydraulic fracture parameters which are from the base case in our analysis; Second, we change these model parameters by specified percentage from the reference values, such as increase or decrease 20%, 50%; then, at the last step, we collect these results from each group of parameters, plot sensitivity diagrams and analyze which parameter influence NPV function most/least. Our sensitivity study can be shown in **Fig. 2.14**. Here we consider variables in the number of HF stages (HFnum), HF drilling cost (HF cost), fracture permeability (Kf), HF half-length (Xf), stimulated reservoir volume permeability (SRV), matrix permeability (KM) and natural fracture effective permeability (KN).

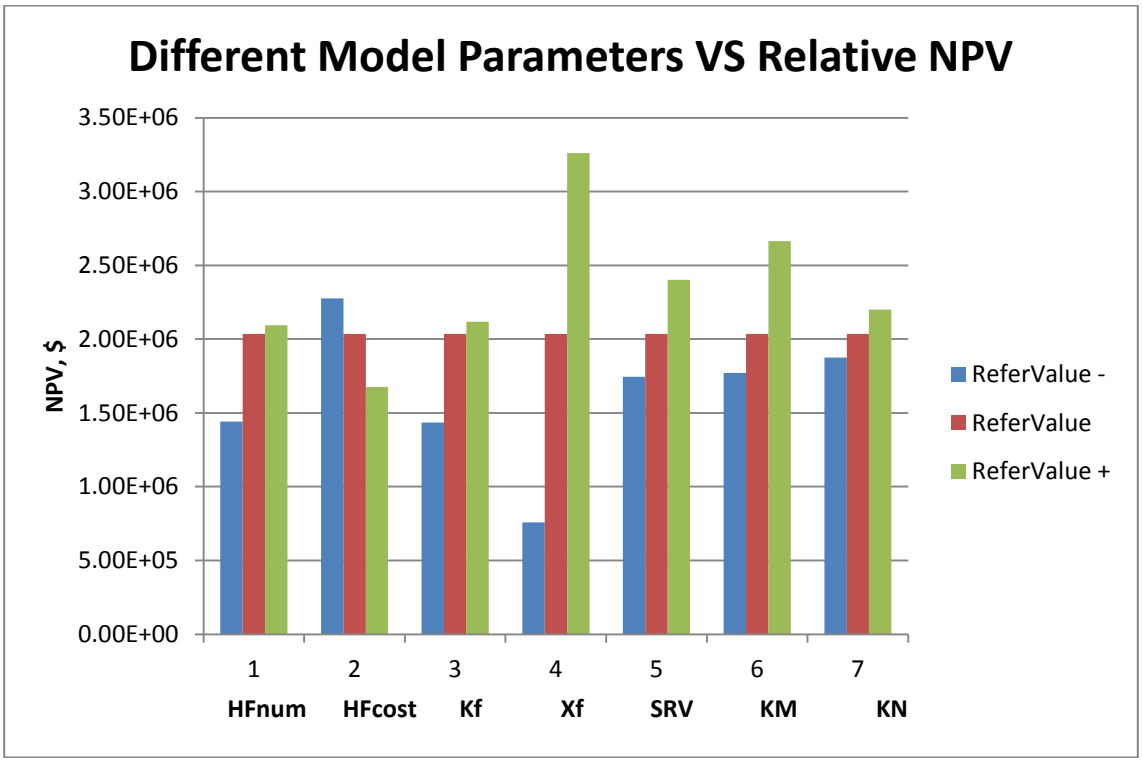

Fig. 2.14 Sensitivity diagram of shale gas reservoir, for 20 years production period

From **Fig. 2.14** and **Table 2.3**, the HF half-length has the largest influence to gas production rate. The second important parameter is the matrix permeability. It shows that the larger permeability matrix has, the easier is to produce gas out and consequently the higher NPV is. Besides these parameters, the permeability and number of hydraulic fracture stages plays important role for NPV calculations. Based on this analysis, we set clearer optimization tasks, put focus on the hydraulic fracture network design to optimize HF stage locations and numbers, and generate different permeability maps of nature fracture as groups of test cases to apply the algorithms.

Table 2.3 Reference values of model parameters and changing range

Model Parameters	Parameter Values			Relative NPV Range		
	Low	Reference	High	Low	Reference	High
HF Number (HFnum)	8	12	14	1.44E+06	2.04E+06	2.09E+06
Costs per HF (HFcost)	1.00E+05	1.20E+05	1.50E+05	2.28E+06	2.04E+06	1.68E+06
HF permeability(Kf)	5000	10000	150000	1.43E+06	2.04E+06	2.12E+06
HF Half-length(Xf)	180	250	340	7.58E+05	2.04E+06	3.26E+06
SRV Permeability (SRV)	0.0003	0.0005	0.001	1.74E+06	2.04E+06	2.40E+06
Matrix Permeability(KM)	0.0001	0.00015	0.0003	1.77E+06	2.04E+06	2.66E+06
Natural Fracture Efficient Permeability (KN)	0.00015	0.0003	0.0005	1.87E+06	2.04E+06	2.20E+06

Furthermore, we also put emphasis on each single parameter and plot the cumulative NPV curves to show their sensitivities. To calculate NPV, we use the equation in chapter 3 and analyze its response for each parameter. And we choose the basic economic assumptions that were used to build the realistic optimization objective function to present NPVs. The economics model considers gas price assumptions (EIA, 2013) and escalation factors (Holdith, 1978). The solid lines in **Fig. 2.15** represent the gas price starting from the $3.2/MCF initial value at 2013 and is escalated at 10%/year with ceiling price $8.5/MCF. We

will use this assumption to show the influences to NPV by different parameters, and compare the NPV values with cases that do not have escalation rate for the gas price.

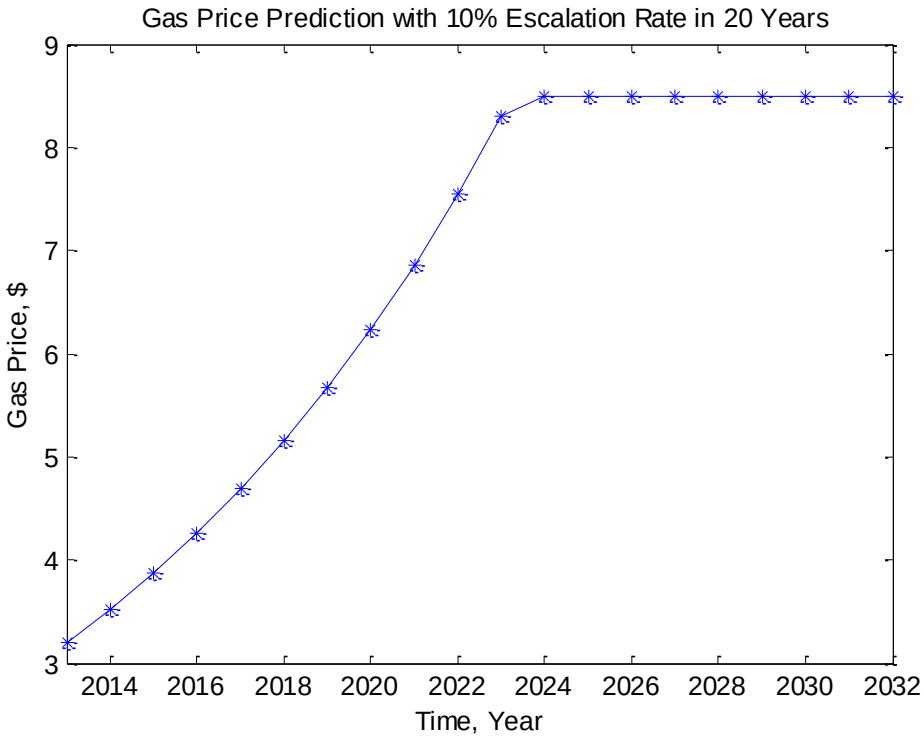

Fig. 2.15 Gas price prediction for 20 years with 10%/year escalation rate

In the sequence, **Fig. 2.16** to **Fig. 2.22** depicts the sensitivity analysis for the parameters shown in **Fig. 2.14**. All the solid lines are the cumulative NPV curves with 10% per year escalation factor, whereas all the dashed lines have constant gas price. We can see that by using the escalation factor in the gas price larger NPV can be achieved. Therefore, in this case, higher gas prices can work on our favor. All the larger reference values have larger cumulative NPV curves.

Fig. 2.16 and **Fig. 2.18** show that HF costs and half-length influence NPV largely, and NPVs are increased as the same ratios as the reference values changed. **Fig. 2.17** and **Fig.**

2.19 show different trend when the reference values grow. It shows that even though we increase the HF numbers and HF permeability, NPVs cannot be improved largely. The reason is that when we increase these two parameters, the cost of hydraulic fractures are also increased which results a little improvement to NPV. This is also the reason why we need pay attention to the optimizations of HF numbers, which give the optimal number of HF and at same time save as more cost as we could. **Fig. 2.20** shows that matrix permeability improves NPV with higher permeability in the matrix grids, and also much higher than the natural fracture permeability and SRV zones shown in **Fig. 2.21** and **Fig. 2.22**. The reason is that values of natural fracture and SRV zones are not big enough based on realistic assumptions.

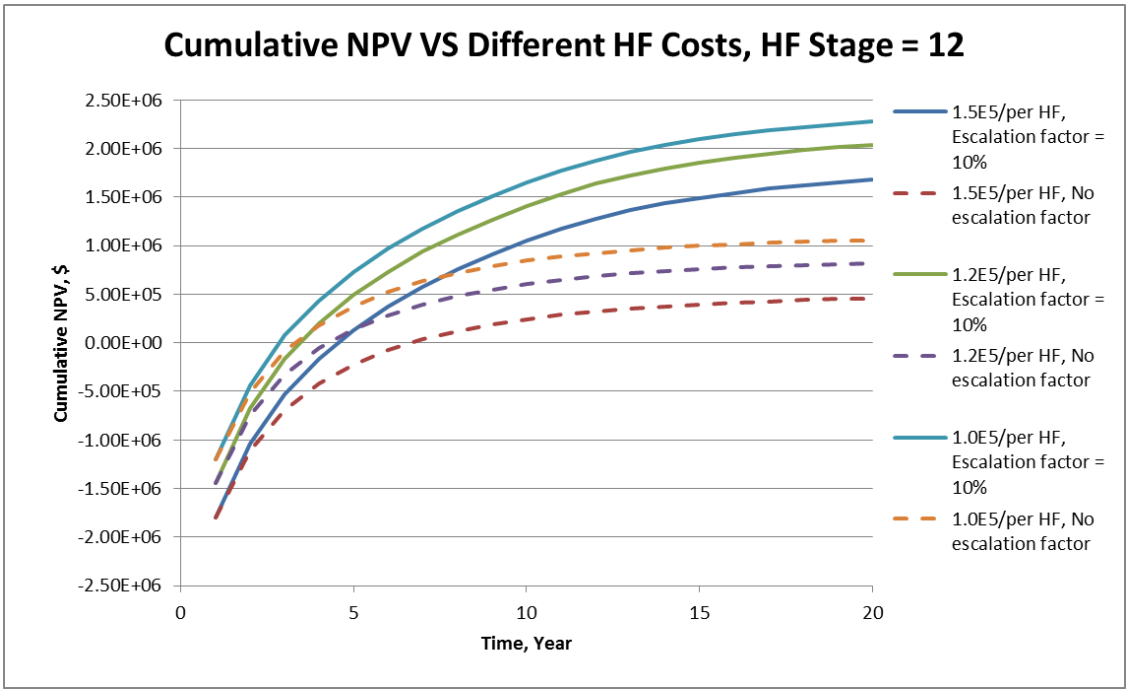

Fig. 2.16 Cumulative NPV curves by different value of HF costs, given HF stage = 12, solid line is gas price with escalation factor 10%/year, dash line has no factor

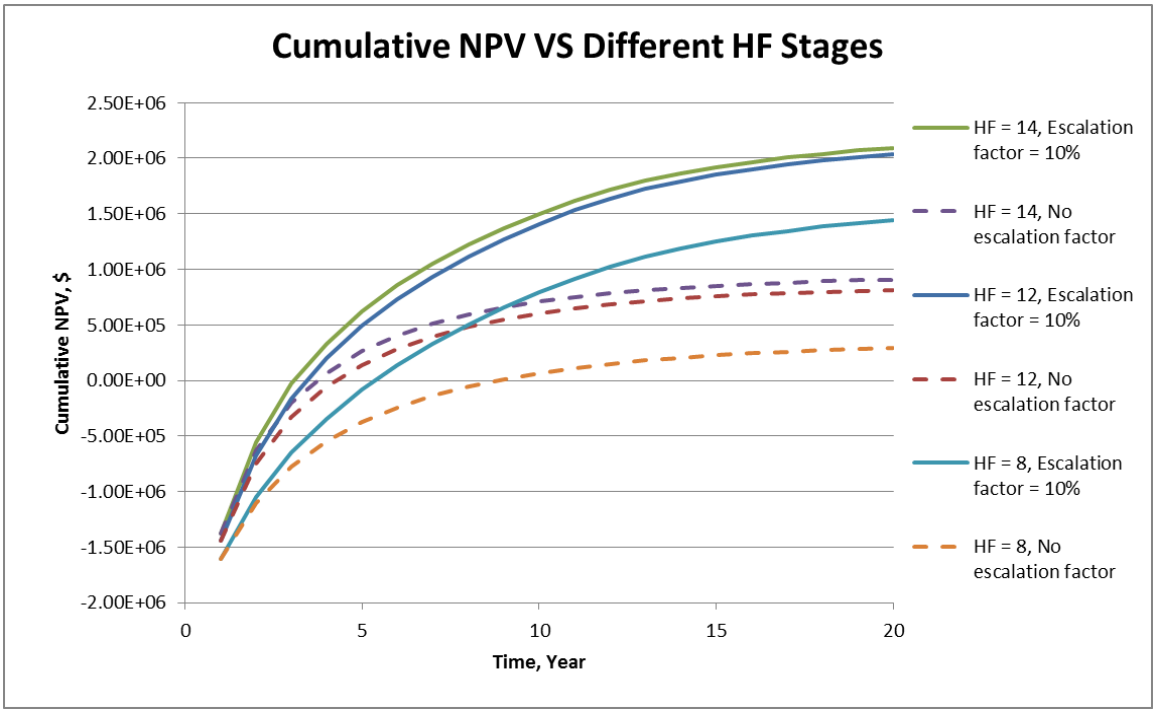

Fig. 2.17 Cumulative NPV curves by different number of HF stage, solid line is gas price with escalation factor 10%/year, dash line has no factor

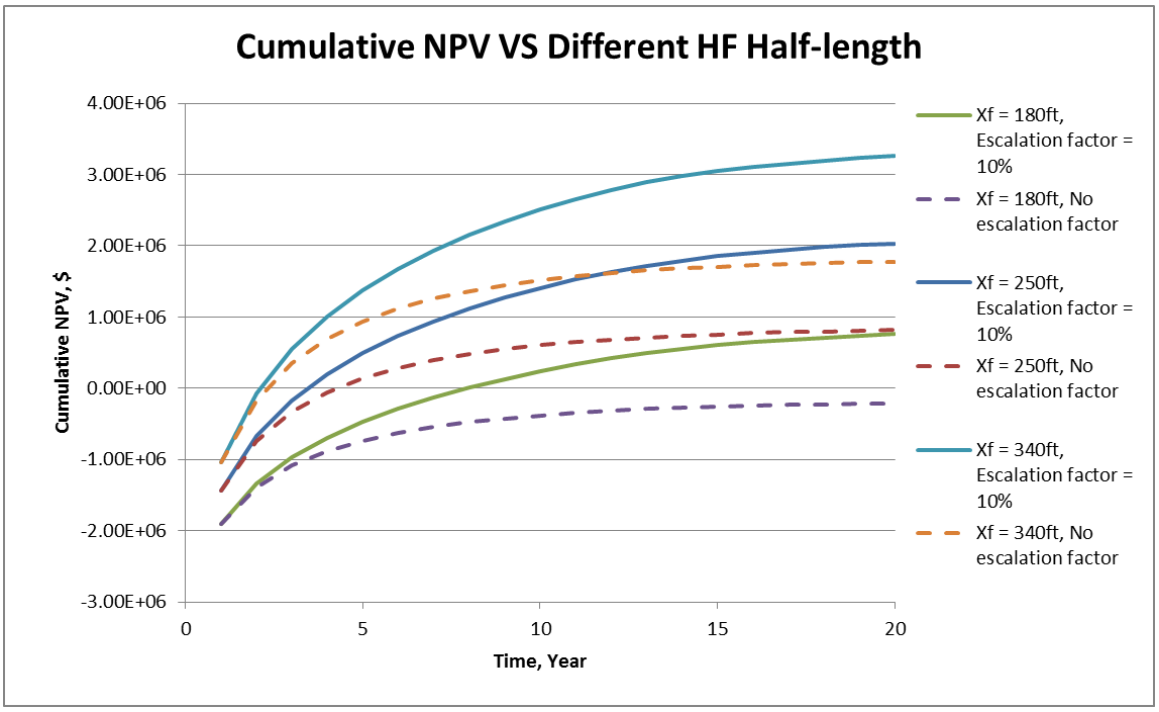

Fig. 2.18 Cumulative NPV curves by different values of HF half-length, given HF stage = 12, solid line is gas price with escalation factor 10%/year, dash line has no factor

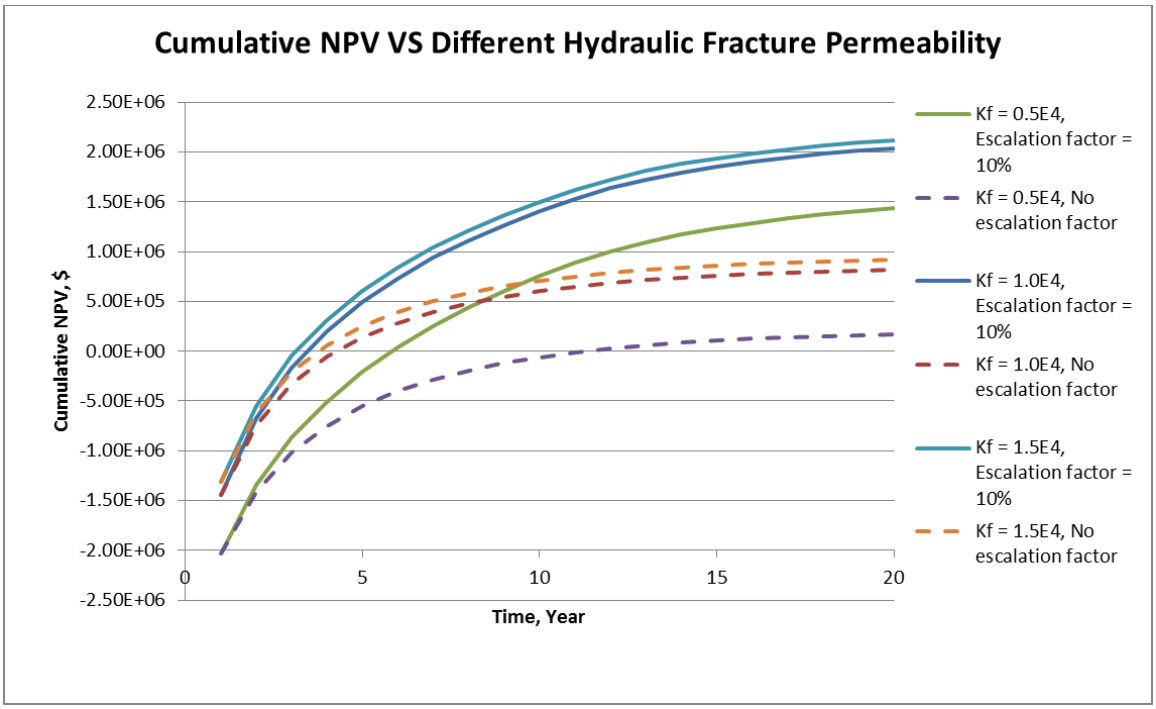

Fig. 2.19 Cumulative NPV curves by different values of HF permeability, given HF stage = 12, solid line is gas price with escalation factor 10%/year, dash line has no factor

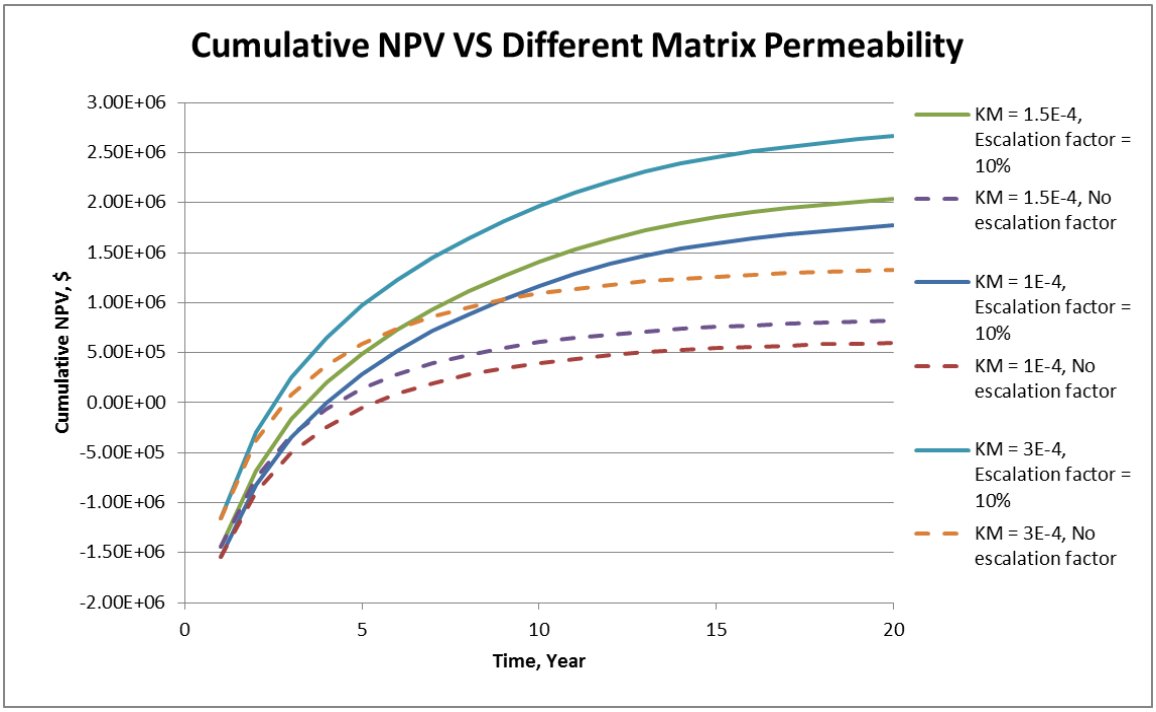

Fig. 2.20 Cumulative NPV curves by different values of matrix permeability, given HF stage = 12, solid line is gas price with escalation factor 10%/year, dash line has no factor

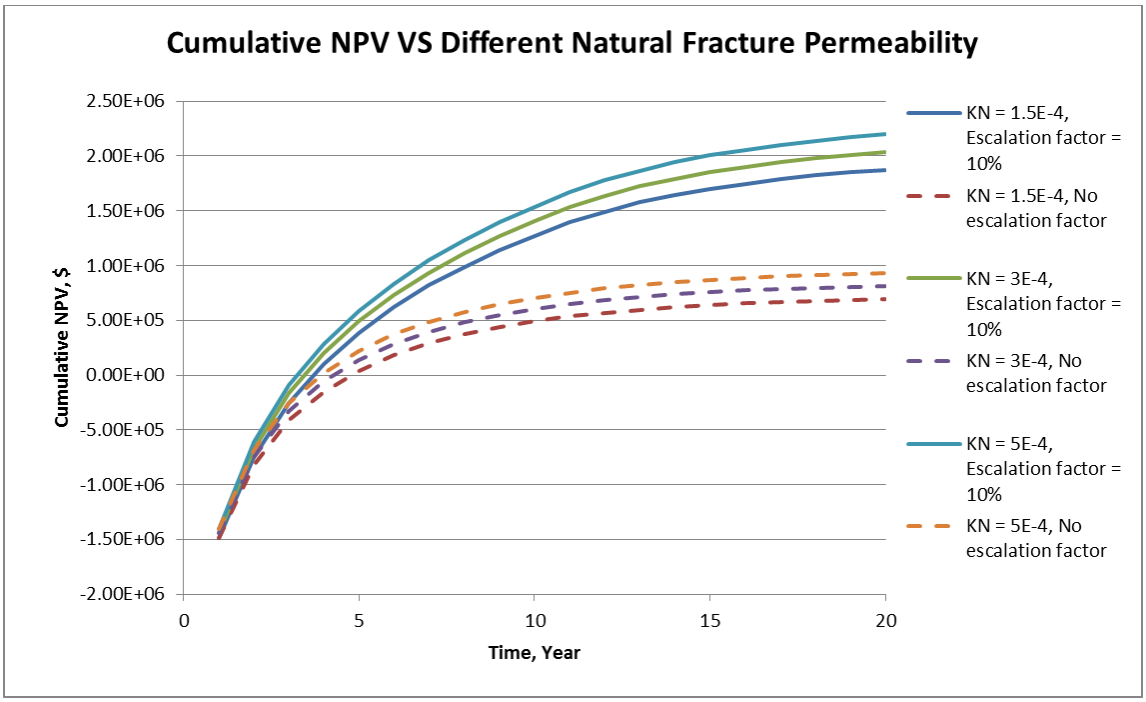

Fig. 2.21 Cumulative NPV curves by different natural fracture efficient permeability values, given HF stage = 12, solid line is gas price with escalation factor 10%/year, dash line no factor

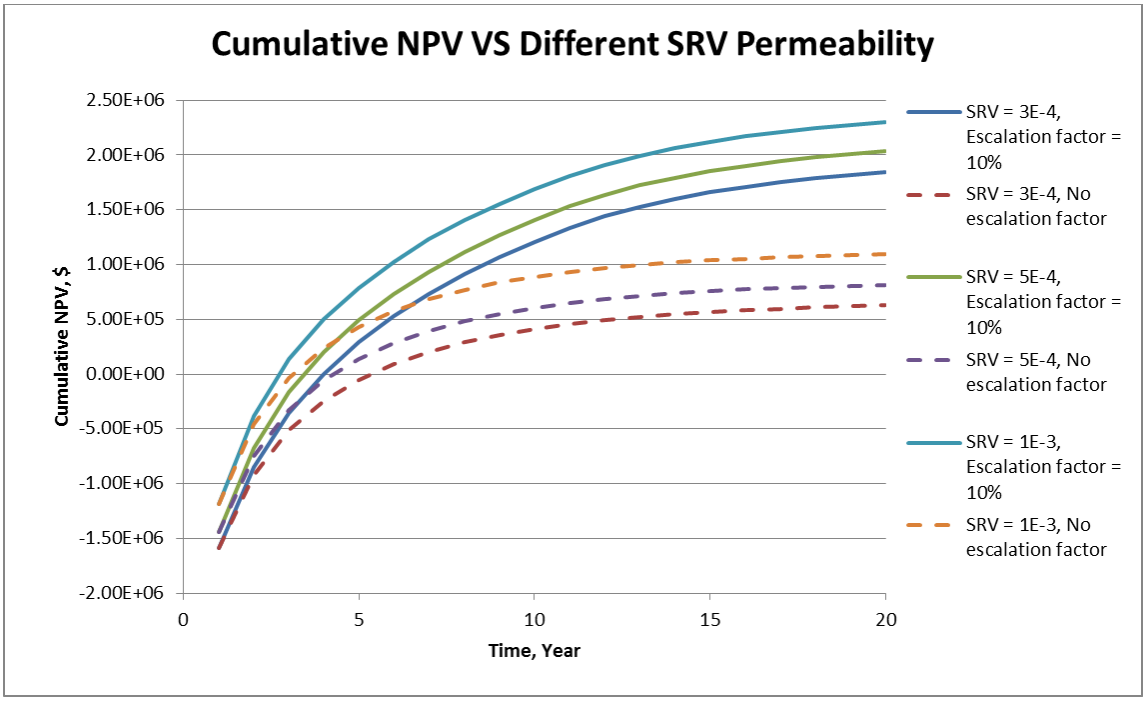

Fig. 2.22 Cumulative NPV curves by different values of SRV permeability, given HF stage = 12, solid line is gas price with escalation factor 10%/year, dash line has no factor

All these figures were testes by evenly spacing HF stages, and homogeneous permeability maps for matrix and natural fracture systems. With given number of HF stages, the cumulative NPV curves have the same trends as the cumulative gas production rates. However, for the heterogeneous permeability maps, the situation will be more complex. Even though we have the same stage number, the locations of HF stage influence NPV largely in heterogeneous case. In this case, the cumulative NPV by different values of model parameters will also change. This is important evidence that finding the optimal locations of HF stages is a paramount step as our optimization work.

2.5 MATLAB Coupling to the Optimization Process

To run the optimization process efficiently, the proposed shale gas reservoir model was built and integrated in the MATLAB (MATLAB R2012b) optimization framework. This framework initializes and updates the required input files for the ECLIPSE reservoir simulator at each iteration. The MATLAB/ECLIPSE coupling is depicted in **Fig. 2.23**.

The framework starts from a basic ECLIPSE model. After we build up the model, and have a base input deck in ECLIPSE, we choose MATLAB to control all of the update. MATLAB is used to write the sub-files which contain the HF parameters for the optimization, call ECLIPSE and read the results to calculate NPV. In order to implement the optimization, MATLAB also combine the control vectors within the algorithms, which we will introduce in the next chapter.

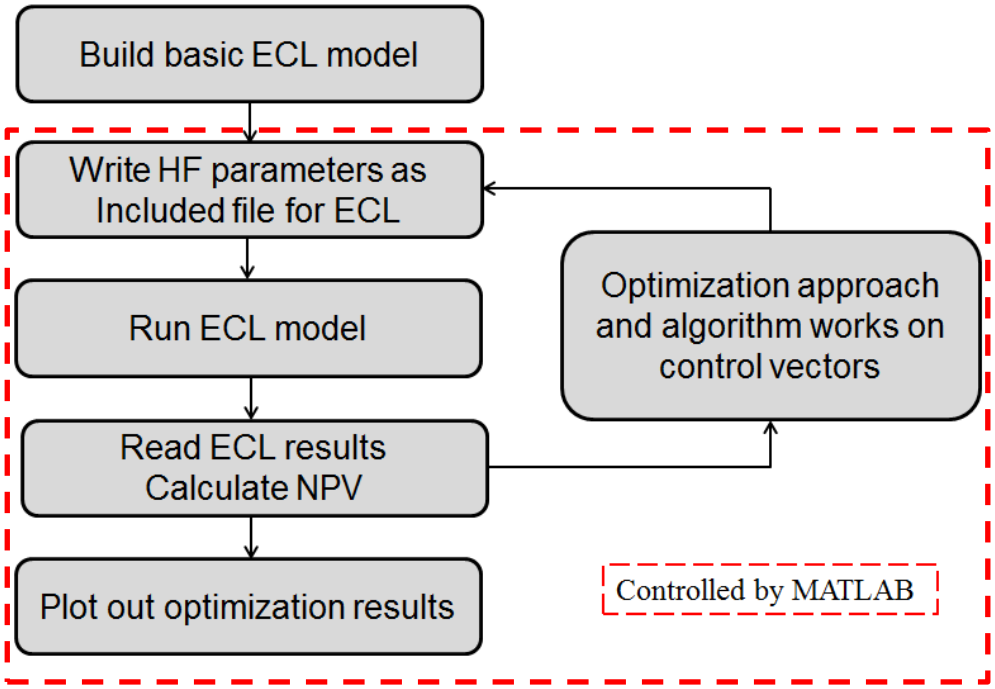

Fig. 2.23 Flowchart of code connection between MATLAB and ECLIPSE

CHAPTER III

ALGORITHMS FOR OPTIMIZATIONS

3.1 Introduction

In this chapter, we introduce the numerical optimization algorithms to be used in the hydraulic fracture stage optimization to be addressed in the next chapters. First, we present the objective function to be maximized. Then, we introduce three algorithms for the optimizations, being two gradient-based methods, Finite Different method and SPSA (Spall, 1992) and a gradient-free method CMA-ES (Hansen, 2006). Details of these algorithms are listed out and numerical cases are discussed to explain how these algorithms work.

3.2 Objective Function

In reservoir engineering, it is a common objective to optimize (maximize) some sort of economic objective functions, throughout the lift-cycle of the reservoir development. In particular, for unconventional reservoirs, the goal is to seek for the best locations of hydraulic fracture (HF) stages, and in turn the optimal numbers that can result in a maximum economical production of the reservoir. In our case, this is translated into maximizing the net present value (NPV) of the life-cycle of the reservoir.

In general, the objective function should contain measure terms describing any user-specified performance. In hydraulic fracture production problems, the NPV function contains the terms accounting for the cost of each hydraulic fracture and the number of hydraulic fracture stages. In addition, the objective function not only considers the gas production and its economic effect, but also well drilling cost and operation cost. Since the production period

is as long as 20 years, the discount rate that is expresses as annual interest rate is also added into the function. Mathematically the objective function can be written in the form:

$$J(u) = \sum_{k=1}^{K}\left[\sum_{j=1}^{N_{prod}} \frac{\left(Q_{g,j}{}^{k} \cdot r_g - r_w - O_j\right)\cdot \Delta t^k}{(1+b)^{t^k/365}}\right] - \sum_{j=1}^{N_{prod}} \left(C_w \cdot j + H_j C_f + H_j C_p\right). \qquad (3.1)$$

Here, the first summation term expresses the discounted revenue from the well operations and the second term accounts for drilling and HF costs (Holt, 2011). Each parameter of $J(u)$ is defined as follows: *K* is the total number of simulation time steps, *k* is the time index, Δt^k [year] is the length of time period, and *b* is the discount rate [%/100/year]. N_{prod} is the number of production wells, $Q_{g,j}{}^{k}$ is gas production rate for a producer *j* [Mscf/day] at year *k*, and r_g is constant gas price [$/Mscf]. In order to describe project expenses, we use O_j [$/day] as the operating cost of the well j, C_w [$] as the base cost of drilling a horizontal well, C_f [$] as the hydraulic fracturing cost per stage, H_j as the number of HF stages along the well j, and, finally, C_p [$] as the drilling penetration cost of a gridblock. **Table 3.1** provides values for the main variables of the objective function $J(u)$ that will be used for the rest of this work.

Table 3.1 Parameter values for the NPV function. (Schweitzer, 2009; Bruner, 2011)

Property	Unit	Value
Gas price (at the wellhead)	$/ft^3	3.2
Cost of disposal water	$/bbl	1.0
Discount rate	%/100	12.5
Base cost for drilling per well	$	2.00E+06
Penetration cost per gridblock	$	6.00E+03
Cost per HF stage	$	1.50E+05
Operating cost per well	$/day	60

Once the objective function is appropriately defined, based on Eq. 3.1, we define the optimization problem as follows: Maximize NPV with respect to the HF stage locations. Mathematically, this leads:

$$u^* = arg \max_{u \in U} J(u) \tag{3.2}$$

where u is the control vector that records locations of HF stages and $J(u)$ is the objective function listed in Eq. 3.1. In this case, the optimization solution u is a discretized vector with integer numbers.

The control vector u^* in Eq. 3.2 contains the optimal number of HFs along the horizontal wellbore of interest and their respective locations. Although in this study we fix several of the parameters associated with the geometry of the fractures, such as half-length of all HFs to be a user-defined value, it does not prevent us from incorporating them in the control variable as well and be subject to the optimization problem. It is important to note that Eq. 3.2 is usual formulated for a continuous control vector $u \epsilon R^2$. Numerical simulators, however, can only represent fracture stage locations as discreet numbers associated with gridblock indices. Thus, conversion of the continuous optimization problem into integer programming problem is another challenge that will be described in our methodology.

In this thesis, we implement several algorithms to solve the above integer programming problem. Simultaneous Perturbation Stochastic Approximation (SPSA) and Covariance Matrix Adaptation Evolution Strategy (CMA-ES) which will be described next are applied as optimization approaches. In addition, we consider gradient based method by brute force perturbations, such as the Finite Difference (FD) approach. Although these methods are different conceptually, they all are suitable for integer programming problems such as HF placement. Application of these optimization techniques allows departing from a

common practice of placing HF stages evenly in the reservoir, and permits one to deal with highly heterogeneous geologic systems that require HF spacing with non-even intensity. We compare results obtained from these algorithms in the following chapters in terms of performance, computational time and accuracy.

3.3 Simultaneous Perturbation Stochastic Approximation (SPSA)

The simultaneous perturbation stochastic approximation (SPSA) (Spall, 1992) method is especially efficient in high-dimensional problems as it provides a good solution for a relatively small number of measurements of the objective function. SPSA uses only objective function measurements to compute the optimal solutions.

3.3.1 Methodology of SPSA

The essential feature of SPSA, which provides its power and relative ease of use in difficult multivariate optimization problems, is the underlying gradient approximation that requires only two objective function measurements per iteration regardless of the dimension of the optimization problem. These two measurements are made by simultaneously varying a "proper" random variables in the problem (the "simultaneous perturbation"). This contrasts with the classical ("finite-difference") method where the variables are varied one at a time. If the numbers of control variables are defined as in the optimization models, the finite-difference method takes $2n$ times measurements of the objective function per iterations to form one gradient approximation, while SPSA takes only two measurements. Assuming we have the number N of controls variables, for the objective function $J(u)$, mathematically the formula to calculate gradients is:

$$g_i = \frac{J(u + \Delta u_i) - J(u - \Delta u_i)}{\Delta u_i}, i = 1, \dots, N$$

Δu_i is perturbation vector that could be generated by several random functions. A brief description of SPSA algorithm is depicted in the **Table 3.2** below:

Table 3.2 Algorithm description of SPSA

Algorithm of SPSA
Step 1: Initialization and coefficient selection. Set dimensions of search space p and edges of region want to search in p_{max}, p_{min}. Pick initial guess and non-negative coefficients about a, c, A, α and γ in the SPSA. Set Nspsa as total iteration number.
Step 2: Do the iteration k=1 to Nspsa. a. Gain sequences $a_k = \frac{a}{(A+k)^\alpha}, c_k = \frac{c}{k^\gamma}$. b. Generate by normal distribution a n-dimensional random perturbation vector Δ_k, compute the cost function for $y(\theta_k + c_k\Delta_k)$ and $y(\theta_k - c_k\Delta_k)$ c. Gradient approximation. Generate the simultaneous perturbation approximation to the unknown gradient $g(\theta_k) = \frac{y(\theta_k+c_k\Delta_k)-y(\theta_k-c_k\Delta_k)}{2c_k\Delta_k}$ d. Updating estimate. Use the standard steepest ascent form $\theta_{k+1} = \theta_k - a_k g(\theta_k)$
Step 3: Iteration or termination. Return to Step 2 with $k + 1$ replacing k.

3.3.2 Numerical Case of SPSA

In order to present the solution step of SPSA, we apply it into a test, 2-D Rosenbrock function. Rosenbrock function is defined as:

$$f(x, y) = (1 - x)^2 + 100(y - x^2)^2 \quad (3.3)$$

It has a global minimum at $(x^*, y^*) = [1, 1]$ where $f(x, y) = 0$.

With any initial point (x_0, y_0), SPSA generates its parameters for iterations, and get two random directions by a Bernoulli perturbation. The gradient is calculated with two objective functions by these two directions, and control vectors will be updated by the gradient to get new location (x_1, y_1). We can repeat this process until the termination criteria is satisfied. **Fig. 3.1** shows as example using SPSA and the search path of solving Rosenbrock function. After 500 iterations, we get the final solution $(x^*, y^*) \approx [1, 1]$ which is very close to the optimal value.

The feature of SPSA that approximates the gradient (or the search direction) by two-sided simultaneous perturbation of the control vector u is particularly attractive for multi-dimensional problems for which precise gradient calculation is prohibitively expensive. SPSA could save large computations and times during optimization approach, and it could get the nearly optimization solution.

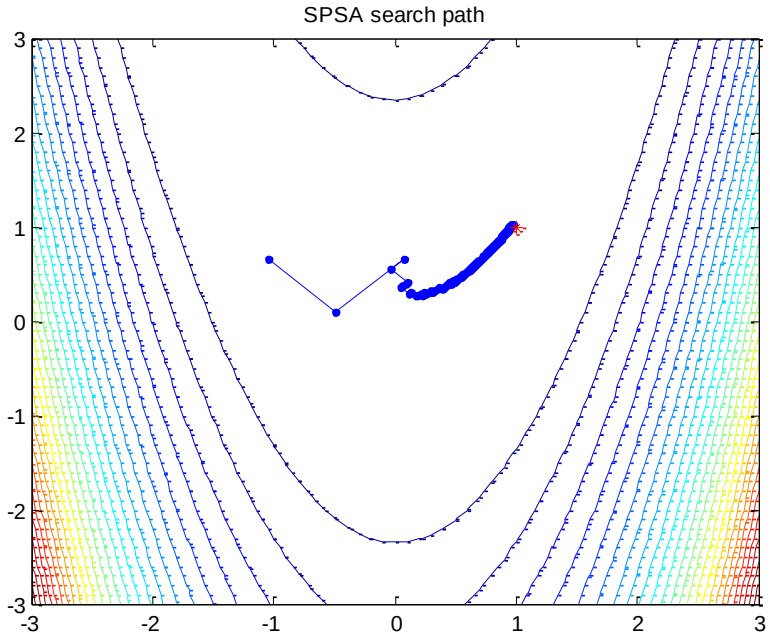

Fig. 3.1 Example of solving 2-D continuous Rosenbrock function by SPSA

3.4 Covariance Matrix Adaptation Evolution Strategy (CMA-ES)

CMA-ES (Hansen, 2006) stands for Covariance Matrix Adaptation Evolution Strategy. Evolution strategies (ES) are stochastic, derivative-free methods for numerical optimization of non-linear or non-convex continuous optimization problems.

3.4.1 Methodology of CMA-ES

In an evolution strategy (ES), we sample a group of new candidate solutions from a normal distribution which could be large dimension variables. In this methodology a covariance matrix records the dependencies between the variables and its distribution. Based on this information, the covariance matrix adaptation (CMA) algorithm updates the covariance matrix of this distribution. **Fig. 3.2** shows how CMA-ES works on a simple two-dimensional problem to find the optimum within a few generations. From generation 1 to 6, it shows the population (dots) is updated through a maximum-likelihood distribution (dotted line) and a certain direction controlled by evolution paths during the optimization.

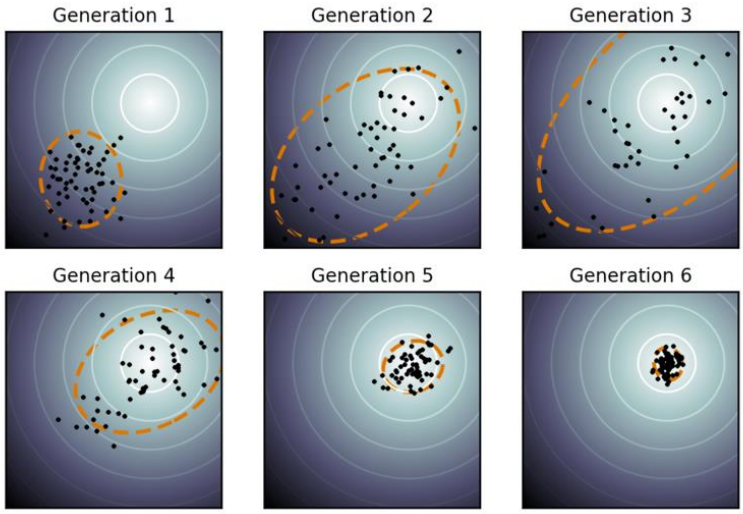

Fig. 3.1 Concept of directional optimization in CMA-ES algorithm (From Wikipedia ”CMA-ES”)

Two main principles for the adaptation of parameters of the search distribution are exploited in the CMA-ES algorithm. First, there is a maximum-likelihood principle based on the idea of increasing the probability of successful candidate solutions and search steps. The mean of the distribution is updated such that the likelihood of previously successful candidate solutions is maximized. The covariance matrix of the distribution is also updated (incrementally) such that the likelihood of previously successful search steps is increased. Both updates can be interpreted as a natural gradient descent.

Second, two paths of the time evolution of the distribution mean of the strategy are recorded, called search or evolution paths. These paths contain significant information about the correlation between consecutive steps. One path is used for the covariance matrix adaptation procedure in place of single successful search steps and facilitates a possibly much faster variance increase of favorable directions. The other path is used to conduct an additional step-size control. This step-size control aims to make consecutive movements of the distribution mean orthogonal in expectation. The CMA-ES algorithm is depicted in **Table 3.3** below:

Table 3.3 Algorithm description of CMA-ES

Algorithm of CMA-ES
Step1: variables' mean $m \in R^n$, step size $\sigma \in R^+$, covariance matrix $C = I$, $p_c = 0, p_\sigma = 0$;
Step2: Set time constant for cumulation$c_c \approx \frac{4}{n}, c_\sigma \approx \frac{4}{n}$, , and learning rate for rank-one, rank- μ update of C: $c_1 \approx \frac{2}{n^2}, c_\mu \approx \frac{\mu_w}{n^2}$, and $c_1 + c_\mu \leq 1$, $d_\sigma \approx 1 + \sqrt{\frac{\mu_w}{n}}$
Step3: Set offspring number$\lambda, w_i, i = 1, \dots, \mu$, μ is parents number for recombination; $\mu_w \approx 0.3\lambda$
Step 4: Do while (iter# < max iter#, or fitness < stopfitness) $x_i = m + \sigma y_i,\ y_i \sim N_i(0, C)$ ……..... Sampling $y_w = \sum_{i=1}^{\mu} w_i y_{i:\lambda},\ \sum_{i=1}^{\mu} w_i = 1$ ….. Calculate objective function and Selection $m \leftarrow m + \sigma y_w$ ……..…..… recombination, update mean $p_\sigma \leftarrow (1 - c_\sigma)p_\sigma + h_c\sqrt{1 - (1 - c_\sigma)^2}\sqrt{\mu_w}C^{-0.5}y_w$ $\sigma \leftarrow \sigma \times \exp\left(\frac{c_\sigma}{d_\sigma}\left(\frac{\|p_\sigma\|}{E\|N(0,I)\|} - 1\right)\right)$ ……. Step-size control $p_c \leftarrow (1 - c_c)p_c + h_c\sqrt{1 - (1 - c_c)^2}\sqrt{\mu_w}y_w$ $C \leftarrow \left(1 - c_1 - c_\mu\right)C + c_1(p_c {p_c}^T) + c_\mu \sum_{i=1}^{\mu} w_i y_{i:\lambda} {y_{i:\lambda}}^T$ …….Covariance matrix adaptation End while

3.4.2 Numerical Case of CMA-ES

We test the same function by CMA-ES, and choose the same initial point as SPSA. Around the point (x_0, y_0), a group of offspring points are generated and evaluated by Rosenbrock function. The function values are sort by fitness and few of points with higher function values are picked out to recombine and update into a new point (x_1, y_1); beside this, evolution paths, covariance matrix and step size should also be updated to make sure the

correct solving direction. After around 30 iterations, the optimization solution $(x^*, y^*) = [1, 1]$ is achieved. **Fig. 3.3** shows as example using CMA-ES and the search path of solving Rosenbrock function.

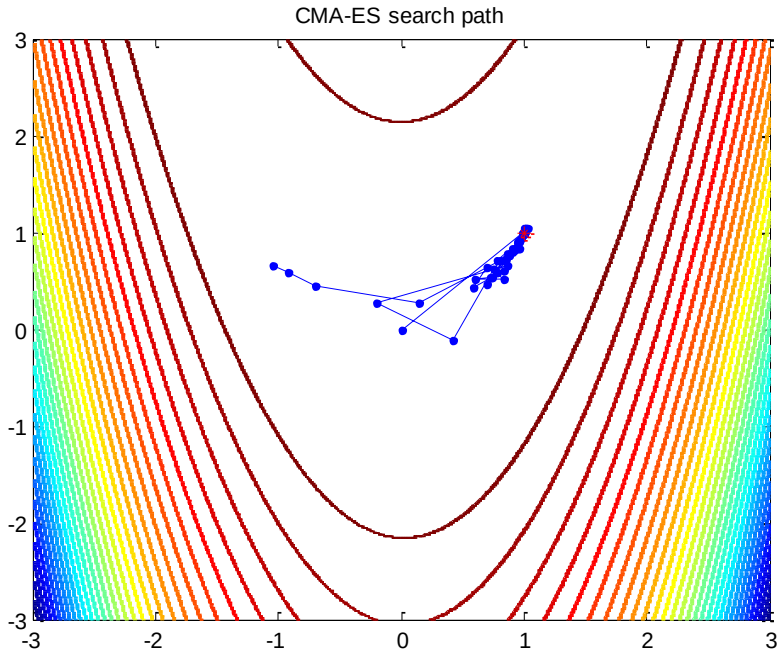

Fig. 3.3 Example of solving 2-D continuous Rosenbrock function by CMA-ES

In each iteration, the function is calculated λ times, by contrast the total computations and time of CMA-ES is larger and longer than SPSA, but the final solution of CMA-ES is closer to the optimal solution. We are aware of these differences not only in these two algorithms in this example, but also in the optimization of hydraulic fracture stages in the following chapters.

3.5 Finite Difference (FD) Method

The FD algorithm is one of the oldest and widely applied optimization techniques (Nocedal and Wright, 1999). This numerical method approximates the solutions to differential equations by using finite difference equations to approximate derivatives with a Taylor Series expansion.

Since this method is well known, we only state the formula form here. Assuming we have the number *n* of controls variables, and the objective function $J(u)$, mathematically the formula to calculate gradients is:

$$\mathrm{g} \approx \nabla \mathrm{J} = \left(\frac{\partial \mathrm{J}}{\partial \mathrm{u}_1}, \frac{\partial \mathrm{J}}{\partial \mathrm{u}_2}, \dots, \frac{\partial \mathrm{J}}{\partial \mathrm{u}_\mathrm{N}}\right)^{\mathrm{T}}, \tag{3.4}$$

$$\mathrm{g}_\mathrm{i} = \frac{\partial \mathrm{J}}{\partial \mathrm{u}_\mathrm{i}} \approx \frac{J(u + \Delta u_i) - J(u)}{\Delta u_i}, i = 1, \dots, n$$

Δu_i is the perturbed control variables in this finite different gradient estimation.

The difference between SPSA and FD is that FD perturbs one control variable at one iteration with calling the objective function one time to compute one element of gradient vector, whereas the SPSA can do to the simultaneously perturbations to all the control variables at one iteration with calling the objective function two times to estimate the whole gradient vector. More details of FD algorithm will be described in Chapter 5, with several tests of applying this method on the HF stages optimizations.

CHAPTER IV

OPTIMIZATIONS WITH FIXED NUMBER OF HYDRAULIC FRACTURE STAGES*

4.1 Introduction

Economic production rate of gas from shale formations depends on the design of well location and hydraulic fracture (HF) stages placement. The optimal locations of wellbore as well as the number and intervals of HF stages are critical for meeting commercial production goals.

The need for an optimized approach to get HF stages placement in organic gas-rich shale is dictated by the high cost of the HF operations (Holditch, 2007). Even though improvements in petrophysical characterization of shale formations and identification of possible HF stages location reduce the solution search space significantly, optimization algorithms are still the most rigorous strategies for obtaining specific values for desired control variables and objective function in a systematic fashion (Cipolla, 2009). The use of our framework, as described next, in addition to the expert knowledge of petrophysics has the potential of enhancing gas reserves and increasing revenues from shale gas development.

Below, we introduce our detailed workflow for horizontal well placement and spacing optimizations of traverse HF stages. To solve the discrete optimization problem, we employ two stochastic algorithms: SPSA and CMA-ES. First, both algorithms are used to place two horizontal wellbores with fixed numbers and locations of HF stages along them. Second,

* Part of this chapter is reproduced with permission of the copyright owner from "Integrated Horizontal Well Placement and Hydraulic Fracture Stages Design Optimization in Unconventional Gas Reservoirs" by Xiaodan Ma, Tatyana Plaksina, Eduardo Gildin, 2013. Paper SPE 167246 presented at SPE Unconventional Resources Conference, Calgary, Alberta, Canada, 5-7 November. Copyright 2013 Unconventional Resources Conference, SPE Further reproduction is prohibited without permission.

with the same methods we optimize locations of all HF stages. Finally, we combine these two optimization problems in a hierarchical workflow with two levels. The upper level calculates the horizontal well trajectory and the lower level places HF stages. Each algorithm will be tested using both homogeneous and heterogeneous permeability cases. Results of the test runs reveal advantages and shortcomings of each combination of algorithms.

Before introducing the optimization framework, it is worth mentioning that the objective function $J(u)$ presented in Equation 3-1 describes several terms used to calculate NPVs, and we want to get the maximize value of NPV after optimizations. Combining the algorithms, SPSA and CMA-ES, described in Chapter 3, we introduce the flowchart in **Fig. 4.1** to present how these two algorithms work during the HF stages optimizations.

The workflow of **Fig. 4.1** starts with setting initial conditions and defining the control vector u. For different algorithms described in the previous chapters, we choose different perturbation strategies to compute the gradient. SPSA chooses the Bernoulli distribution and get two new control vectors u^+, u^-, yielding the reservoir response $\mathrm{NPV}^+, \mathrm{NPV}^-$ for gradients calculation. CMA-ES gets a group of samples around the control vector $\mathrm{X}_{\mathrm{mean}}$ which also yields a group of NPVs, sorts them all and selects certain number of control vectors with larger NPVs to update the control vector $\mathrm{X}_{\mathrm{mean}}$. Update the control vector and repeat the iterations by each algorithm until it satisfies the termination criteria. We will show the optimization tests by each algorithm in the following sections.

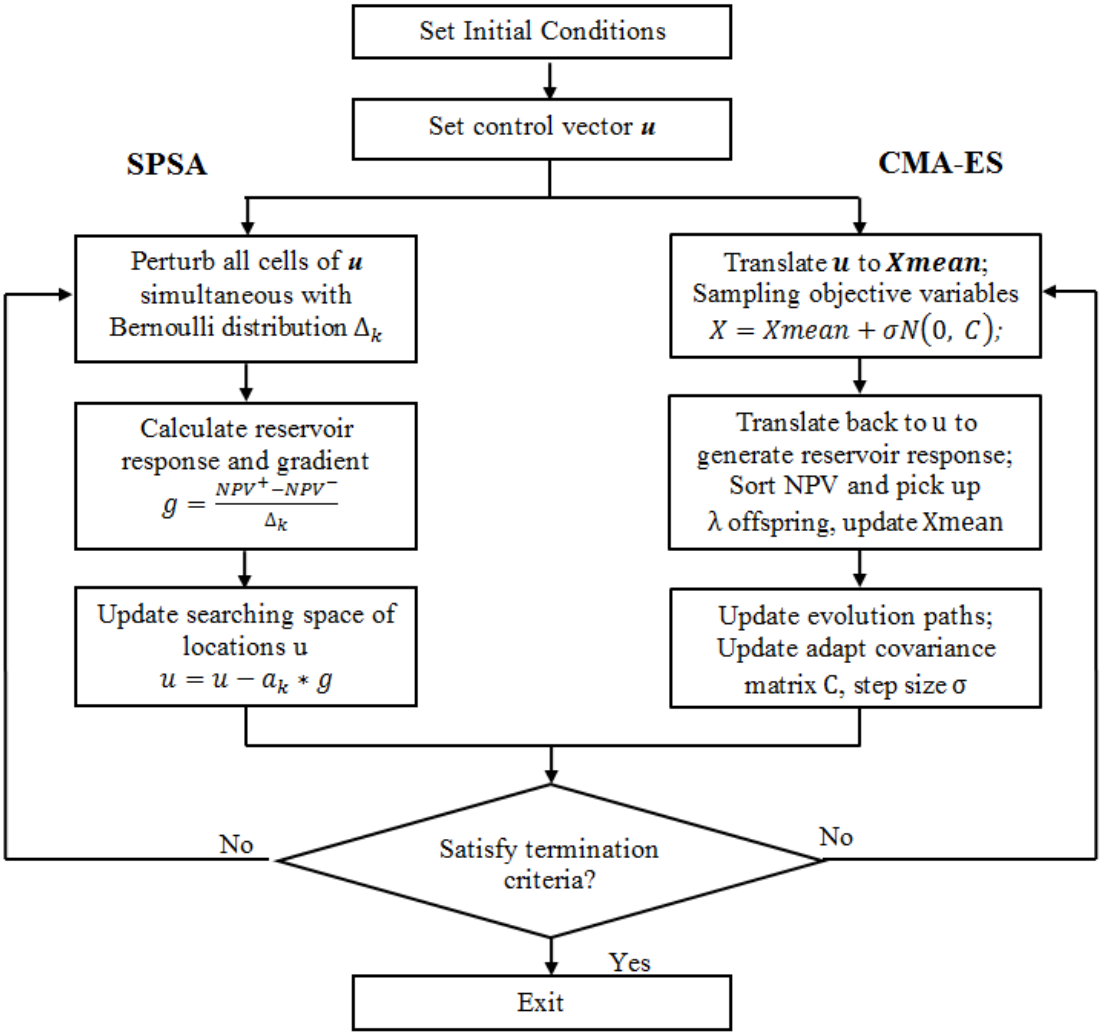

Fig. 4.1 SPSA and CMA-ES flowchart for optimization of fixed HF stage number

4.2 Well Placement Optimization

Horizontal wellbore placement is a complex problem that takes into consideration multiple geological, petrophysical, and operational constraints. In addition to these constraints, our optimization design must accommodate features of a particular simulator, for instance, Cartesian grids. Some global optimization algorithms that honor all the constraints have been already successfully applied to conventional well placement (Yeten, 2003).

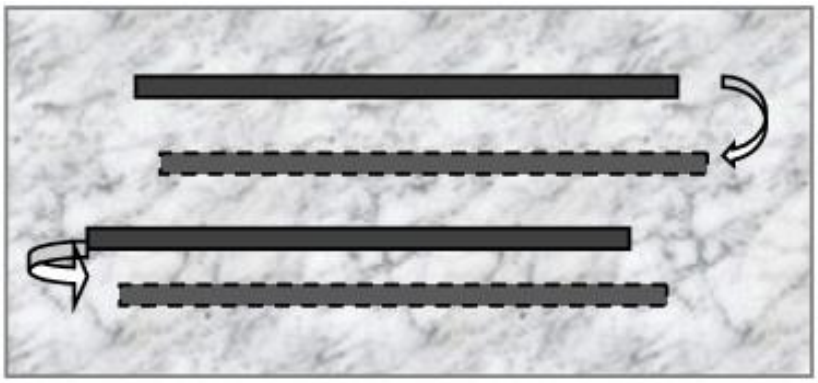

Fig. 4.2 Conceptual model of wellbore placement optimization

The wellbore placement optimization approach can be summarized in the **Fig. 4.2**. We assume that two horizontal wells are placed in the reservoir in the direction from west to east. Each wellbore has fixed HF stages, only the locations of wellbores need to be optimized, which composes the elements of control vector u. The optimization algorithms are applied in this model, which start from initial given wellbore locations. Once the optimization algorithms determine the maximum of the objective function, say, NPV, the wellbore placement is complete.

To apply SPSA and CMA-ES to wellbore placement problem, we define the control vector *u* in terms of X-, Y-, and Z-coordinates of well toe and heel. By fixing the wellbore length at 2000 ft and keeping two horizontal wells parallel, the control vector can be simplified as to find the optimal distance between the two wellbores with only two variables to record locations of wellbores in Y-direction. Mathematically, this problem is formulated with the following constraints:

$$\begin{cases} \max \mathrm{J(u)} \\ \mathrm{s.t.}\, \mathrm{Y_{max}} \geq \mathrm{Y(u)} \\ \mathrm{Y_{min}} \leq \mathrm{Distance(Y(u))} \end{cases} \tag{4.1}$$

These constraints are necessary in order to guarantee the existence of the optimum solution within the feasible domain. The first constraint requires each well to stay inside the reservoir grid and keep some distance to its boundaries. The second one dictates the minimal distance between the wells.

4.2.1 Case I: Homogenous Reservoir

In wellbore placement optimization we assume that two horizontal wells are placed in the reservoir in the direction from west to east, and each wellbore has ten HF stages with zigzag fixed locations. The initial configuration is illustrated in the left figure of **Fig. 4.3** with the left figure. The reservoir has $100 \times 111 \times 1$ gridblocks, and specific reservoir properties are listed out in the appendix.

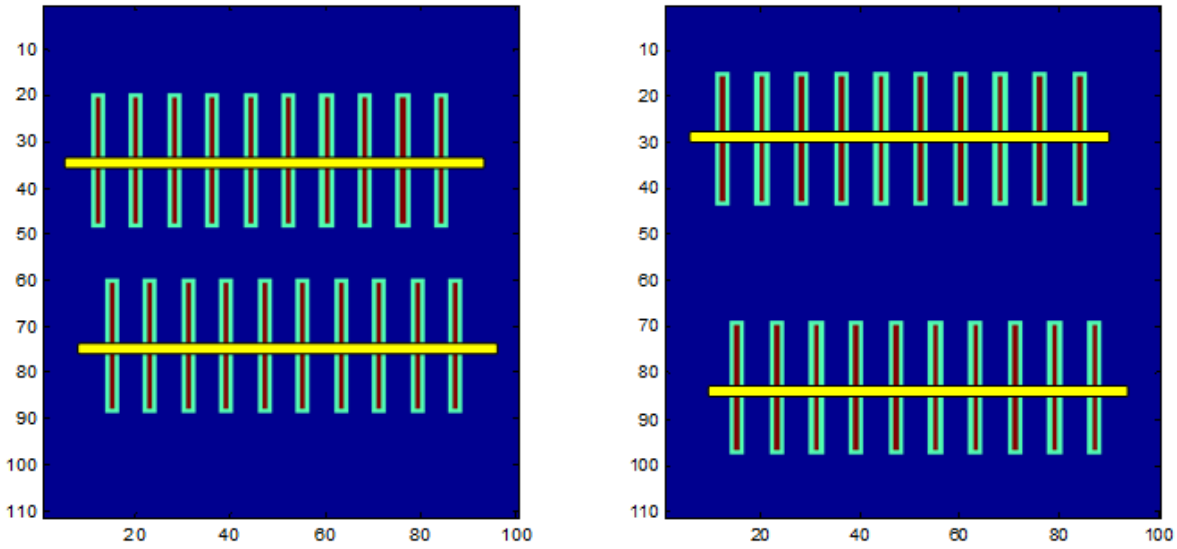

Fig. 4.3 Homogeneous case, one of initial wellbore placement (up) and the optimized result of wellbore locations (down)

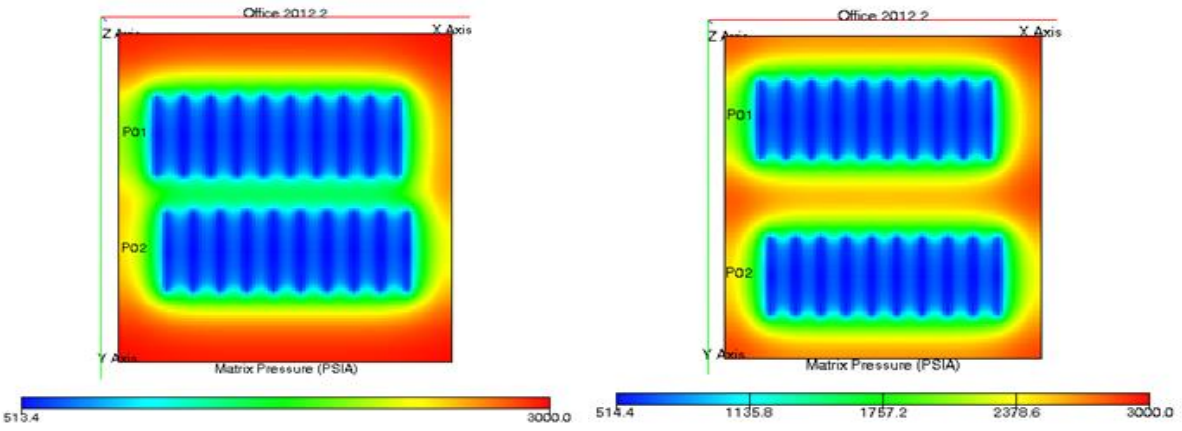

Fig. 4.4 Pressure distribution after 20 years production in the initial case (up) and the optimized results (down), homogeneous case

For the homogeneous case, each algorithm (SPSA and CMA-ES) performs as in **Fig. 4.5**. We can see the difference between the number of iteration calls, and the maximum NPV calculated. We tested these two algorithms with five different initial wellbore locations. The results demonstrate that we obtain the optimal wellbore locations and maximum NPV within several iterations. Fast convergence can be explained with the size of the problem: the control vector in this case has only two dimensions. Comparison between optimization results by SPSA and CMA-ES yields the following observations: both algorithms converge fast to the same NPV value and obtain the same wellbore trajectories corresponding to this maximum NPV (**Fig. 4.3** and **Fig. 4.5**).

Fig. 4.4 shows the pressure distributions for the homogeneous cases after 20 years production. Based on the character of gas adoptions in shale gas reservoir, it will release more gas when pressure drop down. It gives the reason that NPV is improved by the optimization approaches. Given a reservoir model, the distance between two wellbores cannot be too close to each other; otherwise the influence of pressure drop is limited in a certain range and the gas production rate cannot be stimulated to reach the maximum value.

Fig. 4.5 shows the optimization NPV curves by SPSA and CMA-ES. Even though each algorithm has five different cases which have different initial locations of wellbores, we get the same value of optimal NPV and the same solutions for these cases. Since SPSA just call the objective function only twice times per iteration as compared with CMA-ES calling the number of offspring times, the total computational time of SPSA is shorter than CMA-ES, which is just around half times to call ECLPSE.

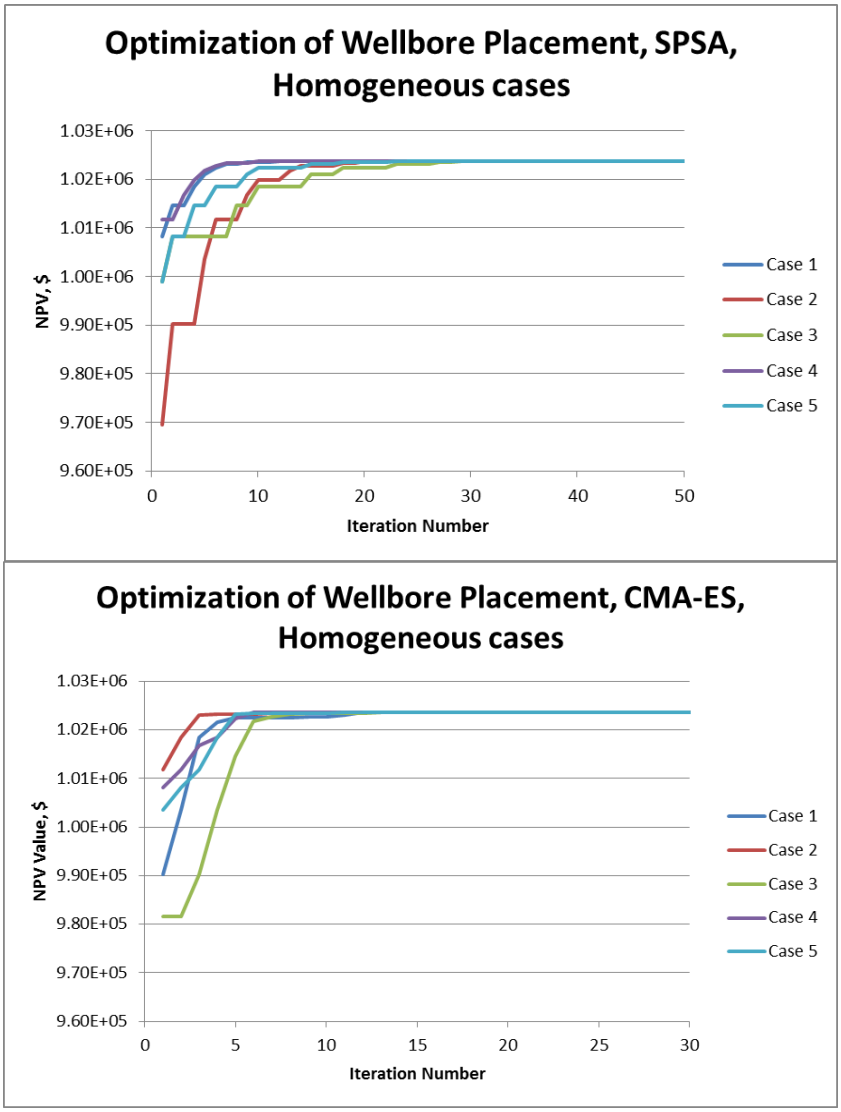

Fig. 4.5 Wellbore placement optimization approach by the algorithms SPSA (up) and CMA-ES (down), homogeneous case

4.2.2 Case II: Heterogeneous Reservoir

In this section, we test the two proposed algorithms with the heterogeneous permeability map shown in **Fig. 4.8**. The initial locations of two wellbore are selected randomly, with fixed number and locations of the HF stages. In this case, we use 10 HF stages and the same reservoir size as in the homogeneous reservoirs.

Fig. 4.6 shows the pressure distribution differences between initial and optimized locations. In the heterogeneous cases, we observe a 10% increase in NVP for both SPSA and CMA-ES (**Fig. 4.6**). Both algorithms finish computation within several iterations, and CMA-ES yields slightly higher optimum value and obtains it with less uncertainty.

Fig. 4.7 shows the results of optimization processes with several different initial wellbore locations on the same heterogeneous permeability map. We find that the curve of NPVs by these two algorithms could not converge at the same optimization results. **Fig. 4.8** gives examples of optimization of wellbore placement distributions for four different initial cases, while **Table 4.1** gives more exactly how much NPV get improved and which grids are the optimization locations of each case.

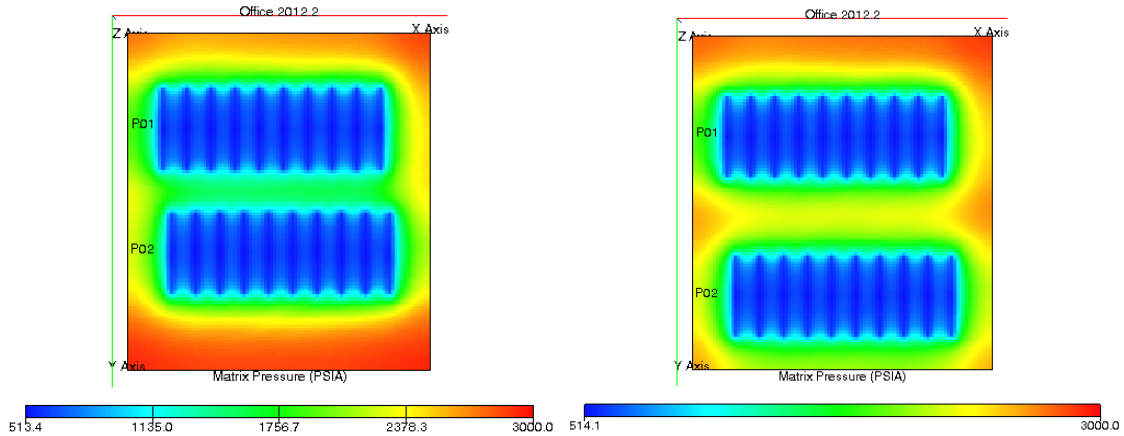

Fig. 4.6 Pressure distribution after 20 years production in the initial case (up) and the optimized results (down), heterogeneous case

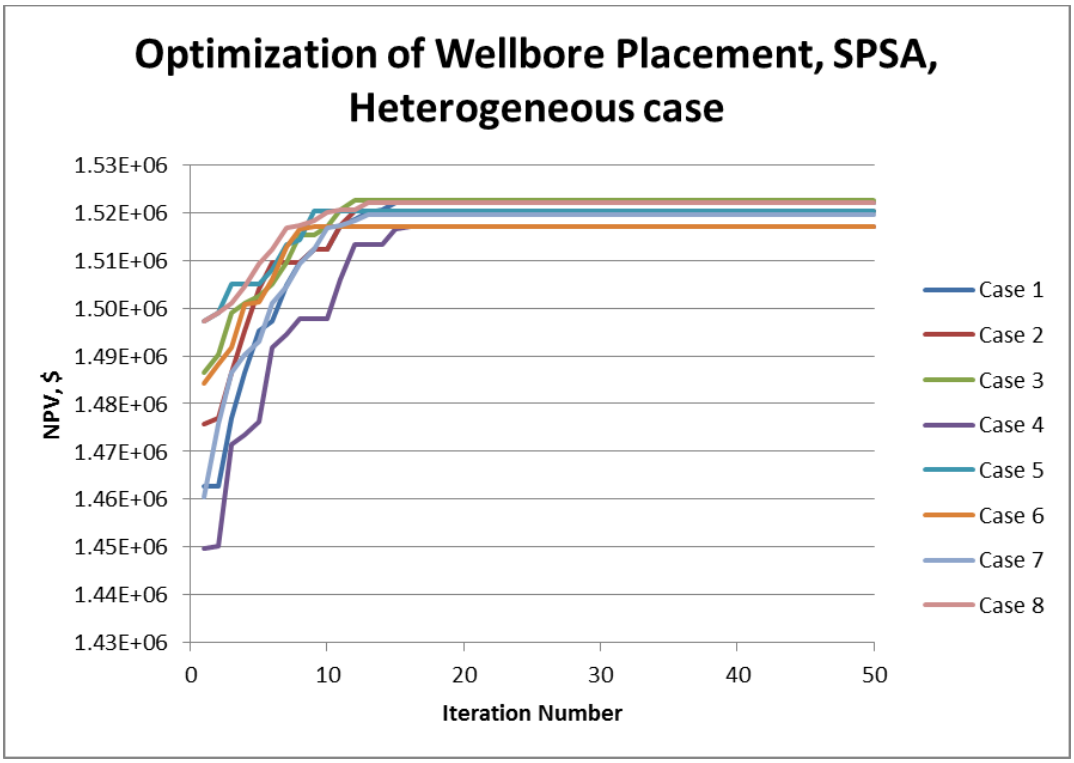

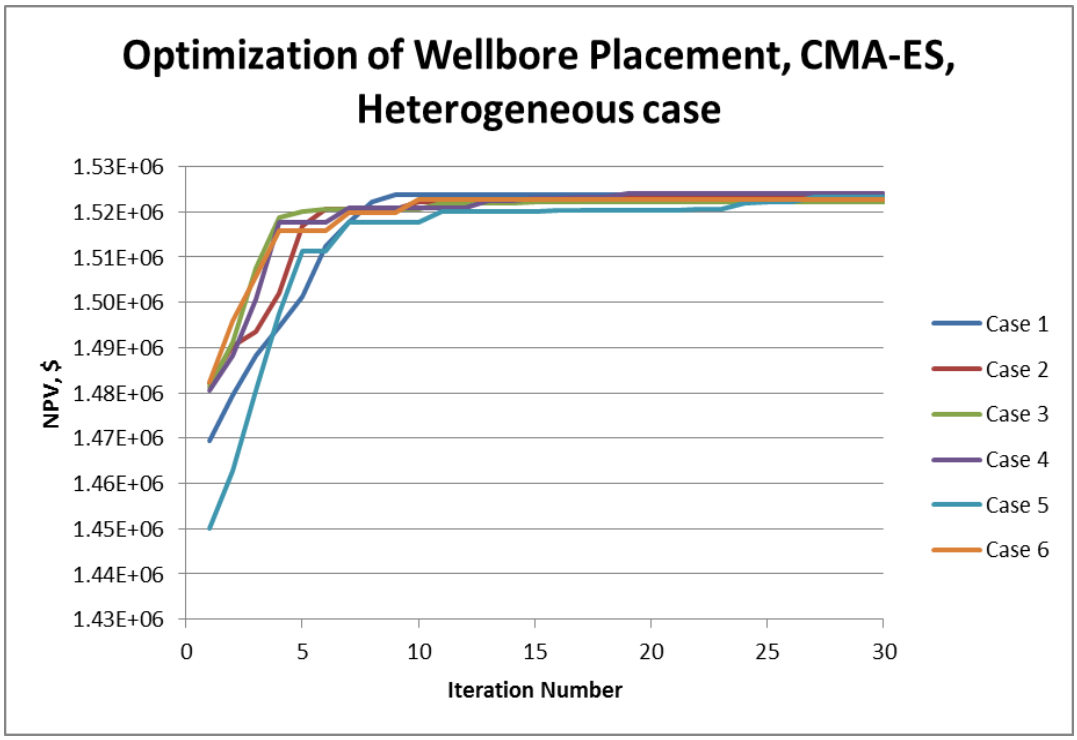

Fig. 4.7 Wellbore placement optimization approach by the algorithms SPSA (up) and CMA-ES (down), heterogeneous case

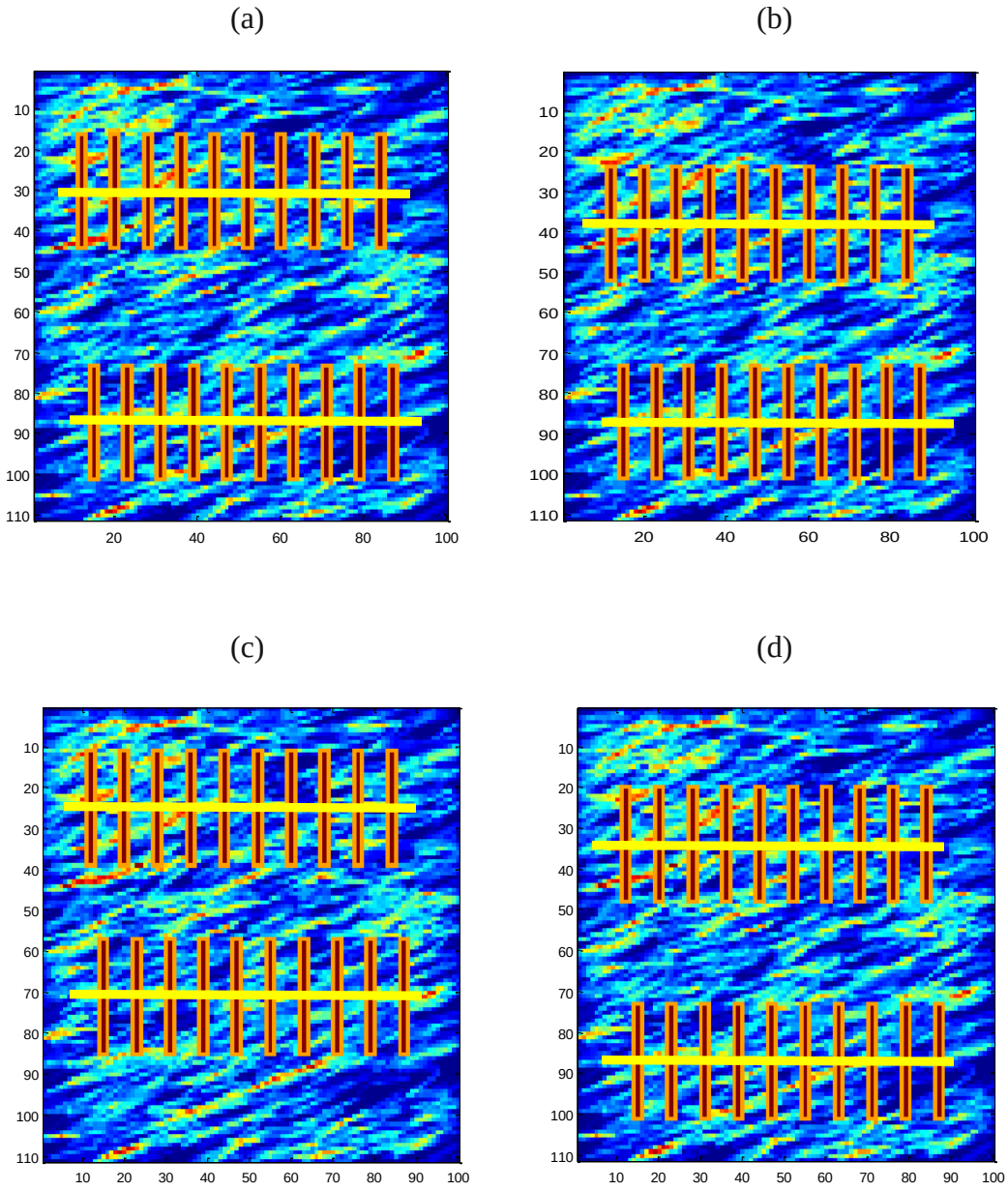

Fig. 4.8 The optimization distributions of wellbore placement for four different initial using the known geologic model in heterogeneous case

Table 4.1 NPVs of four wellbore placement cases in heterogeneous case in Figure 4-8

Cases	(a)	(b)	(c)	(d)
Improved NPV($, 10^5)	1.520	1.519	1.522	1.523
% of Improved NPV	4.11%	4.08%	5.23%	4.51%
Optimization Result	(31, 89)	(38, 90)	(26, 72)	(36, 89)

Although we get the values of optimal NPVs from each case close to each other, they seem to be caught up in local minimum solutions. SPSA shows that it costs less computational time and runs during the optimization approaches, but gets a little bit lower of the optimized values than CAM-ES. The reason why SPSA and CMA-ES do not converge to the global optimization results every time is that all the elements in the control vector are positive integers, and during updating the control vectors, we may lose some accuracy in order to keep integer numbers.

4.3 HF Stages Placement Optimization

In this section, we test the optimization problem with larger control vectors. Similar to wellbore placement, HF stages placement along the horizontal wellbore in a Cartesian grid is also an integer programming problem, but with a larger number of dimensions. Thus, we can apply SPSA and CMA-ES algorithms to this task and observe their advantages and shortcomings. All the HF stages are given as a fixed number, and we need to find their optimal locations as the optimization task.

In HF stages placement optimization we try to establish the optimal locations of the stages along the wellbores. The control vector u in this optimization approach represents interval numbers of grid-blocks between each nearby HF stages (**Fig. 4.9**). This goal is achieved by putting the following constraints on the variables of the control vector u:

$$\begin{cases} max\, J(u) \\ s.t.\, l_{toe} \le u_1 \\ u_n \le l_{heel} \\ l_{min} \le u_i, i = 1,2,\dots,n \end{cases} \tag{4.2}$$

Eq. 4.2 defines the feasible domain of the problem by, first, confining all HF stages to the grid-blocks along the well trajectory (from horizontal well toe l_{toe} to well heel l_{heel}) and, second, keeping the minimal interval distance l_{min}between the stages.

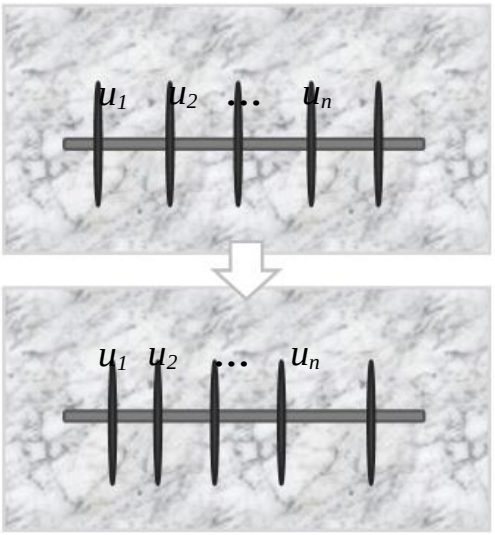

Fig. 4.9 Conceptual model of HF stages placement optimization

4.3.1 Algorithms Applied to a Single Well Case

Considering that we usually have 5 to 10 HF stages for each horizontal well, the control variable of *u* or the dimension of the optimization problem becomes very large when we start adding multiple wells configuration. Therefore, care must be taken when performing the optimization workflows.

We first test a case with a single horizontal well placed in the reservoir's middle zone in the direction from west to east. The number of HF stages is given with number 10. **Fig. 4.10** shows the initial locations of each stage with the minimum interval distance between HF stages on the left figure, and the right one shows the optimized result of HF stages distribution.

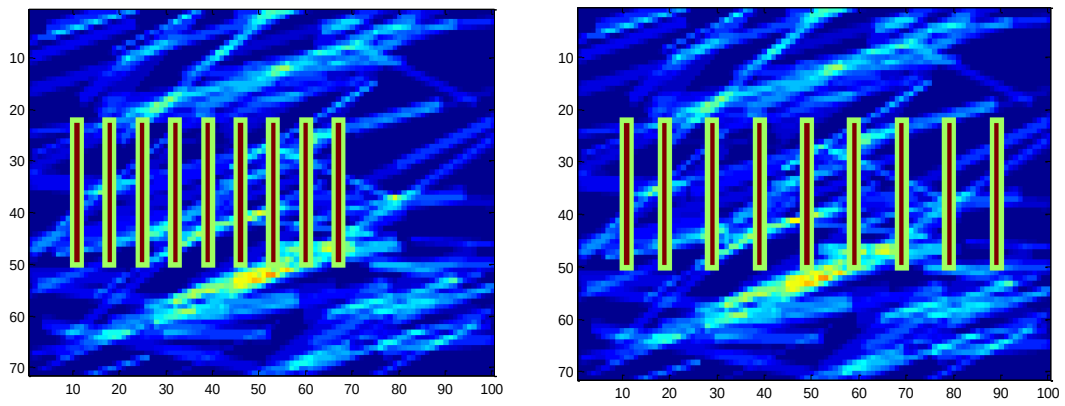

Fig. 4.10 Initial placement of HF stages (left) and one optimized result (right) on a single well

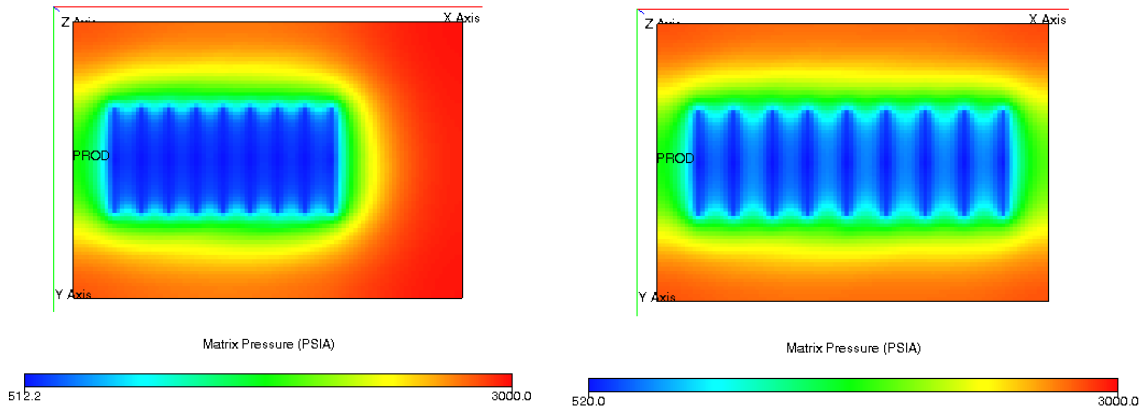

Fig. 4.11 Pressure distribution of initial HF stages placement (left) and one of the optimized result (right) on a single well

Fig. 4.11 shows the difference of pressure distribution between the initial model and the optimized model. After optimization, the zone influenced by pressure drop increases largely leading to increase gas production rate, and in turn, higher NPVs.

Similar to wellbore placement, we run five test cases with the same initial conditions (**Fig. 4.12**) and compare the results as follows. **Fig. 4.12** illustrates that, although the optimization problem is multi-dimensional, each algorithm converges within a small number of iterations.

All the tests starts from the same initial locations of each stage, but not all of the cases could converge to the same optimal NPV and get the same optimization results.

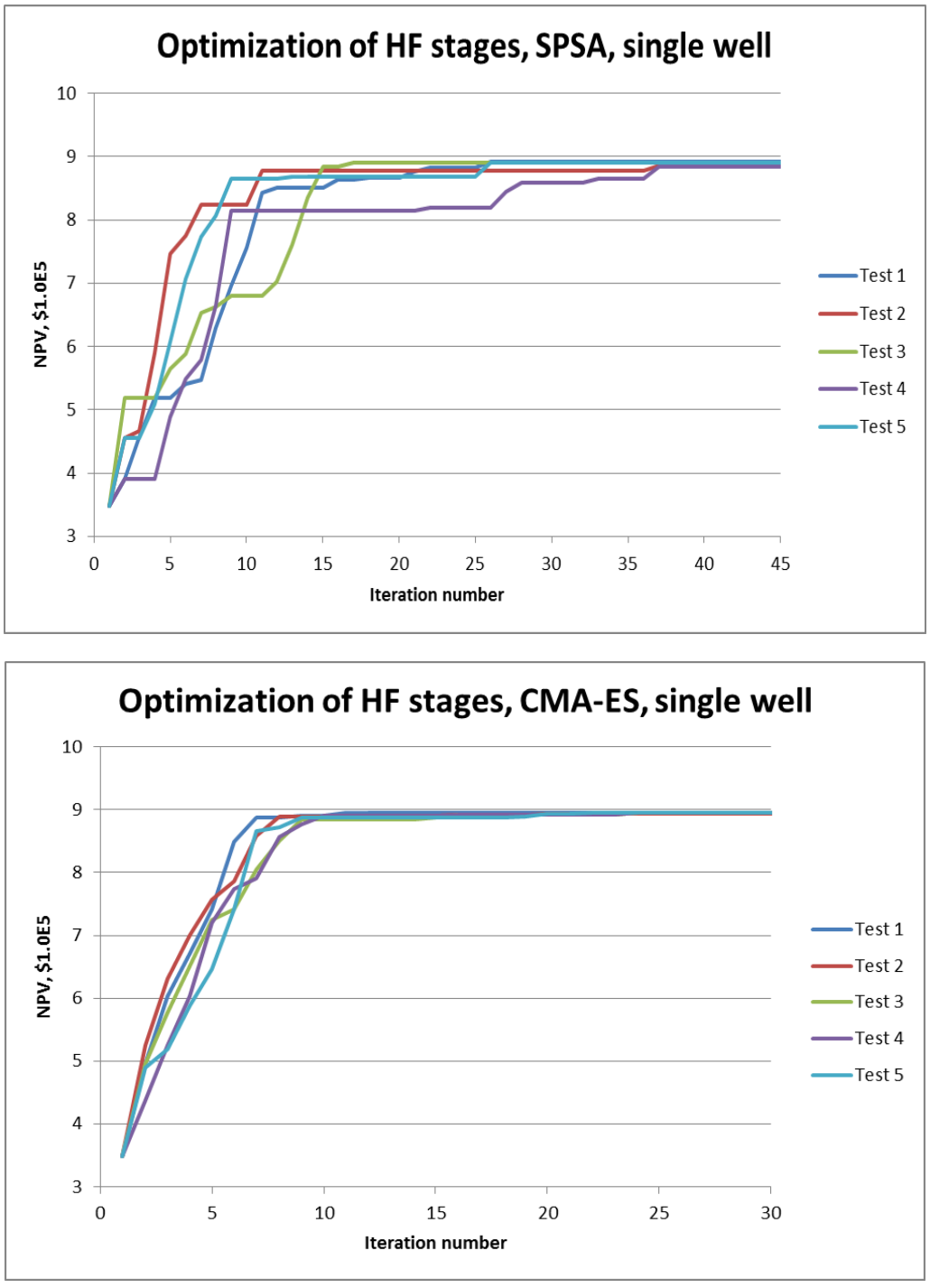

Fig. 4.12 Optimization approaches by the algorithms SPSA (up) and CMA-ES (down) in the case of single well

4.3.2 Algorithms Applied to Two Wells Case

In this section, we consider the previous test cases applied to two horizontal wells placed in the reservoir in the direction from west to east. Each well has ten HF stages with unknown (or random) locations, and locations of the two wellbore are fixed. The control vector for this optimization problem has twice the dimensions as compared to the single well case. In order to analyze the algorithms, we change the locations of HF stages along the two wellbores simultaneously.

In the homogeneous case, we assume that two wells have ten HF stages with evenly spacing distribution as the initial conditions. **Fig. 4.13** gives the initial HF stages distribution and the optimization locations of each HF stages on these two wells. It is clearly showing the zigzag distribution of HF stages between two wells.

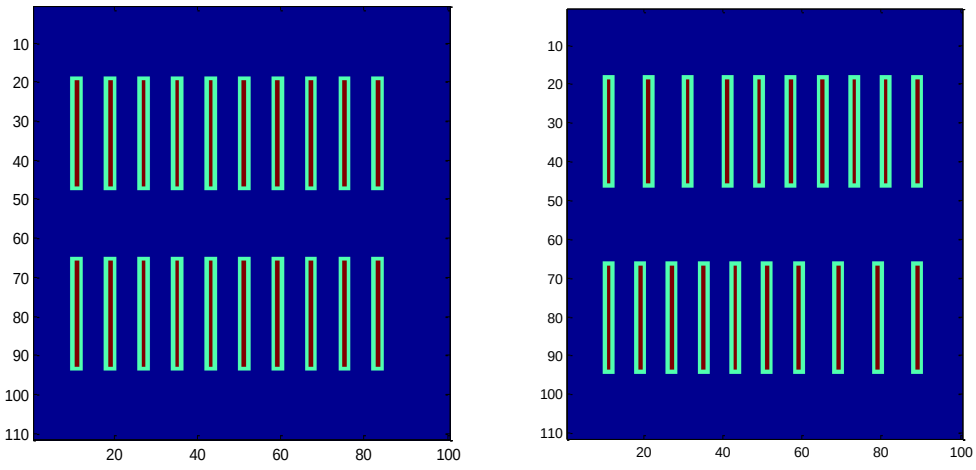

Fig. 4.13 Homogeneous case, initial HF stages placement on two wells (left) and one optimized result (right)

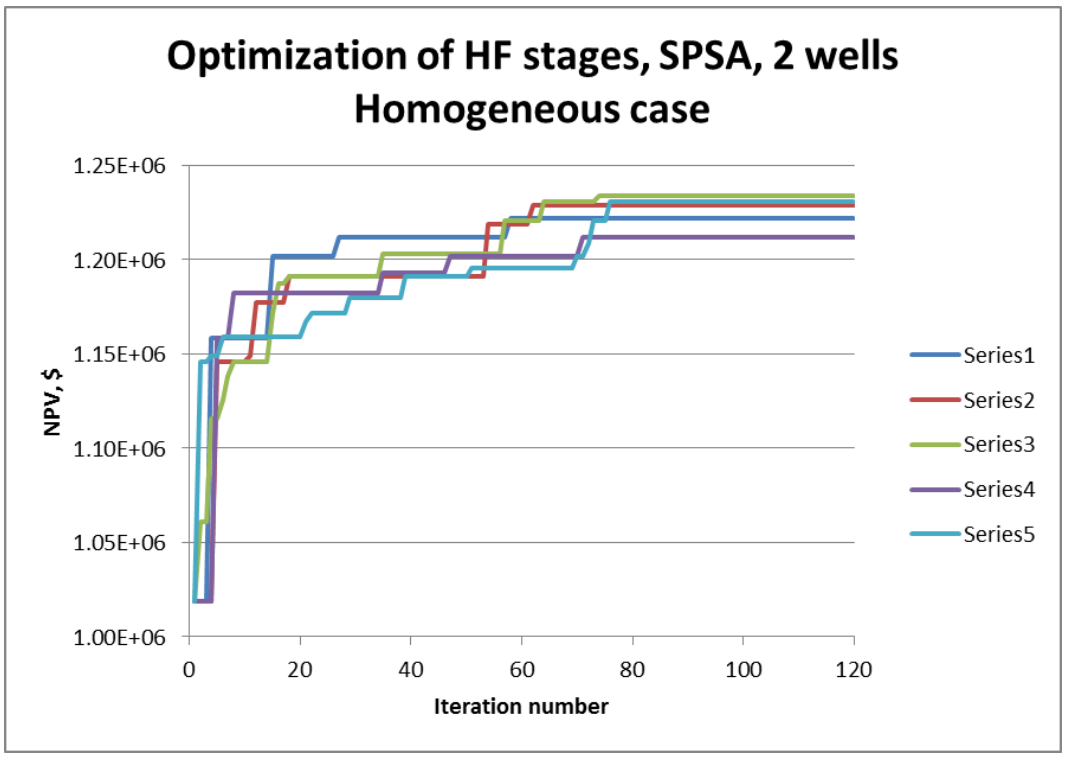

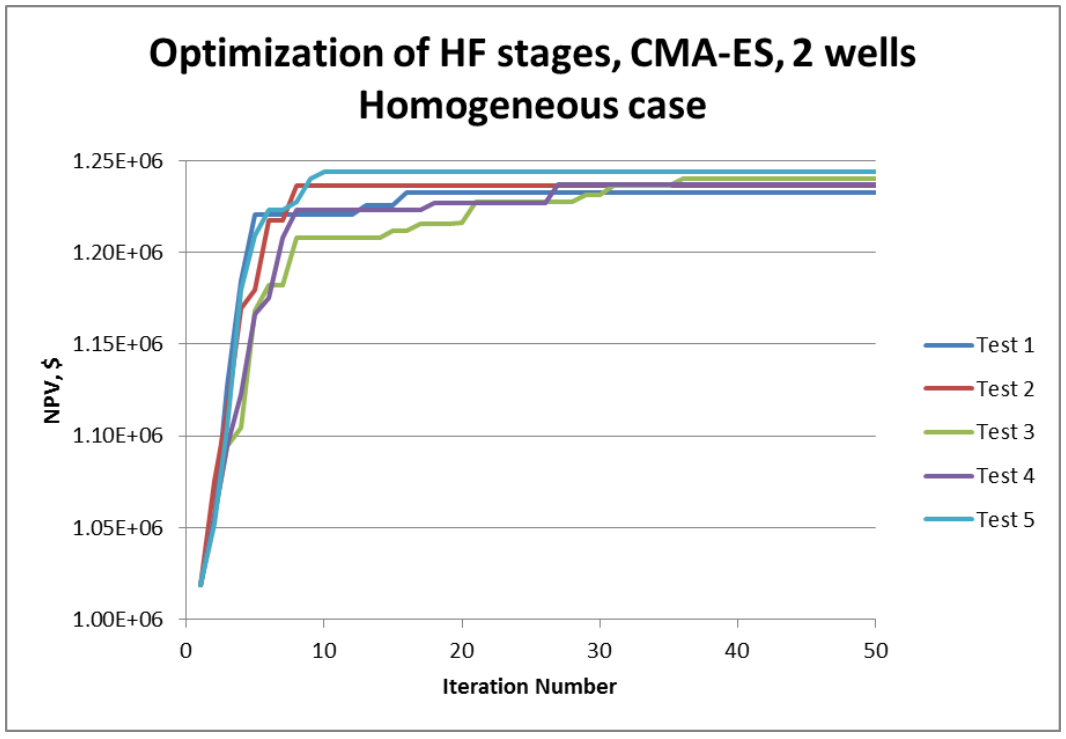

Fig. 4.14 Homogeneous case, optimization approaches of HF stages by the algorithms SPSA (up) and CMA-ES (down)

The results for the application of both algorithms to the two well cases can be seen in **Fig. 4.14**. It shows that both algorithms have the capability of solving problems with large number of dimensions. CMA-ES obtains better solutions with higher total computational time because it needs to calculate a group of offspring samples with more computations. However, it provides the results with less uncertainty and outputs higher NPV values compared to SPSA.

For the case of heterogeneous reservoir, we make the comparisons of pressure distribution between initial conditions and the optimized results. **Fig. 4.15** explicit shows that more grid-blocks are improved to produce gas by these two algorithms. Also, a non-symmetrical distribution of pressure drop can be observed, considering that this is a heterogeneous reservoir.

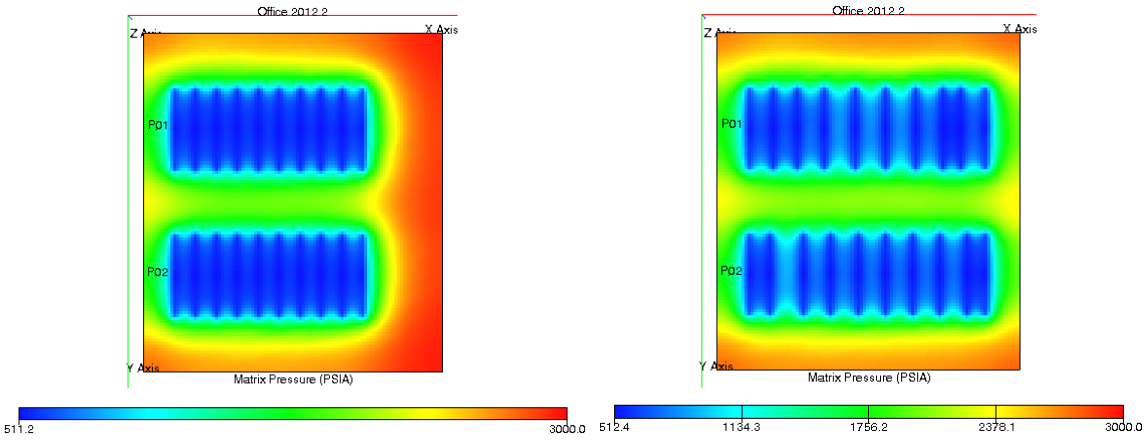

Fig. 4.15 Pressure distribution of initial HF stages placement (left) and one of the optimized result (right) on two wells

The convergence of these two algorithms for the case of heterogeneous can be observed in **Fig. 4.16**. During the optimization process of heterogeneous cases, the iteration numbers by the SPSA algorithm increases two times more than the homogeneous cases in

order to obtain the improved NPV curve. By comparison to SPSA, the total iteration number for CMA-ES algorithm increases slightly more than its performance in the homogeneous cases. Also, the final improved NPV by SPSA have much larger value range than CMA-ES does.

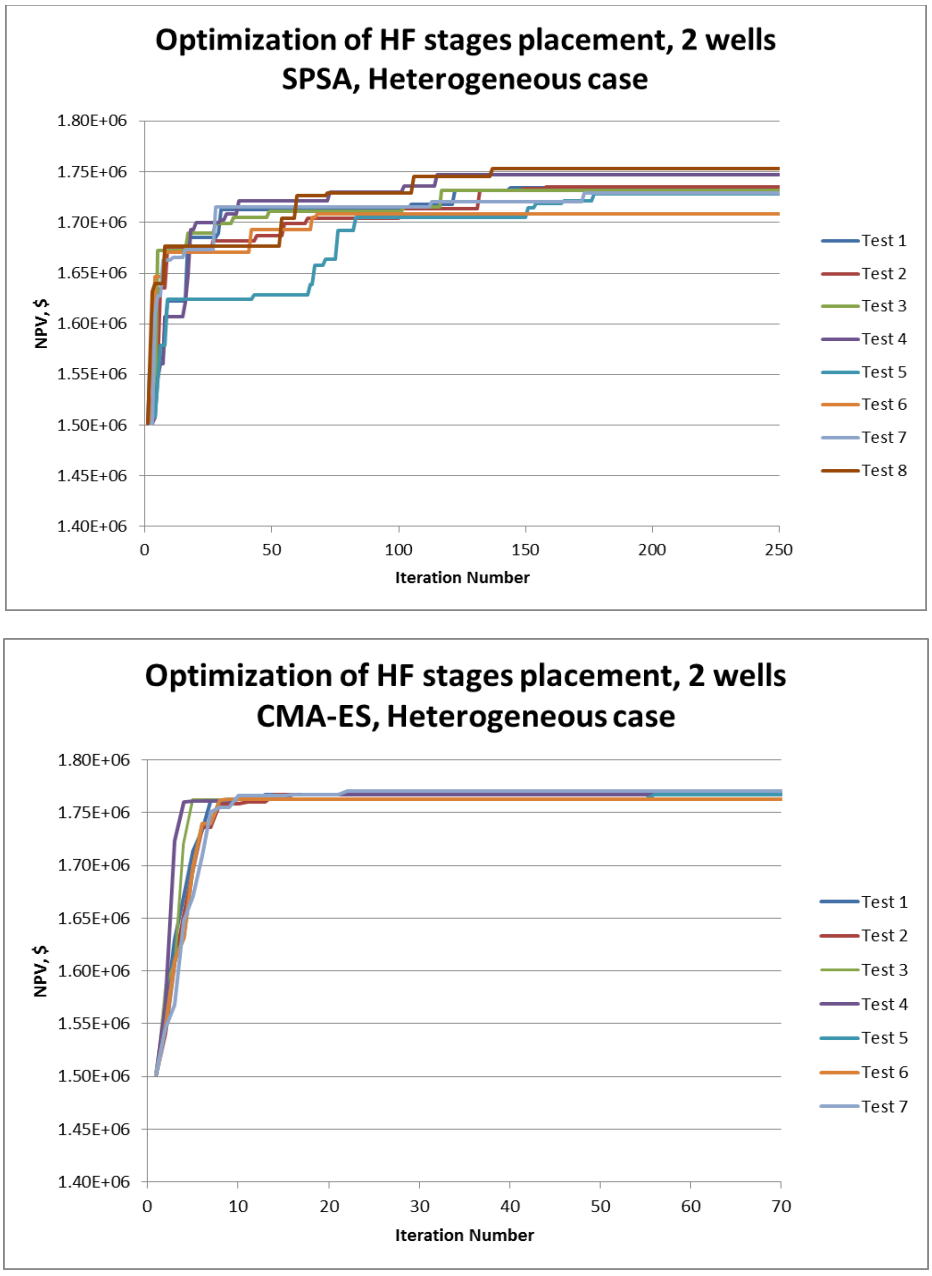

Fig. 4.16 Heterogeneous case, optimization approaches by the algorithms SPSA (up) and CMA-ES (down)

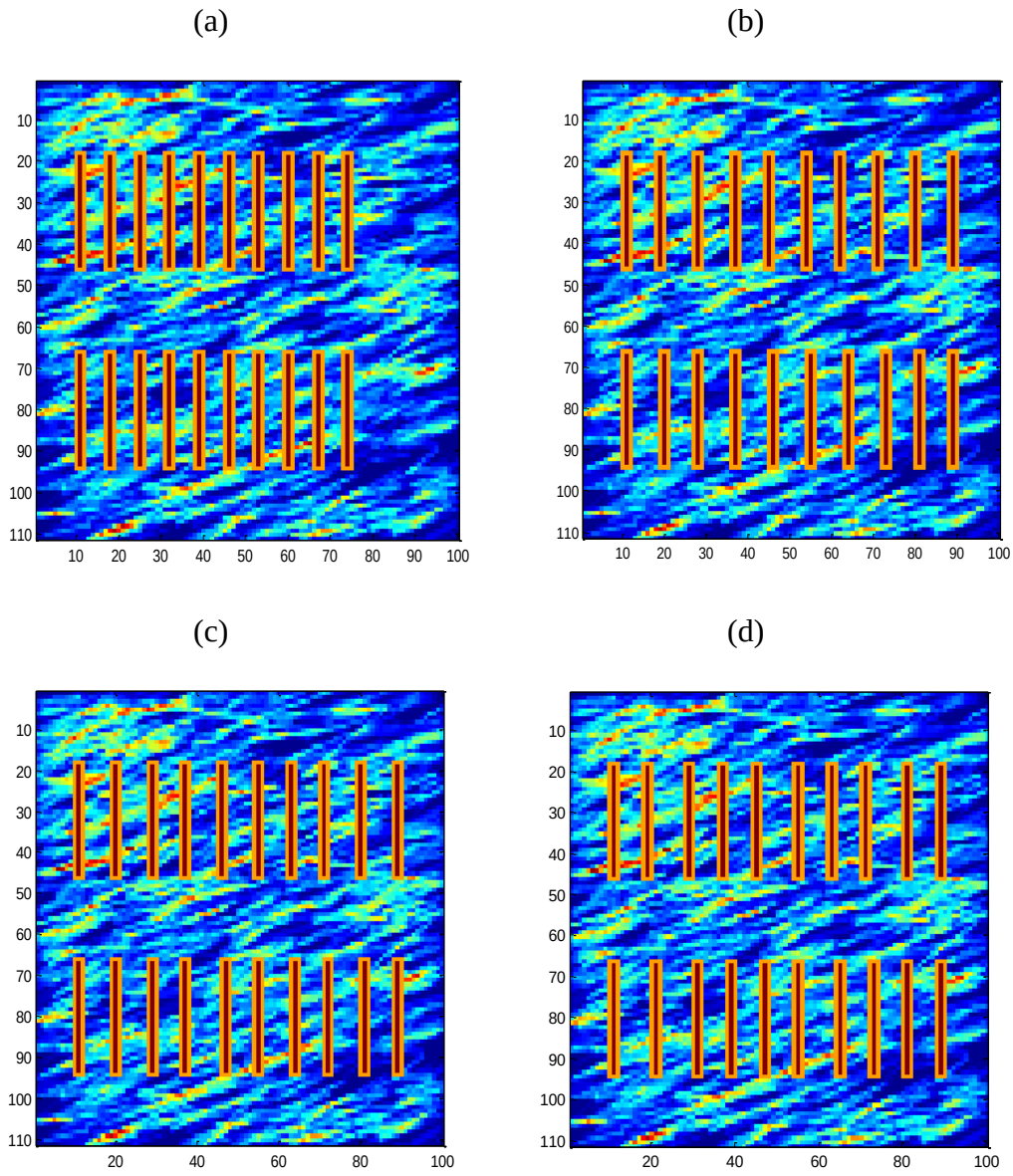

Fig. 4.17 Initial case (up-left) and three optimization distributions of HF stages placement using the known geologic model in heterogeneous case

Table 4.2 Initial HF stages placement and three optimized results in heterogeneous case shown in Figure 4-17

Cases	(a)	(b)	(c)	(d)
Improved NPV($, 10^5)	1.5015	1.7672	1.7675	1.7474
% of NPV Improved	--	17.70%	17.72%	16.38%

Although the heterogeneous case tests start with the same initial conditions, i.e., have the same HF stages locations for two wells, the optimized locations do not fall in the same grid numbers (**Fig. 4.17**). **Table 4.2** shows the difference of optimized NPV improvement for both cases in **Fig. 4.17**.

4.4 Joint Wellbore and HF Stages Placement – Hierarchical Optimization

Finally, in this section we juxtapose the two previous optimization workflows within a hierarchical framework. Our hierarchical optimization approach can be summarized as in the **Fig. 4.18**. Considering multiple well configuration, the two-level structure first selects the wellbore placement as described in the previous section and then places HF stages in the way that maximizes the objective function of NPV for this particular well location. Once the maximum value of NPV is approximated, the next wellbore placement is evaluated.

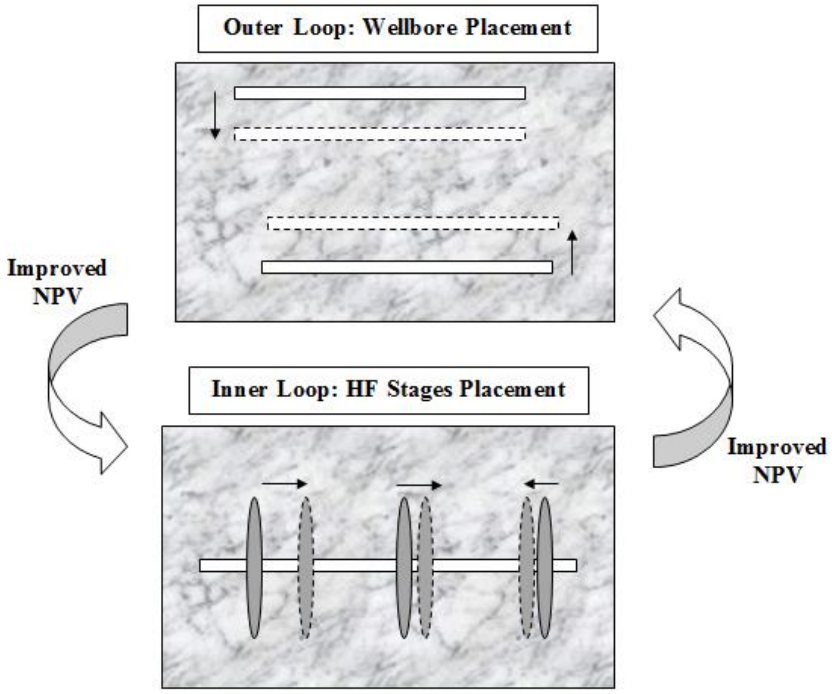

Fig. 4.18 Conceptual model of the hierarchical optimization framework

This hierarchical approach searches for the best wellbore location on the upper level of the framework. Once the current location of the well is calculated, it is keep fixed and passed to the lower level. On this level, one of the chosen algorithms computes optimal locations and spacing of HF stages by varying the control vector and evaluating the objective function.

Within the same iteration loop, SPSA and CMA-ES first compute trajectories of the horizontal wells and then pass them to HF stages optimization. Once the optimum value of NPV is determined, the corresponding control vector with the wellbore trajectories and HF stages locations is recorded and perturbed in the next iteration. The control vector of this hierarchical workflow is a composition of the control vectors from the above-mentioned optimization problems with the identical constraints of Eq. 4.1 and Eq. 4.2. In what follows, we discuss the results of all three optimization workflows, compare them with respect to SPSA and CMA-ES, and quantify parameter uncertainty.

4.4.1 Hierarchical Optimization in Homogeneous Case

In our investigation of the hierarchical optimization workflow that combines wellbore and HF stages placement, we run test cases similar to those discussed in the previous sections. However, optimization of the wellbore trajectories requires an extended control vector. The control vector contains two sets to control variable, namely, the wellbore locations and HF stages, which represents the operations in X-direction and Y-direction with multi-dimensions respectively.

Similarly as the previous sections, each well has ten HF stages with unknown (or random) locations and is placed at some distance from one another. Here, we optimize

locations of the wellbores and all HF stages along them simultaneously. **Fig. 4.19** gives the initial conditions of the wellbore placement and HF stages location, and one case of optimized results for these variables. **Fig. 4.20** shows different ranges of pressure distribution by initial conditions before hierarchical optimization and one case of optimized results. The distance between two wells is increased and HF stages are not evenly spaced after the optimization process but show more diagonal symmetric, which enlarges the largest production zone in this reservoir map and then improves NPV.

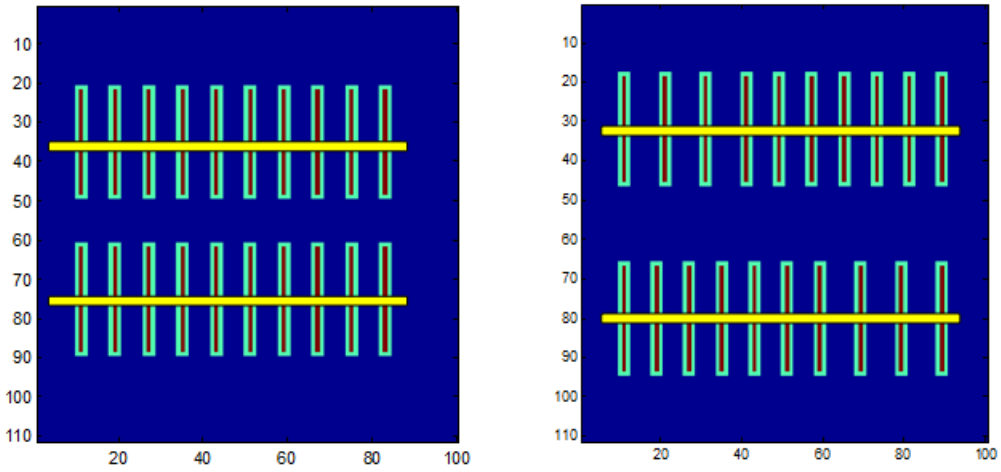

Fig. 4.19 Homogeneous case, initial condition of hierarchical optimization (left) and one optimized result (right)

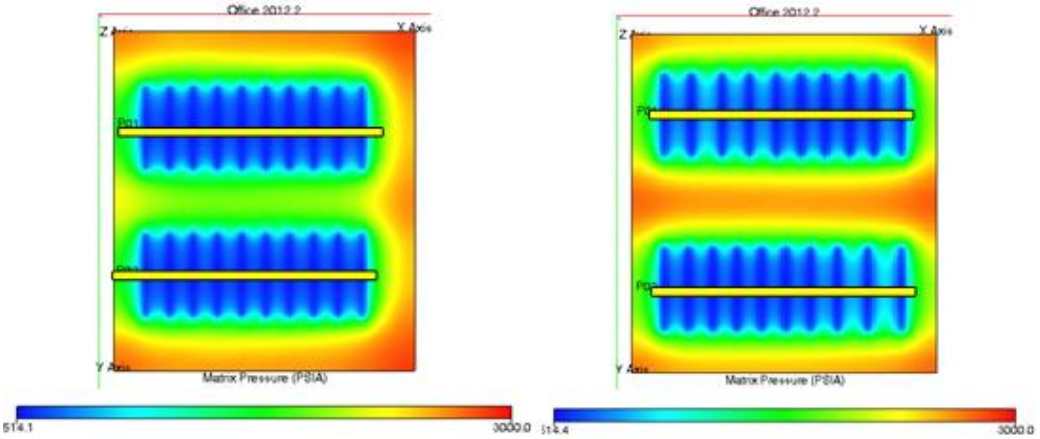

Fig. 4.20 Homogeneous case, pressure distribution of initial condition before hierarchical optimization (left) and one optimized result (right)

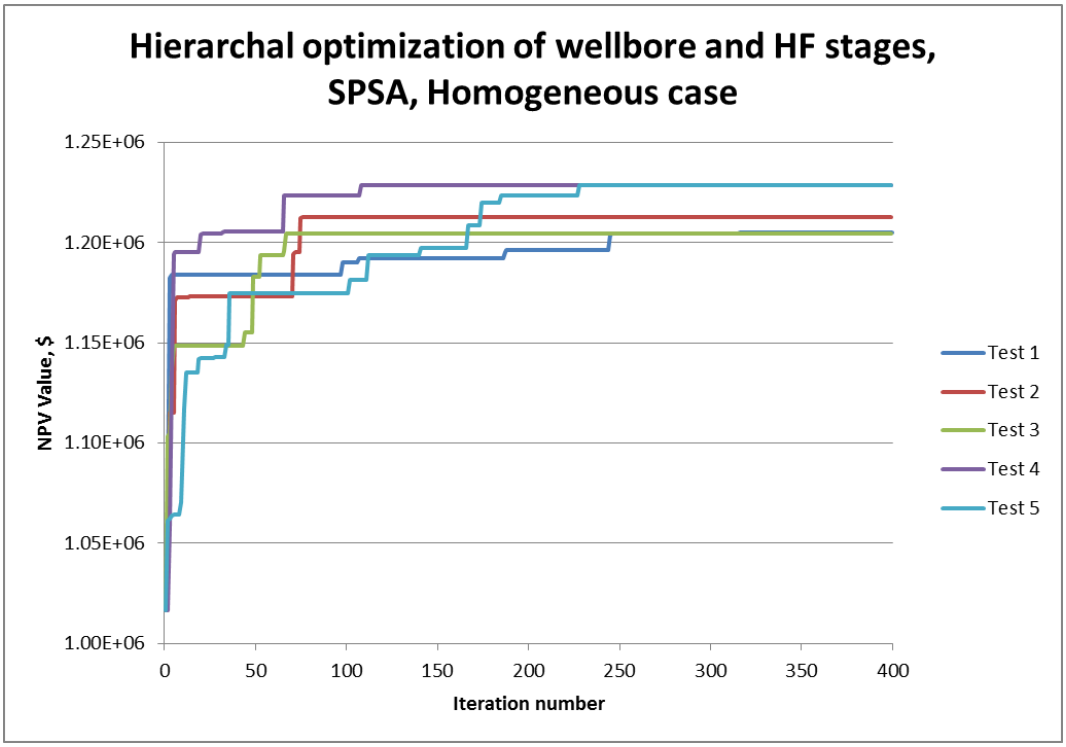

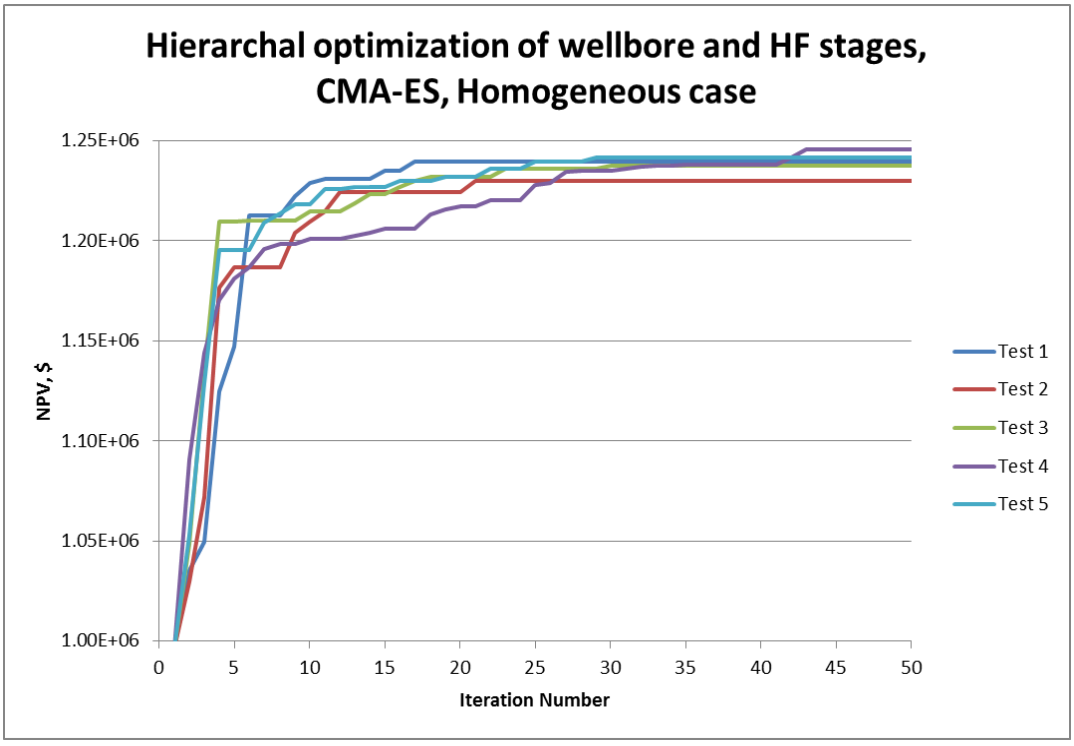

Fig. 4.21 Homogeneous case, hierarchical optimization approach by the algorithms SPSA (left) and CMA-ES (right)

Comparisons between NPV values of the homogeneous cases from **Fig. 4.5**, **Fig. 4.14** and **Fig. 4.21** demonstrate that the optimal arrangement of HF stages along the wellbores has larger impact on gas production rate and NPV than the location of the wellbores. This observation explains why in most cases of the hierarchical optimization problem we get the same optimized HF stages locations while the wellbores locations can oscillate around certain spots in the reservoir.

4.4.2 Hierarchical Optimization in Heterogeneous Case

Fig. 4.22 and **Fig. 4.23** illustrate a significant increase in the total number of iterations for the heterogeneous cases, which has roughly the double of the computational time than the homogeneous cases. As a result of a larger search space, uncertainty of the optimization results also increases for both algorithms.

Comparisons between the optimization results from the heterogeneous permeability cases above show that the hierarchical optimization by SPSA and CMA-ES gives acceptable optimization solutions (**Fig. 4.22**). Although the optimal NPV values from SPSA are lower than those from CMA-ES, SPSA gives the results saving half of total computational time. From these tests, both SPSA and CMA-ES demonstrate good performance for multi-dimensional problem in reasonable computational time.

Table 4.3 shows several optimized NPVs and several groups of percent values improved from initial cases. Comparing the percent of improved NPV in **Table 4.1**, we find that the optimization of HF stages locations could improve NPV much more than the optimization of wellbore placements. Either optimizing HF stages locations or wellbore placements are important ways to get higher NPV and more gas production rate.

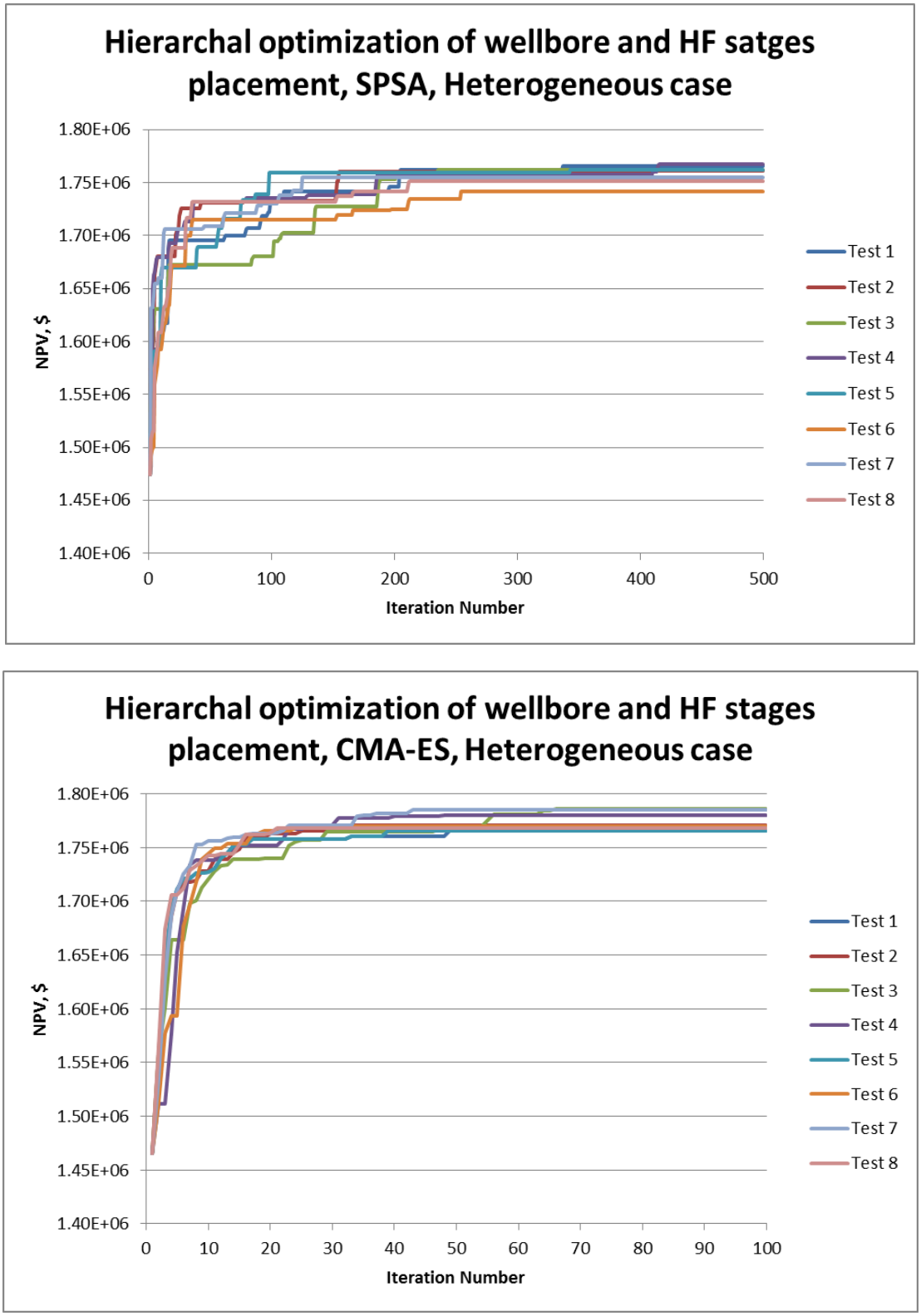

Fig. 4.22 Heterogeneous case, hierarchical optimization approach by the algorithms SPSA (up) and CMA-ES (down)

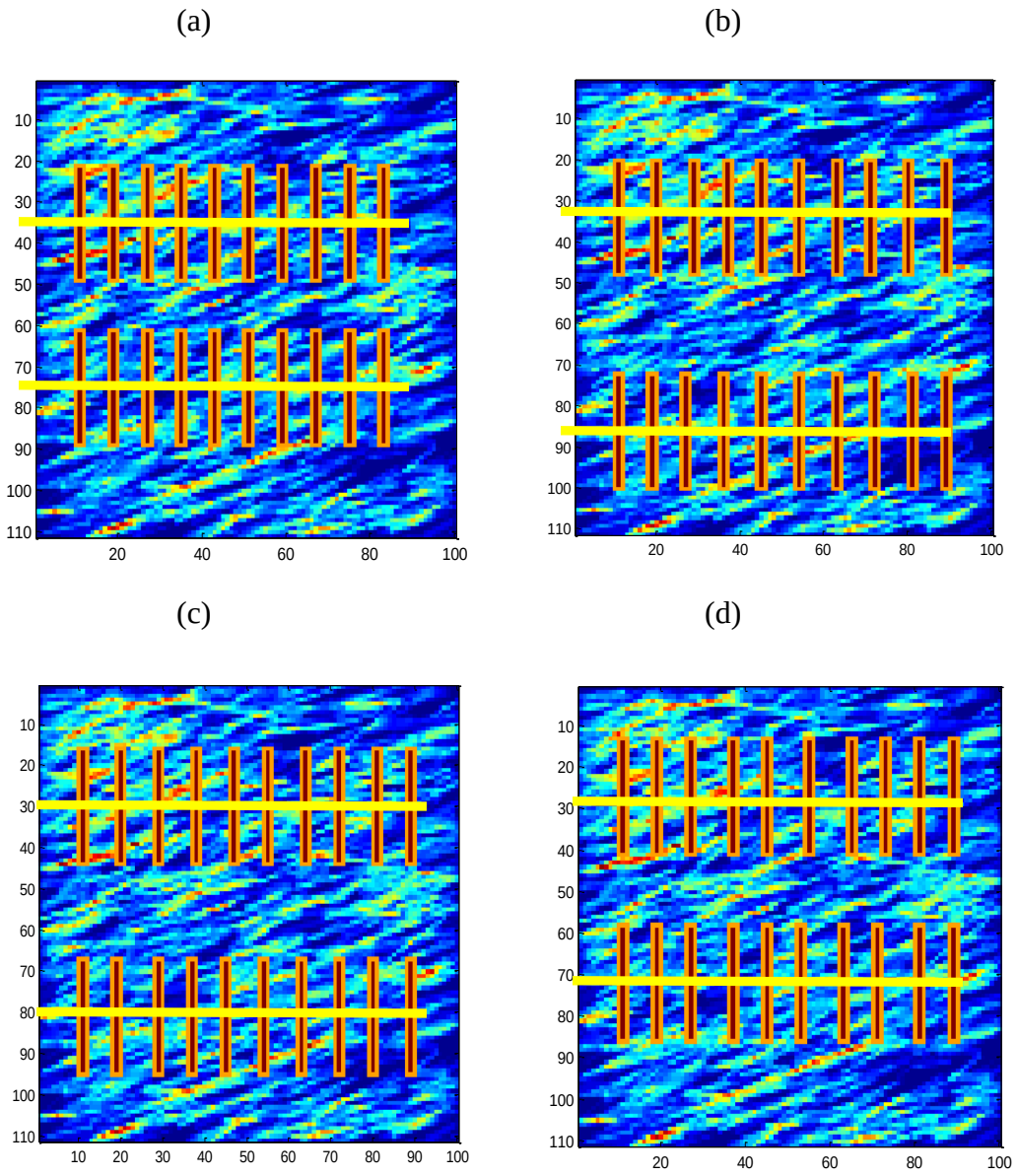

Fig. 4.23 Initial case (up-left) and three optimization distributions of hierarchical optimizations using the known geologic model in heterogeneous case

Table 4.3 Initial HF stages placement and three optimized results in heterogeneous case shown in Figure 4-23

Cases	(a)	(b)	(c)	(d)
Improved NPV($, 10^5)	1.4747	1.7693	1.7885	1.7518
% of NPV Improved	--	19.98%	21.28%	18.79%

4.5 Discussions

In these optimization approaches, although the problem formulation remains the same for both algorithms, SPSA and CMA-ES yield the optimal solutions in different ways. SPSA approximates the gradient (or the search direction) by two-sided simultaneous perturbation of the control vector u. This feature is particularly attractive for multi-dimensional problems for which precise gradient calculation is prohibitively expensive. To summarize, SPSA saves computational time and obtains nearly optimal solution, but it does not guarantee convergence to the global optimum every time.

In comparison to SPSA, CMA-ES is more versatile because it is suitable for both continuous or integer problems. This flexibility allows incorporating into the control vector some variables that are continuous by nature (for instance, lengths or angles). In addition to this, CMA-ES tends to outperform SPSA and give a better approximation of the optimum solution. During each iteration, CMA-ES costs more by calling the simulators times more often than SPSA. The details of computation times are listed in **Table 4.4**. Comparing the results between SPSA and CMA-ES, it reveals that CMA-ES obtains the optimal solution with less uncertainty and its NPV values are higher than those of SPSA. This implicitly confirms the global optimization nature of CMA-ES and SPSA's tendency to get stuck in local optima.

In this section, we developed automatic optimization strategies for the wellbore placement problem, HF stage placement problem, and the hierarchical workflow that combine wellbore and HF stages placement in shale gas reservoirs. Each problem gives a clearly optimization task and respective constrains. The numerical experiments discussed above show promising results and render the feasible optimization problem. The comparison

between gradient-based and gradient-free algorithms revealed their advantages and shortcomings that point us to the direction of hybrid algorithms that combines the beneficial features of the both types of the optimization methods. We also observed that even though the problems of HF stages placement have large dimension numbers, the two algorithms, SPSA and CMA-ES, allows obtaining good results in reasonable time with acceptable uncertainty.

Table 4.4 Compare computational times between SPSA and CMA-ES with cases tested in Chapter 4

Calling ECLIPSE Times	SPSA	CMA-ES
Well Placement, Homogeneous	60	180
Well Placement, Heterogeneous	60	180
HF Placement in 2 wells, Homogeneous	200	500
HF Placement in 2 wells, Heterogeneous	400	500
Hierarchical Placement, Homogeneous	600	650
Hierarchical Placement, Heterogeneous	1000	1000

CHAPTER V

OPTIMIZATIONS WITH UNFIXED NUMBER OF HYDRAULIC FRACTURE STAGES*

5.1 Introduction

In the past, a number of automatic optimization algorithms of well placement have been devised and applied to problems in conventional reservoir engineering and management. In an analogous fashion, the problem of HF placement can be recast as a well placement problem, in which the number of fracture stages and their locations are determined by optimizing a pre-defined objective. Well placement strategies in conventional reservoirs were extensively researched in the last 15 years with stochastic and deterministic approaches (Brouwer, 2004; Bangerth, 2006). Some efficient well placement algorithms, however, are yet to be adopted in HF network design (Holt, 2011).

The situation of HF stages optimization in this chapter is different from Chapter 4, which has been given less information than the cases showed above. In this chapter, we apply the same of stochastic optimization algorithms to the HF placement problems, but here they have not fixed dimension number of control vectors, which means that we need to determine the number of HF stages as well as locations during the optimization approaches. More specifically, we investigate the simultaneous perturbation stochastic approximation (SPSA) method and the Covariance Matrix Adaptation Evolution Strategy (CMA-ES) to measure

* Part of this chapter is reproduced with permission of the copyright owner from "Optimization of Placement of Hydraulic Fracture Stages in Horizontal Wells Drilled in Shale Gas" by Xiaodan Ma, Tatyana Plaksina, Eduardo Gildin, 2013. Paper URTeC 1580378 presented in Unconventional Resources Technology Conference, Denver, Colorado, USA, 12-14 August. Copyright 2013 AAPG. Further reproduction is prohibited without permission.

their efficiency in optimization approaches, and compare their performance for a shale gas production problem.

We organize our study in the following way. First, we present the mathematical rigorous formulation of the problem. Secondly, we describe the reservoir model used for the numerical simulator test runs. Then, we discuss the optimization algorithms with their advantages and drawbacks, and we analyze the results of our numerical experiments with the proposed methods. Finally, we conclude the study with possible directions for future research.

5.2 Gradient-based Optimization on HF Stages Placement Problem

The gradient-based methods discussed in this chapter borrow ideas from two papers, Wang, Li and Reynolds (2007) and Zhang et al. (2010). These two papers focus on finding an optimal number and locations of injector wells, which convert a discrete variables problem to a continuous variables problem in conventional reservoirs. The main process of their optimization is as follows. First, assume that vertical injector wells are initially positioned within every grid block of a 2D model, except for the fixed grid blocks that contain a vertical producer well. Second, set the constraints of the continuous differentiable variables, with arbitrarily chosen single well injection rate and a constant total injection rate, and fed into the reservoir simulator. Third, the simulator runs these scenarios and computes a gradient by adjoint algorithms based on given objective functions. Eliminate the grid-blocks that have certain gradient values which cannot be used for the potential locations of inject wells.

Following the same idea for the optimization process of well placement problem, we consider the optimization HF stage placement problem discussed above entails the search for the optimal number of fracture stages and their best location along the horizontal well.

Mathematically, the locations of HF stages are represented by a control vector u (**Fig. 5.1**), with the assumption that all the gridblocks penetrated by the horizontal well contains a possible HF stage. Since each element i of the control vector u indicates presence or absence of a HF stage inside the gridblock i, it can only take the value of 0 or 1. 0 means that this gridblock doesn't have any HF stage, as well as 1 means there has HF stages inside of this gridblock. Once the gradient of the objective function is calculated, the element of u that has the smallest value is set to zero, and then updated to the new control vector for next iterations. In other words, the fracture stage is eliminated from this grid, and zero value of the selected gridblock is stored permanently and no new fracture stage will be placed there in the subsequent iterations.

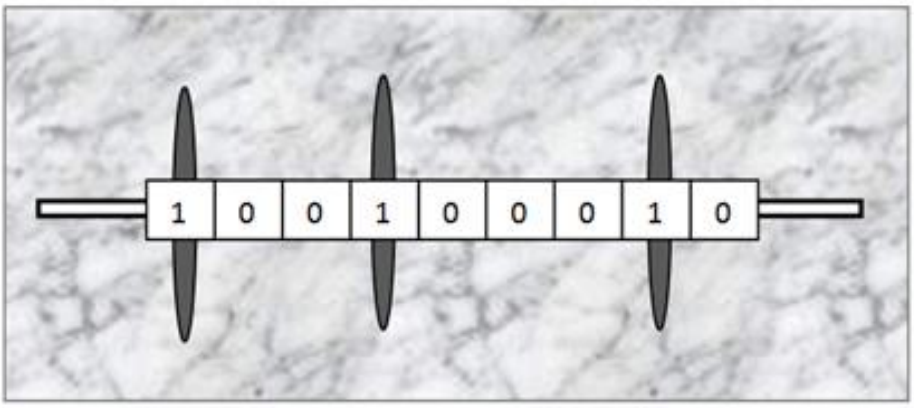

Fig. 5.1 Control vector used for represent HF stages

For the gradient-based optimization methods, we present specific optimization algorithms and their application to eliminate HF stages placement. The methodology used for the optimization of HF stages is equivalent to the well placement optimization problem in conventional reservoirs. In the following cases, we recast the optimization by a “fracture elimination problem”. After the initial assumption that all the gridblocks penetrated by the

horizontal well contains a HF stage, the proposed search algorithms will select those grid blocks that should be eliminated and other corresponded to be kept. This will yield the final configuration for the optimal number and locations of HF stages.

5.2.1 Algorithms for Gradient-based Optimizations

In this section, we introduce two algorithms of Finite Difference (FD) and Simultaneous Perturbation Stochastic Algorithm (SPSA) methods for the optimization of HF stages placement.

The FD algorithm is one of the oldest and widely applied optimization techniques (Nocedal and Wright, 1999). Gradient-based fracture stage elimination is similar in idea and implementation to the wellbore placement method proposed by Wang, Li and Reynolds (2007). A variant of this method is presented in Holt (2011). More specifically, at initial step all gridblocks penetrated by a horizontal well contain one HF stage. Then the gradient of the objective function (or the optimum search direction) is approximated with the following formula:

$$g \approx \nabla J = \left(\frac{\partial J}{\partial u_1}, \frac{\partial J}{\partial u_2}, \dots, \frac{\partial J}{\partial u_N}\right)^T \tag{5.1}$$

$$g_i = \frac{\partial J}{\partial u_i} \approx \frac{J(u + \Delta u_i) - J(u)}{\Delta u_i}, i = 1, \dots, N$$

where g is the gradient of the control vector u, $J = J(u)$ is the objective function evaluated at u, and N is the dimension of the control vector ($i = 1, \dots, N$). **Fig. 5.2** shows the flowchart of FD apply on the HF stages optimization. **Fig. 5.3** gives more clearly how perturbation works by FD methods at the first iteration. It will very expensive if there has lots of gridblocks along the horizontal wellbore.

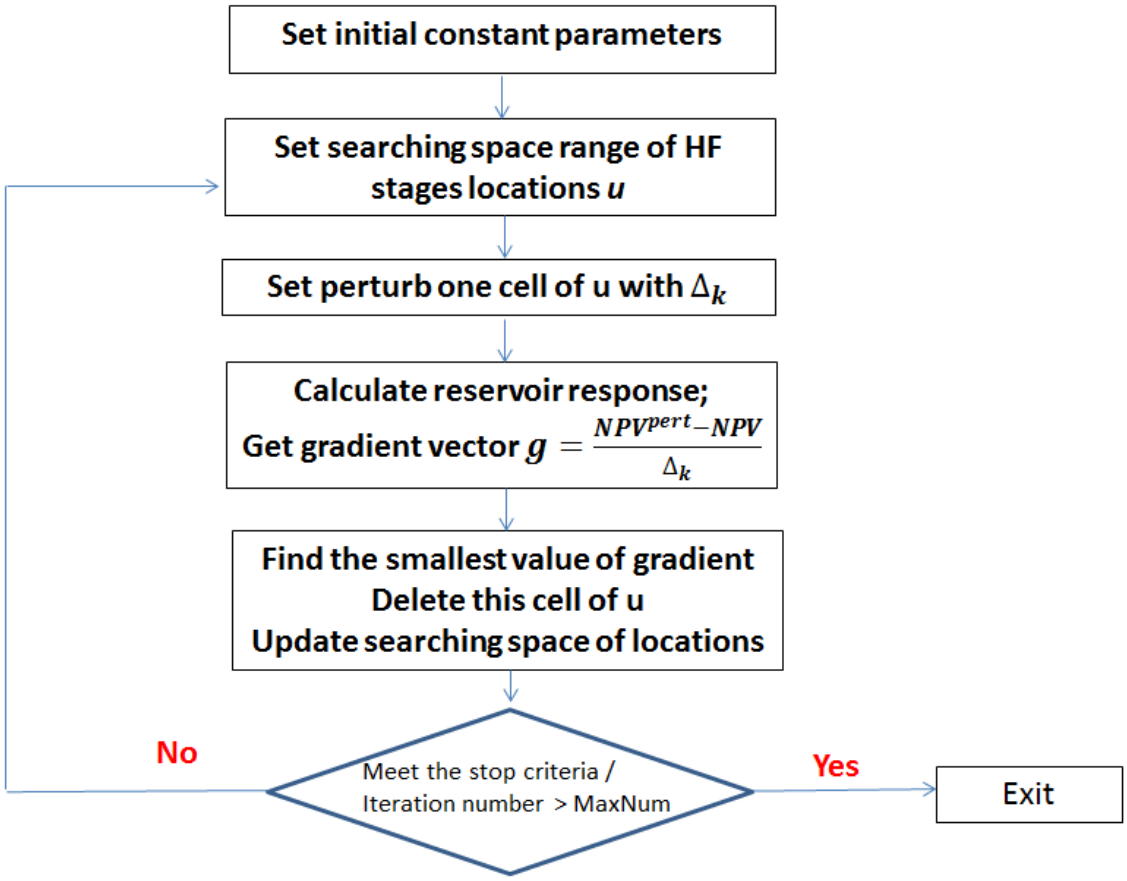

Fig. 5.2 FD flowchart for HF stages optimization

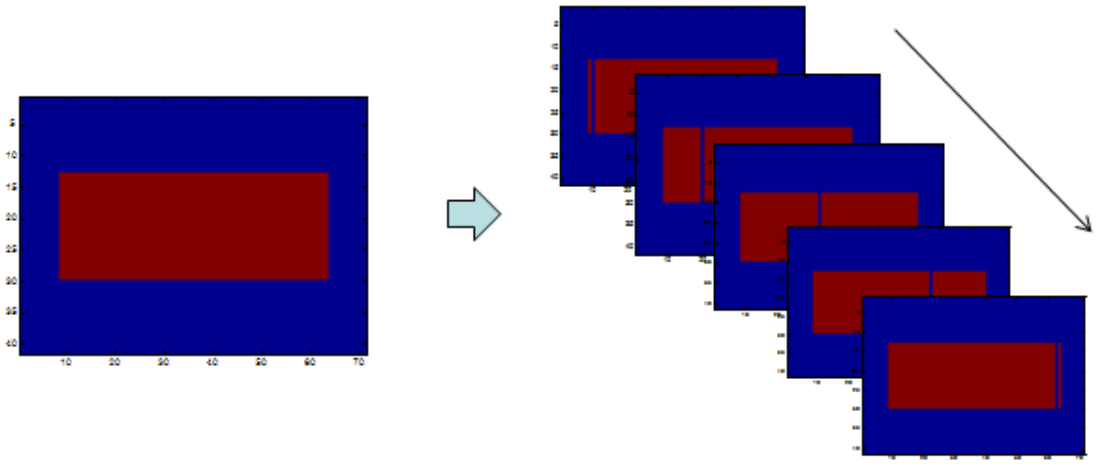

Fig. 5.3 Example of FD perturbation at 1st iteration

The next optimization algorithm we consider is an integer version of the SPSA method (Spall, 1998). SPSA has been developed for use with large dimensional optimization problems where the gradient information is not easy or available to compute. SPSA in general works with the approximation of the gradient by a stochastic perturbation of the control vector. By choosing a "proper" random direction Δ_k from a distribution (Bernoulli) in the search space per iteration, one finds an ascent direction by computing the two-sided simultaneous perturbation using the selected random direction. The gradient vector is calculated by an approximate estimate with two function calls. Compared with finite-difference perturbation, SPSA fewer forward calls (two random perturbations) than the finite differences (perturbation for the entire control vector).

In the original algorithm, SPSA algorithm can only operate on unbounded continuous sets and is not suited for discrete optimization. The modified SPSA algorithm has been proposed and analyzed to the discrete well placement problem (Bangerth, 2006). In this section, we begin by implementing and evaluating the SPSA algorithm for the HF placement problem. Our goal is to extend the application of the SPSA to the mixed integer problem of combined HF placement and stages control optimization. **Fig. 5.4** shows the flowchart of SPSA apply on the HF stages optimization.

The optimization is a discrete integer programming problem while the control vector *u* is discrete and bounded by the number of gridblocks along horizontal wellbore domain. A few parameters of SPSA that give initial constraints of the step lengths and stability of the algorithm have to be chosen carefully. In the SPSA algorithm used to solve this problem, the directions are updated after the computations of the approximate gradient. In the random perturbation step, we choose the Bernoulli random values rather than Gaussian and uniform

random vectors. **Fig. 5.5** gives an example of perturbation by Bernoulli distribution at the first iteration. All the cells are perturbed simultaneous at one iteration. This perturbation represents the simultaneous perturbation applied to all search space components and call two-side objective functions to approximate the gradient vector. For the stages placement problem in this paper, we limit the step size of the optimization line search to a single gridblock.

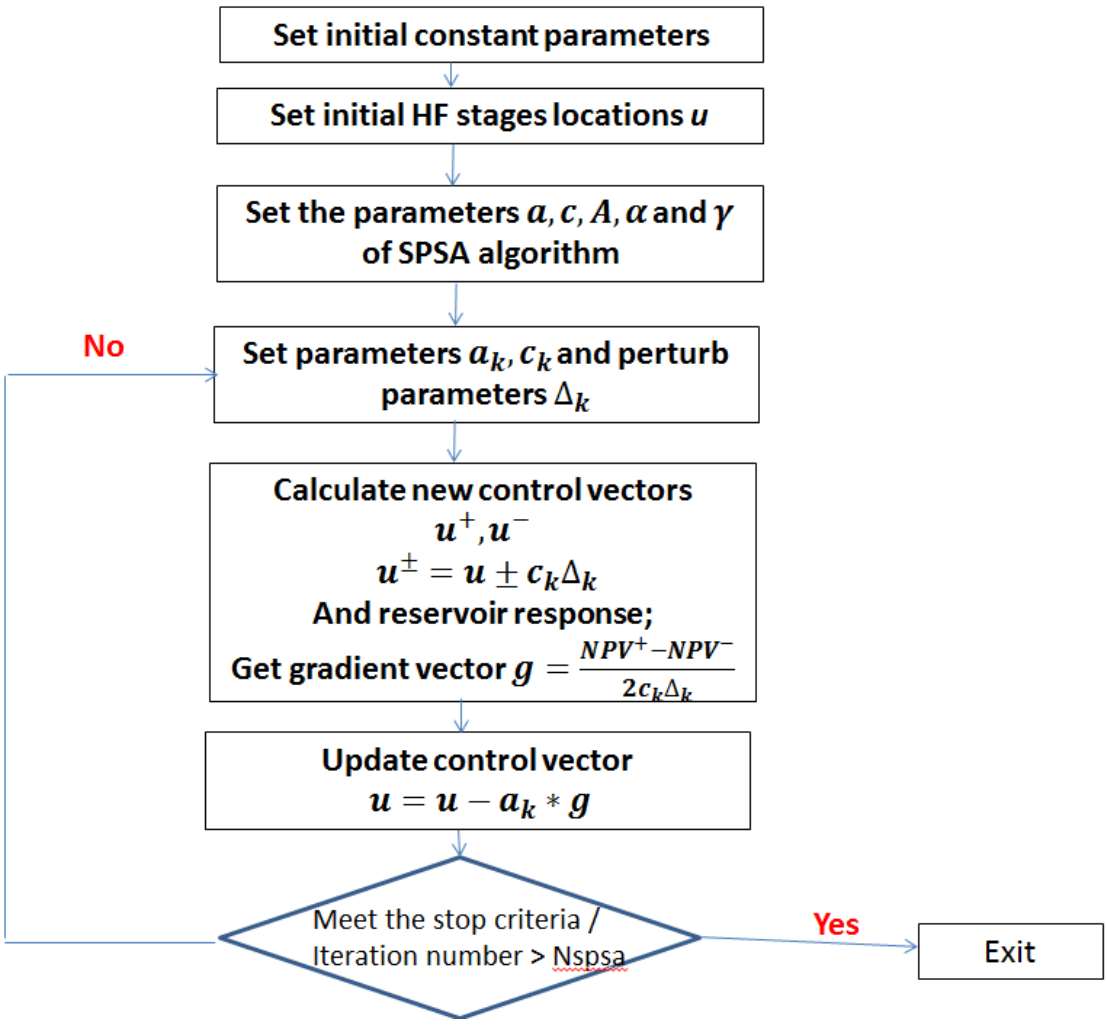

Fig. 5.4 SPSA flowchart for HF stages optimization

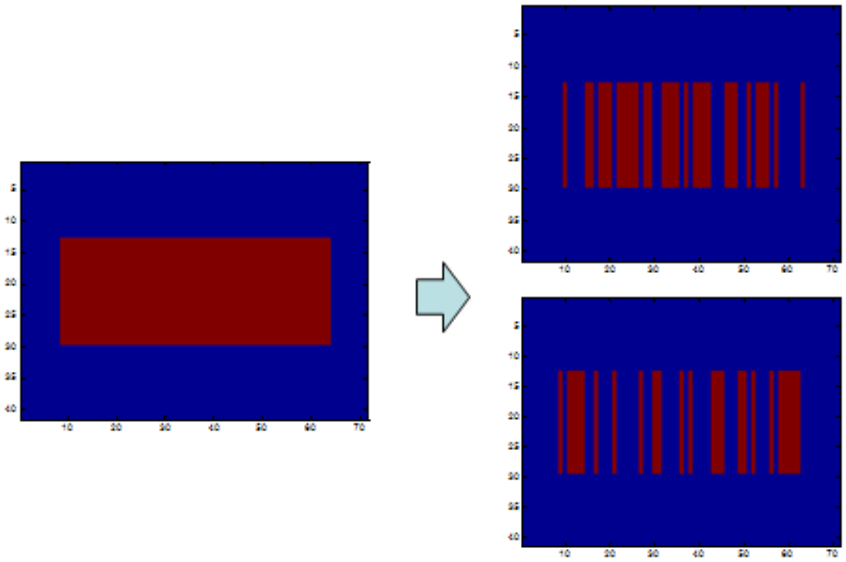

Fig. 5.5 Example of SPSA perturbation at 1st iteration

5.2.2 Test Experiments and Case Results

In this section, we present results of several numerical experiments in order to evaluate the performance of FD and SPSA for HF stages optimization. The two test cases presented below consider naturally fractured shale gas reservoirs with homogeneous and heterogeneous permeability maps. For the reservoir with homogeneous permeability, we choose the reservoir properties listed in the appendix. For the heterogeneous reservoir, we assume that natural fractures are not uniformly distributed.

We assume that the horizontal well is placed in the reservoir middle zone with direction from west to east. Within a given boundary of integer search space, we can compute the objective function and calculate the gradient of each active HF stages. After several steps of elimination (see previous sections for more in depth explanations), the NPV attains the highest value, yielding the optimized HF placement as well as the optimized number of stages, which are shown for homogeneous permeability map in **Fig. 5.6** and **Fig.**

5.7. The corresponding NPV attained values by these two algorithms are also plotted in **Fig. 5.8**. SPSA is computationally more efficient than FD because it does not perturb every gridblock one by one at the same iteration. For the two cases considered, SPSA approaches the FD optimized results by saving about a half times of calling simulator than FD does.

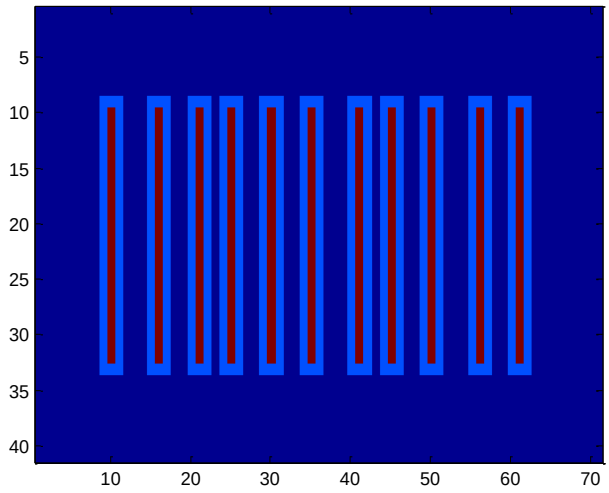

Fig. 5.6 Optimization of HF stages placement in homogeneous case by FD

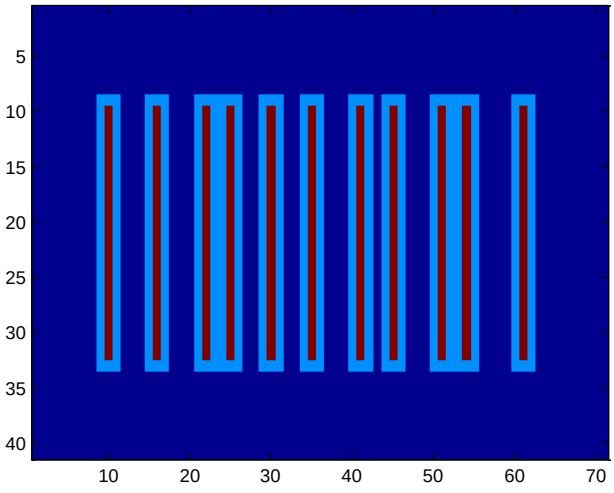

Fig. 5.7 Optimization of HF stages placement in homogeneous case by SPSA

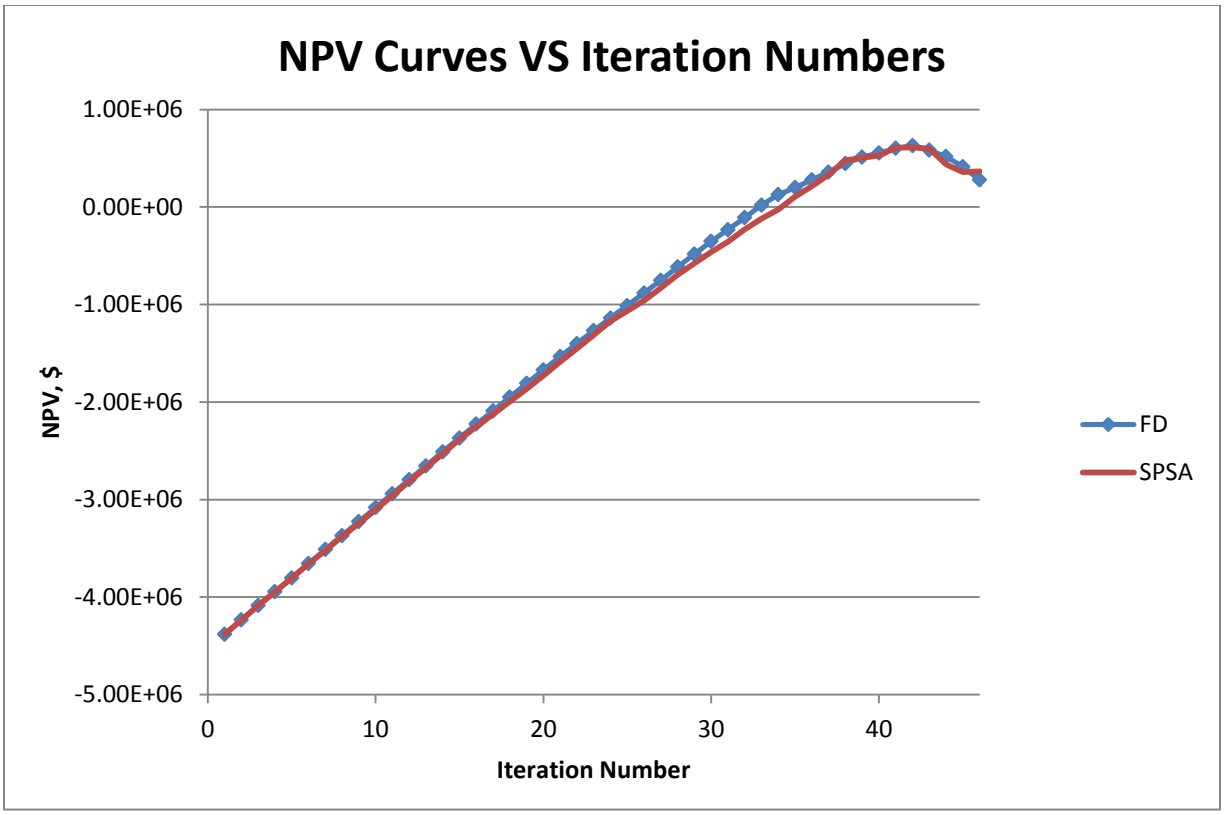

Fig. 5.8 NPV curve of HF stages placement optimization in homogeneous case by FD and SPSA

5.3 HF Stages Placement Optimization with Realistic Constrains

When placing HF stages along horizontal wells, we need to consider realistic constrains regarding the actual physical locations. Depending on collected geo-mechanical information, we cannot put HF stages on every place along the wellbore, since some places may be difficult to penetrate or drill. The distances between HF stages are also needed to be controlled. For the shale formation that is friable, if the distance between two HF stages is very small, it's very possible to have "honeycomb" fracture network near wellbore zone. It only could stimulate the zone near wellbore, but fails on fracturing by HF stages to enlarge permeability far away from wellbore. If the distance between two HF stages is too large, we may lose to build up an effective fracture networks between natural fracture and HF stages.

Based on these considerations, we need enhance our strategies and incorporate new optimization approaches with more realistic constrains.

In the following sections, we will give description on the improved optimization approaches with their flowchart, and test the two algorithms, SPSA and CMA-ES, based on with several cases.

5.3.1 Assumptions and Flowcharts for the Improved Approach

In order to have more realistic constrains on our model, we add one more assumption to the problem of HF stages placement. During the processes to find optimal locations for each HF stage, we need to keep a certain distance between two stages. In our models, we choose 100 ft as the minimum distance. In order to translate this constrain into the model design, we have to keep a certain number of gridblocks (specified) between the grids that possibly have HF stages.

Before starting the optimization algorithms, we need have a general idea for HF stages placement since we do not know how many HF stages we could put along the wellbore. In this section, we choose a shale gas model with grid size 111x100x2 to test all the optimization algorithms. If we choose the evenly spacing distribution of HF stages for a single horizontal well, different HF intervals yield different number of HF stages. **Fig. 5.9** shows that two patterns of HF stages distribution with intervals 100 ft and 160 ft. For each given HF stage interval, the numbers of gridblocks between two stages are different. Since we have a fixed length of horizontal wellbore, the total searching space is also fixed.

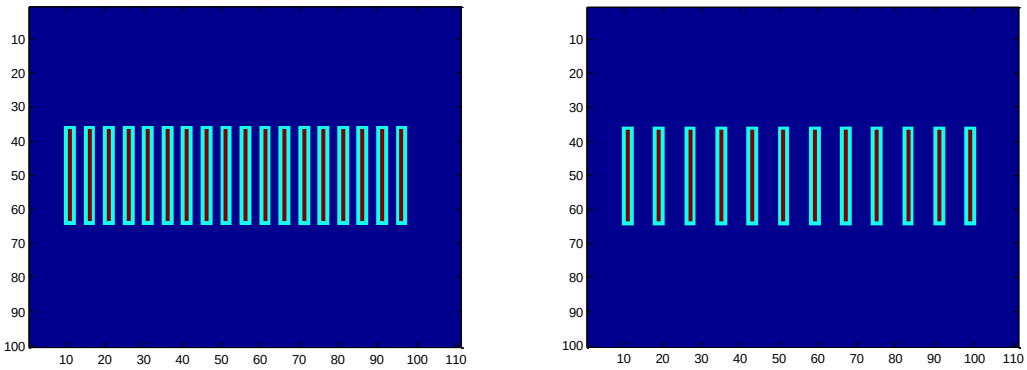

Fig. 5.9 Two patterns of HF stages distribution with intervals 100 ft and 160 ft

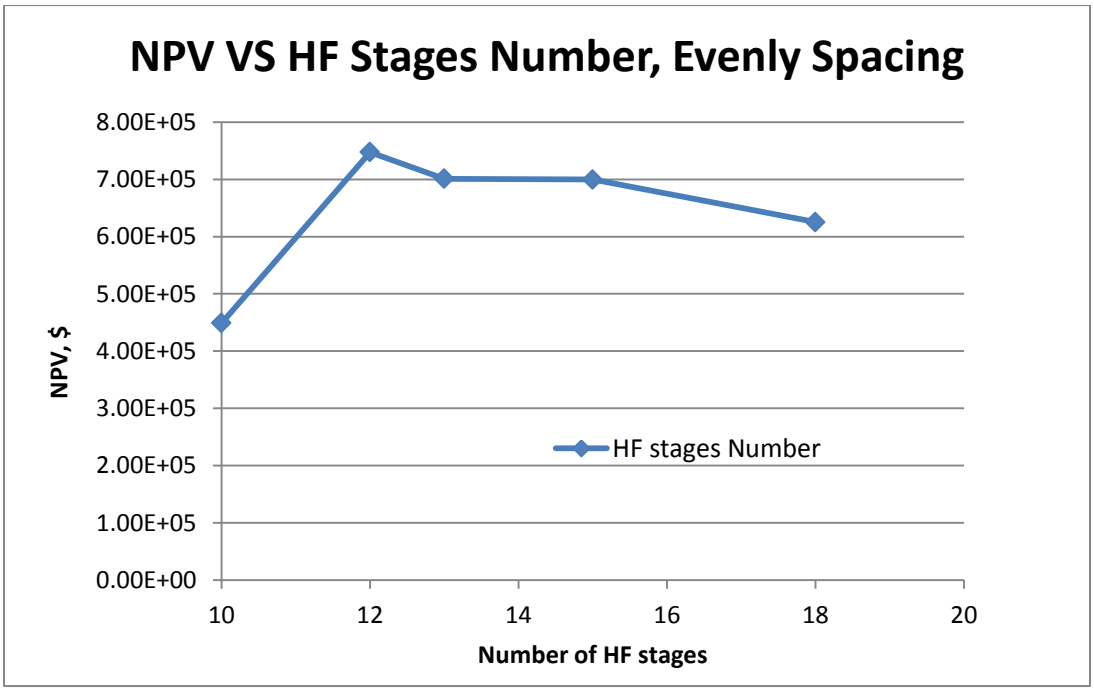

Fig. 5.10 NPV curve corresponding to different number of HF stages

Fig. 5.10 shows the NPV curve corresponding to different number of HF stages. From this graph curve, we first suggest that the number 12 of HF stages is the initial optimal number for our shale gas model, however, the locations of these 12 HF stages may not be the

final optimal gridbocks. From number 12 to 16, they has a possibility to be the optimal number with much higher NPV and more reasonable locations.

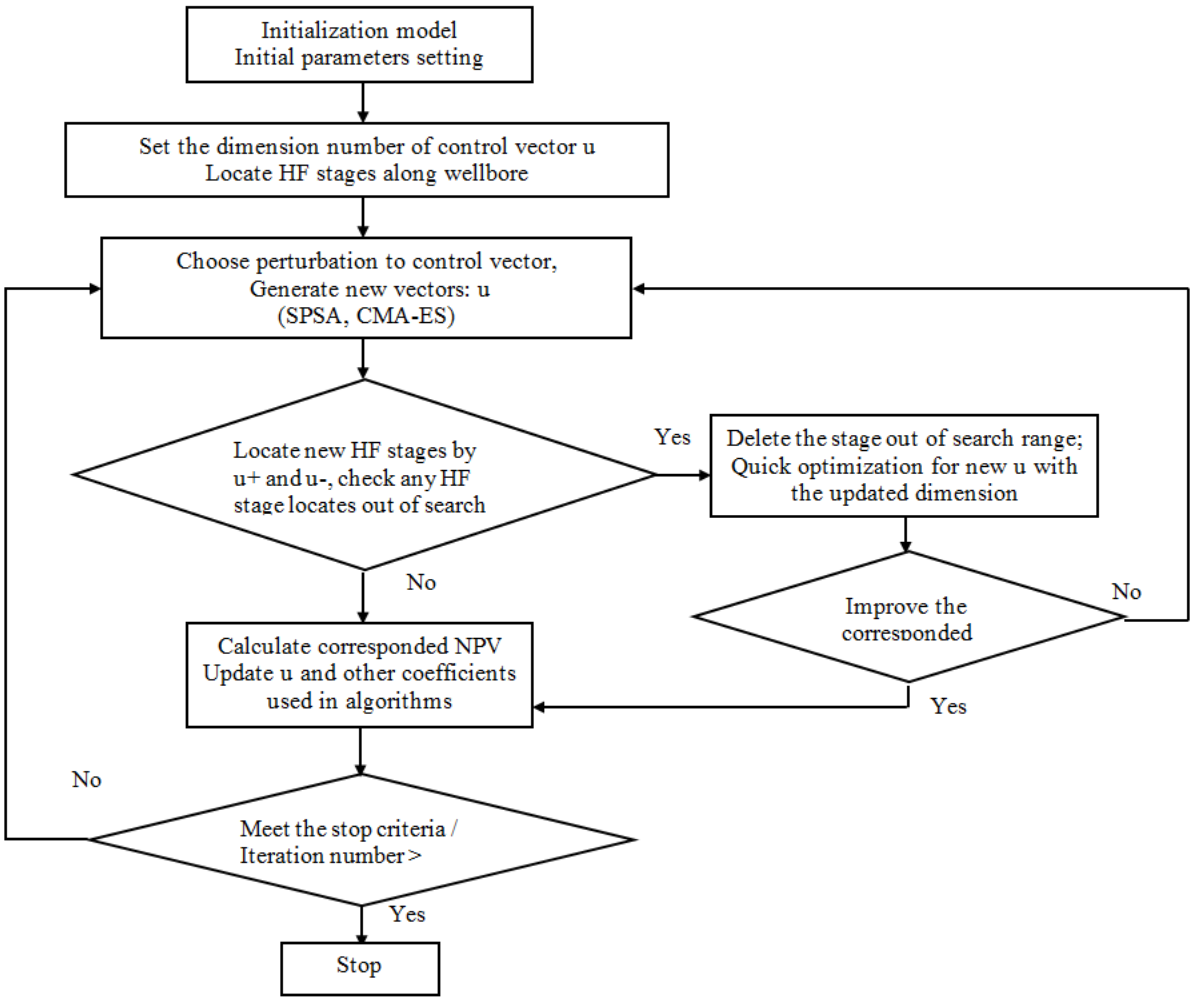

Fig. 5.11 Flowchart of the optimization approach with more realistic constrains

To achieve the global optimization objective, we apply SPSA and CMA-ES to the shale gas model with the control vector that represents intervals between HF stages. **Fig. 5.11** shows the methodology and flowchart of this optimization approach. In the initial setting part, we put HF stages with the minimum interval pattern. After control perturbations, we will

have new pattern of HF stages distribution with updated stage number and corresponding NPV. Comparing the updated NPV with the value from the initial pattern or former iterations, if the updated NPV get improved, i.e., is higher than the former ones, and then we will accept this HF stage pattern and update the control vector with this new dimension number. Along with iterations, HF stages will be eliminated to the optimal number as well as locations of stages are determined with non-evenly spacing.

In order to test the validly and efficiency of this methodology, we apply both SPSA and CMA-ES to several test cases. First, we will test them in the model with single horizontal well, representing a "not too" large dimension for the control vector; Second, two horizontal wells will be considered in the same shale gas model, and we will discuss the distribution of hydraulic fracture networks between these two wells, which has larger dimension numbers of the control vector.

5.3.1 Optimization for Non-fixed HF Stages Number on Single Well

In this section, we test the algorithms, SPSA and CMA-ES with a homogeneous case and single well. The reservoir size is $111 \times 100 \times 1$ gridblocks, and the horizontal well is in the middle of reservoir. The initial condition of HF stages is that HF stages have evenly spacing with the minimum intervals between each stage. From this assumption, we have 18 HF stages as initial case. The optimized values and HF distribution can be sum in **Fig. 5.12** and **Fig. 5.14**.

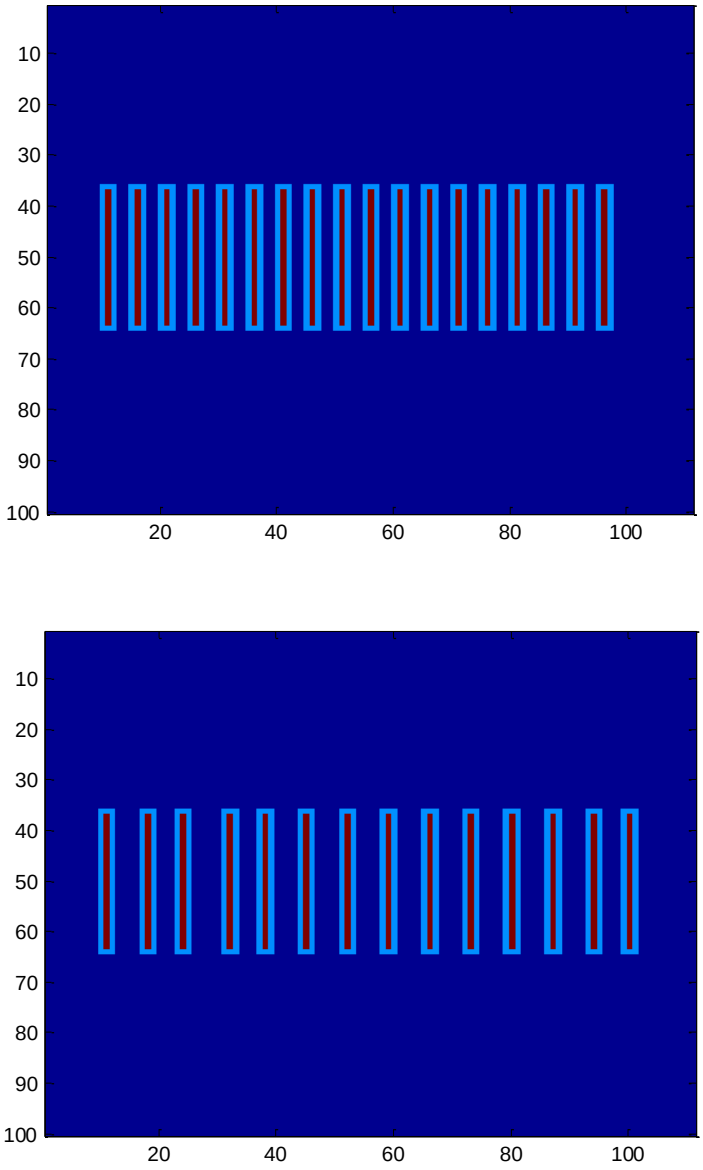

Fig. 5.12 Initial and the optimal number and locations of HF stages for single well

Fig. 5.14 shows more clearly the optimization process and how the HF stages are eliminated. Starting with the initial 18 stages, we add perturbation for the control vector which yields new locations of HF stages. If one of the new HF stage locates out of the searching space, we eliminate this stage and perform the quick optimization process to the

rest 17 HF stages inside searching space. If the optimized NPV from the quick optimization is larger than the NPV by initial 18 HF stages, we accept this new HF stage number and one HF stage is eliminated. We continue with this algorithm, that is, perturbe again and repeat the optimization process until a certain criteria is reached.

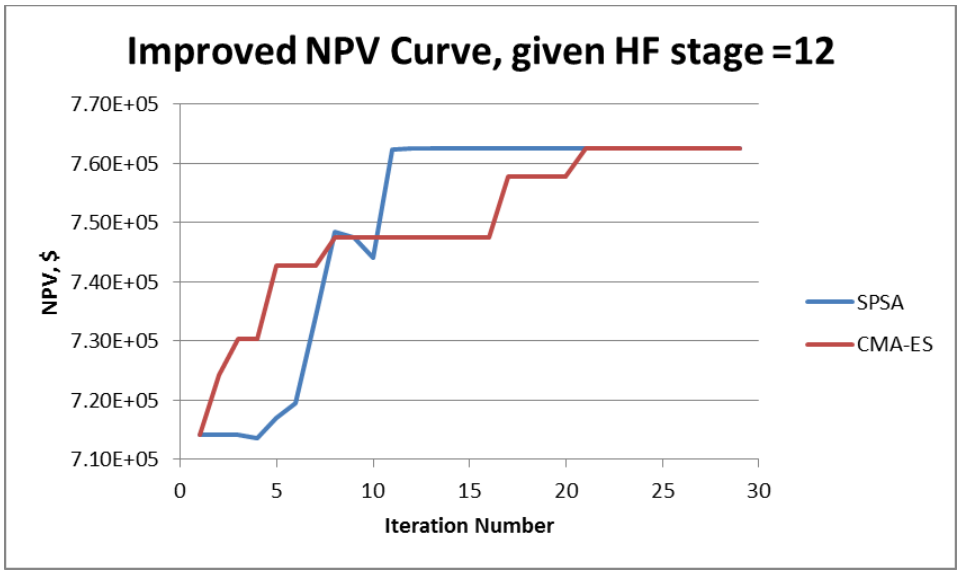

Fig. 5.13 Optimization to NPV with given 12 HF stages

From **Fig. 5.10** which gives us an initial guess of optimal HF stage number**,** we can see that for evenly spacing 12 HF stages is the optimal number for this homogeneous case. So given this number of HF stages, we test the optimization process described in Chapter 4 and get the improved NPV curves shown in **Fig. 5.13**. The optimized NPV value of 12 HF stages is much smaller than the optimal 14 HF stages shown in **Fig. 5.14**, which also prove the accurate of this elimination optimization process.

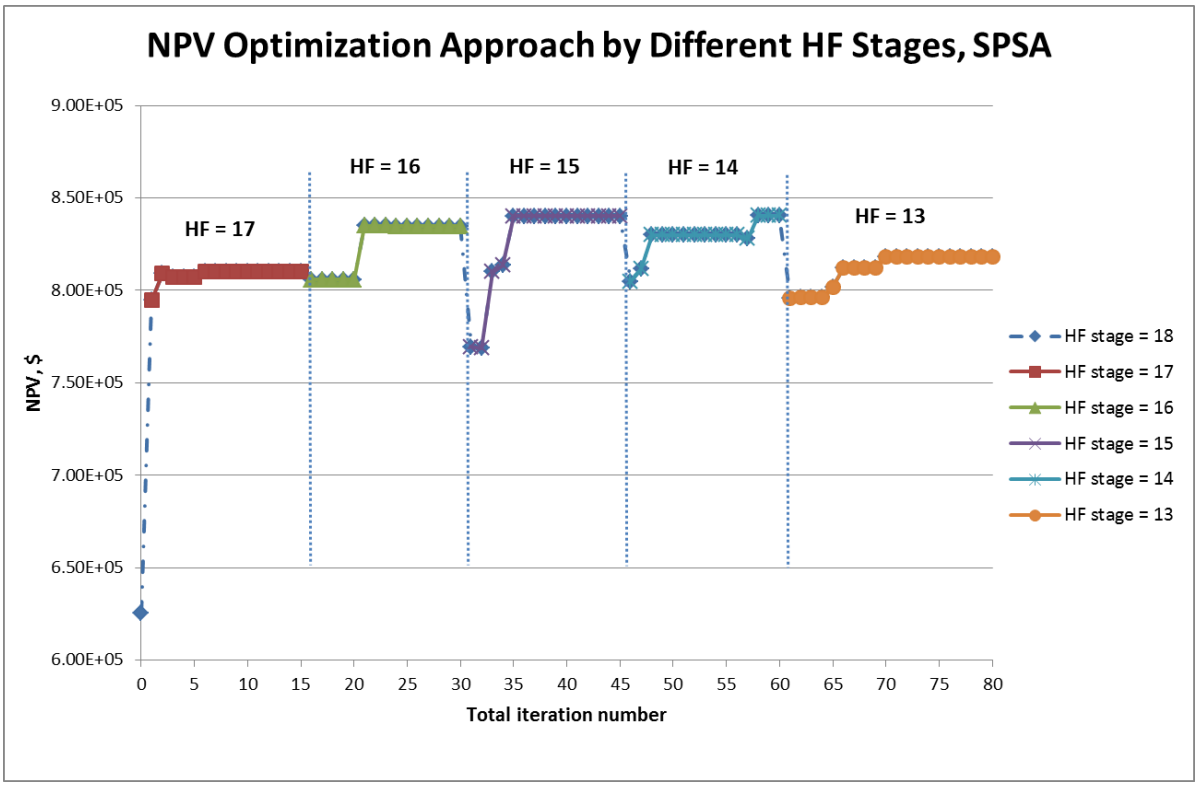

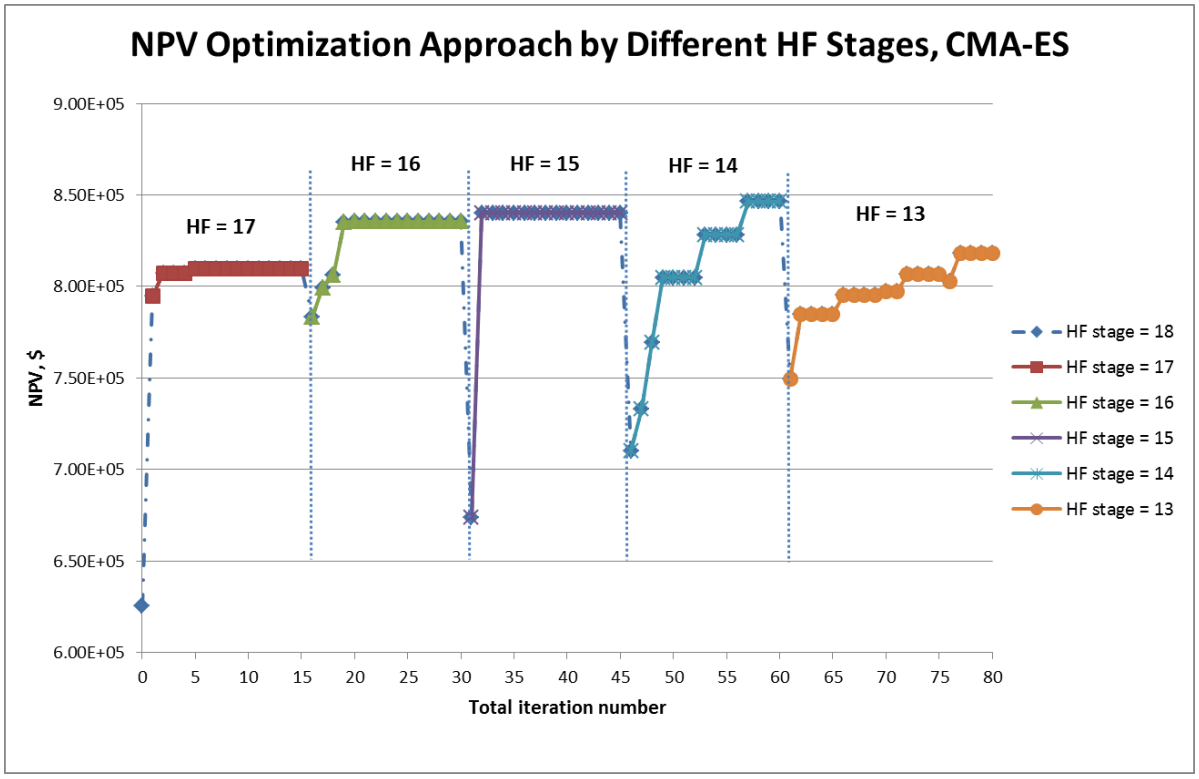

Fig. 5.14 The optimization and elimination process by SPSA and CMA-ES, single well

5.3.2 Optimization of HF Stages Networks with Non-fixed HF Stages Number

In this section, we test the algorithms, SPSA and CMA-ES with a homogeneous case and two wells. Still use the same reservoir size $111 \times 100 \times 1$ gridblocks, and two horizontal wells are parallel and symmetrically in reservoir. The initial condition for the HF stages is that the HF stages are evenly spaced respecting the the minimum intervals between each stage. After running the algorithms as in the flowchart of Fig. 5.11, we obtain the optimal locations and in turn, the optimal number of HF stages. In this case we obtain the 15 HF stage per well, which is shown in **Fig. 5.15**.

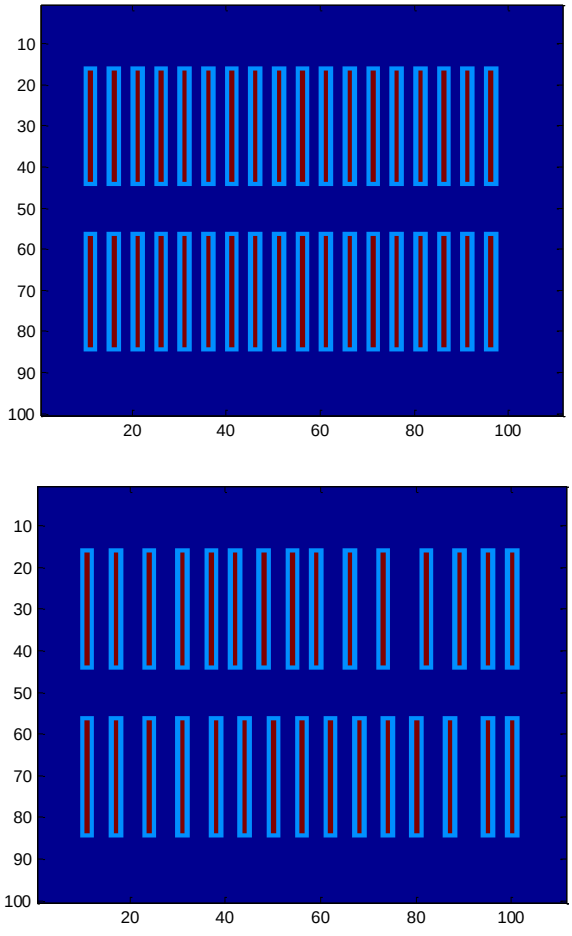

Fig. 5.15 Initial and the optimal number and locations of HF stages for two wells

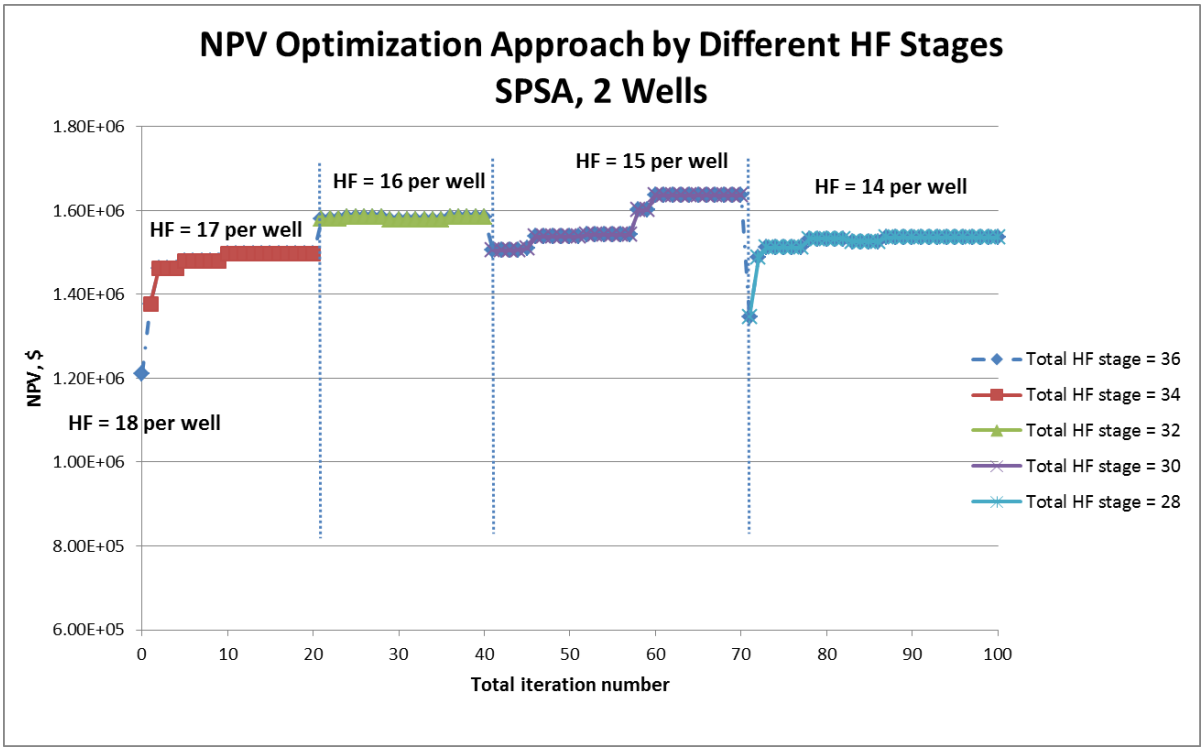

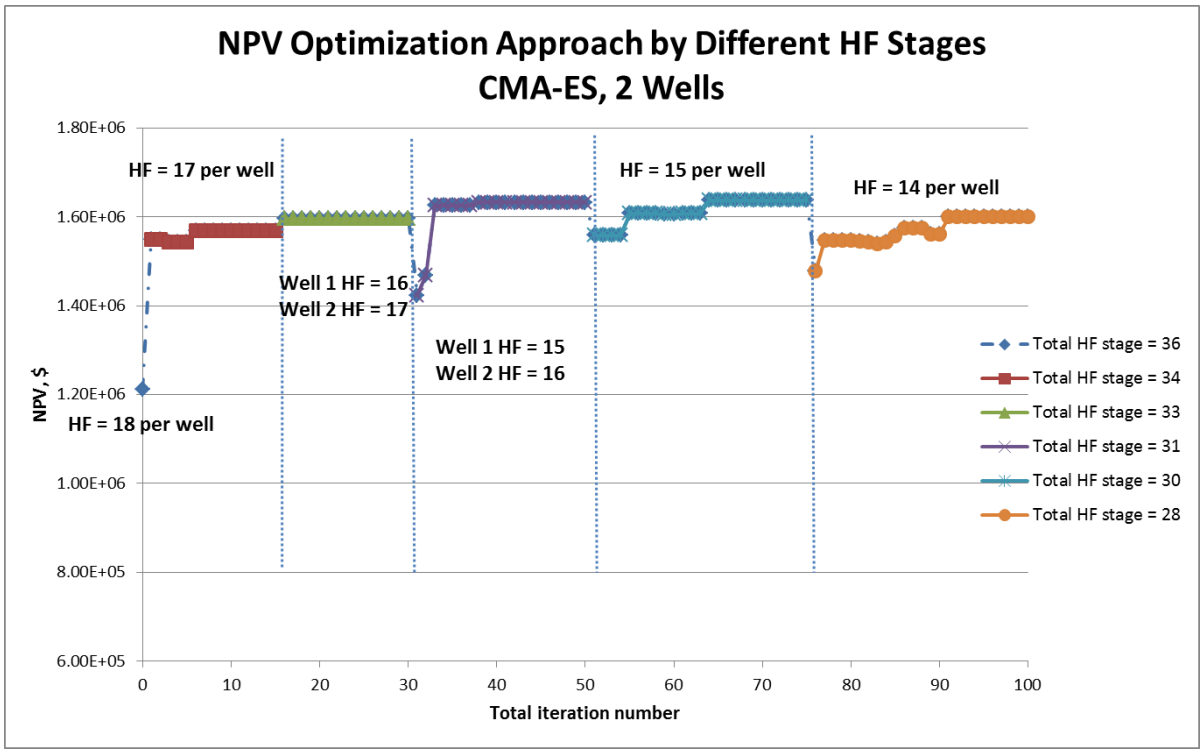

Fig. 5.16 The optimization and elimination process by SPSA and CMA-ES, two wells

Compare initial case and the optimal case, we find that the number of HF stages is eliminated in **Fig. 5.15**. Beside the number, the locations of HF stages also show non-evenly spacing distribution. Given a search spacing grids, this stage distribution could produce the maximum NPV. **Fig. 5.16** shows how the optimization process eliminates HF stages and determines the optimal number of HF stages. SPSA eliminates one HF stage synchronous for each well per iteration while CMA-ES shows that it may eliminate one stage for each well but in the different iterations. As a final result, we have number 15 as the optimal HF stages for each well, which is larger than the case of single well. The reason why we get larger HF stages number is that we have more cost on wellbore drillings. Since we put one more horizontal well in the same reservoir, we need to produce more gas rate to balance out this additional cost.

5.4 Uncertainty Quantification and Discussions

Optimization of multi-stage hydraulic fracture (HF) placement is a challenging problem not only in terms of the multidisciplinary tasks involved, but also in relation to its numerical issues, especially when automatic optimization algorithms are used. Its complexity stems out of requirement to achieve maximum revenue while minimizing operating costs that are subject to geological and economic constraints. In addition, the highly uncertain environment in which the HF jobs take place, may lead to numerical optimization problems that need to take into account uncertainty in the parameter spaces, and in turn, large number of parameters to be optimized. Thus, without a solid optimization approach, knowledge of experienced engineers and large suites of simulations will yield suboptimal and inefficient results.

In this chapter, we developed automatic optimization strategies for the HF placement problem with non-fixed number in shale gas reservoirs. These optimization strategies, FD, SPSA and CMA-ES, could give the configurations of HF stages number and locations based on economic consideration and production optimizations. FD gives a way to determine the optimal number and locations of HF stages; however, it is very expensive to use this method. SPSA applied to HF stage elimination method shows that it could reduce the times calling ECLIPSE and save computational costs.

We also give some numerical experiments with more realistic assumptions. SPSA and CMA-ES are tested in these cases, and give the optimization results about the optimal number and locations of HF stages. Compared with HF stage elimination methods, this optimization strategies shows more advantages on optimization approaches rather than the brute-force approach. And it shows more flexible to deal with larger dimension problems in reasonable time. Even though with more realistic assumptions, the numerical experiments discussed above show that our framework allows obtaining good results, improve NPV with fewer HF stages and optimal locations.

CHAPTER VI

CONCLUSIONS AND RECOMMENDATIONS

6.1 Conclusions

In this work, we presented a hierarchical workflow for the placement of both horizontal wells and hydraulic fracture stages in shale gas reservoirs. Some specific conclusions that can be made from this work are as follows:

The proposed shale gas reservoir model was built and integrated in the MATLAB optimization framework; Parameters of Hydraulic fracture were set using realistic date from Barnett Reservoirs, and were taken into account in the sensitivity analysis, providing sensitivity diagrams and in turn, the optimization problem targets.

The frameworks of FD, SPSA and CMA-ES algorithms were also built in MATLAB for production optimization approaches. These proposed algorithms were designed in such a way that they can work with several control variables, ranging from a couple of them to several fracture stages and horizontal wellbores.

We developed several automatic optimization strategies for different dimension problems. The numerical experiments discussed above show that our frameworks improve NPV with fewer HF stages and could determine the optimal locations. The algorithms used in this study show ability on controlling different number of dimensions in the discrete optimization problems.

In the gradient-based approach, Finite Difference (FD) method gives a way to determine the optimal number and locations of HF stages; however, it is very expensive to use this method. As an alternative, we introduced SPSA and tested using several

configurations. SPSA shows that it could perturb all variables at the same iteration saving the total computational times.

We also introduced the CMA-ES algorithm as an alternative to gradient-based optimizations. Problems with small dimension for their control vectors, i.e., wellbore placement problem, the numerical experiments of gradient-based SPSA and gradient-free algorithms CMA-ES show good optimization results within reasonable iteration numbers. In this case, SPSA shows convergence faster than CMA-ES. In the optimization problem with large dimension, such as HF stage placement problem and the hierarchical workflow that combine wellbore and HF stages placement, the numerical experiments tested by SPSA and CMA-ES show results with uncertainty range, and opening the possibility of the algorithm being stuck at a local minima. The total computational time also increased a lot compared with the single well problem. The comparison between SPSA and CMA-ES revealed their advantages and shortcomings. SPSA shows that its convergence at first few iterations being faster than CMA-ES, but it slows down and gets nearly optimization results rather than approach to the global optimization solutions. Comparing the final optimization results, CMA-ES shows more ability on controlling larger dimension problems than SPSA does.

6.2 Recommendations

There still have several aspects to improve the optimization processes:

1. For the real field projects from unconventional reservoirs, we need to pay more attention to more realistic conditions, such as geo-mechanical and petrophysics information, which could help us make decisions to the locations to drill and hydraulic fracturing stages

placement. Adding the engineering judgment to the hierarchical optimization can improve on the computations as a good initialization can be obtained.

2. Another idea is about analyzing uncertainty from the reservoir properties and fracture parameters. The shale gas model we tested in this thesis has reservoir properties or HF parameters that were selected within certain ranges. However, in practice they have uncertainty accounted with their ranges.

3. Finally, we can consider more complex wellbore placement with certain angle trajectories. Here, the wellbore placement optimization only considers the straight horizontal wellbore which simplify the optimization problem a lot. We could add more dimensions to the control vectors to handle the situation of wellbore drilled with different trajectories.

REFERENCES

Al-Ahmadi, H. A. and Wattenbarger, R.A., 2011. Triple-porosity Models: One Further Step Towards Capturing Fractured Reservoirs Heterogeneity. SPE 149054

Arthur, J.D. and Langhus, B. and Alleman, D. 2008. An Overview of Modern Shale Gas Development in the United States. Available at http://www.all-llc.com/publicdownloads/ALLShaleOver viewFINAL.pdf.

Bangerth, W., Klie, H., Wheeler, M.F., Stoffa, P.L., and Sen, M.K. 2006. Optimization Algorithms for the Reservoir Oil Well Placement Problem. Computer Geosciences, Vol. 10, pp. 303 – 319

Bouzarkouna, Zyed, Ding, Didier Yu, and Auger, Anne, 2011. Well Placement Optimization with the Covariance Matrix Adaptation Evolution Strategy and Meta-Models. Computational Geosciences Vol. 16, pp. 75 – 92

Brouwer, D.R. and Jansen, J.D. 2004. Dynamic Optimization of Water Flooding With Smart Wells Using Optimal Control Theory. SPE 78278

Bruner K.R. and Smosna R. 2011. A Comparative Study of the Mississippian Barnett Shale, Fort Worth basin, and Devonian Marcellus Shale, Appalachian basin: U.S. Department Energy, National Energy Technology Laboratory, DOE/NETL/2011/1478, p. 106

Cipolla, C.L. 2009. Modeling Production and Evaluating Fracture Performance in Unconventional Gas Reservoirs. SPE 118536

Cipolla, C.L., Lolon, E.P., Erdle, J.C. and Rubin, B. 2010. Reservoir Modeling in Shale-Gas Reservoirs. SPE 125530

Curtis, J. B. 2002. Fractured shale-gas systems. AAPG Bulletin 86 Vol. 11, pp. 1921 – 1938

Dempsey, B. J., Taki, H., and Druyff J. C., 2001. Case History of Hydraulic Fracture Optimization in Tight Gas Wells with Water Production in the Wind River Basin, Wyoming, SPE 67300

ECLIPSE 300, ECLIPSE Technical description Version 2012.2.0.0

Energy Information Administration, 2010. Shale Gas Production. U.S. Department of Energy, Washington, D.C. Available at: http://www.eia.doe.gov/dnav/ng/ng_prod_shalegas_sl_a.htm.

Energy Information Administration, 2013. Natural Gas Prices. . U.S. Department of Energy, Washington, D.C. Available at: http://www.eia.gov/dnav/ng/ng_pri_sum_dcu_nus_m.htm

Fazelipour,W. 2010. Innovative Simulation Techniques to History Match Horizontal Wells in Shale Gas Reservoirs. SPE 139114

Gorucu, S.E. and Ertekin T., 2011. Optimization of The Design Of Transverse Hydraulic Fractures In Horizontal Wells Placed In Dual Porosity Tight Gas Reservoirs, SPE 142040

Gray, F. D. 2008. Fracture Detection in Unconventional Gas Plays Using 3D-Seismic Data. SPE 114902

Ground Water Protection Council and ALL Consulting. 2009. Modern shale gas development in the United States: A primer. Available at http://www.netl.doe.gov/technologies/oil-gas/publications/EPreports/Shale_Gas_Primer_2009.pdf.

Güyaguler, B. and Byer, T. 2007. A New Production Allocation Optimization Framework. SPE 105200

Handels, M., Zandvliet, M.J., Brouwer, D.R., and Jansen, J.D. 2007. Adjoint-based Well Placement Optimization under Production Constraints. SPE 105797

Hansen, N., 2006. The CMA evolution strategy: a comparing review. StudFuzz Vol. 192, pp. 75–102

Hareland, G., Rampersad, P., Dharaphop, J., and Sasnanand, S. 1993. Hydraulic Fracturing Design Optimization, SPE 26950.

Holditch, S.A, Jennings, J.W., and Neuse, S.H., 1978. The Optimization of Well Spacing and Fracture Length in Low permeability Gas Reservoirs, SPE 7496.

Holditch, S.A. and Tschirhart, N.R. 2005. Optimal Stimulation Treatments in Tight Gas Sands. SPE 96104

Holditch, S.A.. 2007. Hydraulic fracturing: Overview, trends, issues. Presented at DEA Workshop, 20 - 21 June 2007, Galveston, Texas.

Holt S. 2011. Numerical Optimization of Hydraulic Fracture stage placement in a gas shale reservoir (Together with TNO). Thesis dissertation, Department of Geotechnology, Delft University of Technology, Netherlands.

Huffman, C.H., Harkrider, J.D., and Thompson, R.S. 1996. Fracture Stimulation Treatment Design Optimization: What Can the NPV vs Xf Plot Tell Us? SPE 36575.

Jenkins, C.D. and Boyer C.M.. 2008. Coalbed and Shale Gas Reservoirs. SPE Distinguished Author Series.

Lee B., Soleimani A., Dyer S., and Bartko K., 2009. Optimization of Multiple Hydraulic Fractures for Openhole Horizontal Wells by Numerical Modeling - Saudi Arabia Case Study, SPE 124406

Li, L., Jafarpour, B. and Mohammad-Khaninezhad, R., 2013. A Simultaneous Perturbation Stochastic Approximation Algorithm for Coupled Well Placement and Control Optimization Under Geologic Uncertainty. Computational Geosciences Vol. 17: 167 – 188

King, G.E. 2010. Thirty Years of Gas Shale Fracturing: What Have We Learned? SPE 133456

Maas, J.G. 2011. Maas Special CORE Analysis, facts. Available at http://www.jgmaas.com/scores/facts.html. Viewed on 7 July 2011.

MATLAB, matrix laboratory software, version 2012b.

Mayerhofer, M.J., Lolon, E.P., Warpinski, N.R., Cipolla, C.L., Walser, D., and Rightmire, C.M. 2010. What Is Stimulated Reservoir Volume?. SPE 119890

Mirzaei, M. and Cipolla, C.L. 2012. A Workflow for Modeling and Simulation of Hydraulic Fractures in Unconventional Gas Reservoirs Authors. SPE 153022.

Moridis, G.J., Blasingame, T.A. and Freeman, C.M. 2010. Analysis of Mechanisms of Flow in Fractured Tight-Gas and Shale-Gas Reservoirs. SPE 139250

Nemhauser, G.L. and Wolsey, L.A., 1999. “Integer and Combinatorial Optimization”. Wiley-Interscience Series in Siscrete Mathematics and Optimization. John Wiley & Sons, New York, USA

Nocedal, J. and Wright, S.J. 1999. “Numerical Optimization”. Springer Series in Operations Research, New York, USA

Novlesky, A., Kumar A., and Merkle, S. 2011. Shale Gas Modeling Workflow: From Microseismic to Simulation -- A Horn River Case Study.SPE 148710

Orangi, A., Nagarajan, N. R., Honarpour, M. M., and Rosenzweig, J. 2011. Unconventional Shale Oil and Gas- Condensate Reservoir Production, Impact of Rock, Fluid, and Hydraulic Fractures. SPE 140536

Pruess, K., Oldenburg, C., and Moridis, G. 1999. TOUGH2 User's Guide – Version 2.0. Lawrence Berkeley Laboratory Report LBL-43134, Berkeley, CA.

Richardson, M. 2000. A New and Practical Method for Fracture Design and Optimization. SPE 59736

Rubin, B. 2009. Accurate Simulation of Non-Darcy Flow in Stimulated Fractured Shale Reservoirs. SPE 132093

Schweitzer, R. and Bilgesu, H.I. 2009. The Role of Economics on Well and Fracture Design Completions of Marcellus Shale Wells. SPE 125975

Sehbi, B.S., Kang, S., Datta-Gupta A., and Lee, J.W. 2011. Optimizing Fracture Stages and Completions in Horizontal Wells in Tight Gas Reservoirs Using Drainage Volume Calculations. SPE 144365

Spall, J.C. 1992. Multivariate Stochastic Approximation Using a Simultaneous Perturbation Gradient Approximation. IEEE Vol.37: 332 - 341

Wang, C., Li, G., and Reynolds, A.C., 2007. Optimal Well Placement for Production Optimization, SPE 111154

Warpinski, N.R., Mayerhofer, M.J., Vincent, M.C., Cipolla, C.L. and Lolon, E.P. 2009. Stimulating Unconventional Reservoirs: Maximizing Network Growth While Optimizing Fracture Conductivity. SPE 114173

Wilson, K. C., and Durlofsky, L. J., 2012. Computational Optimization of Shale Resource Development Using Reduced-Physics Surrogate Models, SPE 152946

Xie, J., Efendiev, Y., and Datta-Gupta A., 2011. Uncertainty Quantification in History Matching of Channelized Reservoirs using Markov Chain Level Set Approaches. SPE 141811

Yeten, B. 2003. Optimum Deployment of Nonconventional Wells. Ph.D. dissertation, Stanford University, California.

Yu W., Sepehrnoori K., 2013. Optimization of Multiple Hydraulically Fractured Horizontal Wells in Unconventional Gas Reservoirs, SPE 164509

Zhang, K., Li, G., Reynolds, A.C., Yao, J. and Zhang, L., 2010. Optimal Well Placement Using an Adjoint Gradient. Journal of Petroleum Science and Engineering Vol. 73, pp. 220 – 226

APPENDIX A

Table A.1 Reservoir properties and hydraulic fracture parameters used for wellbore placement optimization in Chapter IV

Parameters	***Values***	***Unit***
Model dimensions	2000 x 2220 x 200	ft
Initial reservoir pressure	2950	psi
Reservoir temperature	150	F
Bulk Density	161	lbs/ft3
Bottom hole pressure	500	psi
Horizontal well length	2000	ft
Production Period	20	years
Matrix permeability	0.00015	md
Matrix porosity	0.06	100%
Natural fracture efficient permeability	0.0002	md
Natural fracture porosity	0.00005	100%
Hydraulic fracture conductivity	1	md-ft
Hydraulic fracture spacing	160	ft
Hydraulic fracture height	200	ft
Hydraulic fracture half-length	250	ft
SRV permeability, Zone 1	0.05	md
SRV permeability, Zone 2	0.0005	md
Number of hydraulic fractures per well	10	stages

Table A.2 Reservoir properties and hydraulic fracture parameters used for HF stages placement optimization on two wellbores in Chapter IV

Parameters	***Values***	***Unit***
Model dimensions	2000 x 2220 x 200	ft
Initial reservoir pressure	2950	psi
Reservoir temperature	150	F
Bulk Density	161	lbs/ft3
Bottom hole pressure	500	psi
Horizontal well length	2000	ft
Production Period	20	years
Matrix permeability	0.00015	md
Matrix porosity	0.06	100%
Natural fracture efficient permeability	0.0002	md
Natural fracture porosity	0.00005	100%
Hydraulic fracture conductivity	1	md-ft
Minimum hydraulic fracture spacing	100	ft
Hydraulic fracture height	200	ft

Hydraulic fracture half-length	250	ft
SRV permeability, Zone 1	0.05	md
SRV permeability, Zone 2	0.0005	md
Number of hydraulic fractures per well	10	stages

Table A.3 Reservoir properties and hydraulic fracture parameters test for FD and SPSA optimizations in Chapter IV

Parameters	***Values***	***Unit***
Model dimensions	2000 x 1420 x 200	ft
Initial reservoir pressure	2950	psi
Reservoir temperature	150	F
Bulk Density	161	lbs/ft3
Bottom hole pressure	500	psi
Horizontal well length	2000	ft
Production Period	20	years
Matrix permeability	0.00015	md
Matrix porosity	0.06	100%
Natural fracture efficient permeability	0.0002	md
Natural fracture porosity	0.00005	100%
Hydraulic fracture conductivity	1	md-ft
Hydraulic fracture height	200	ft
Hydraulic fracture half-length	250	ft
SRV permeability, Zone 1	0.05	md
SRV permeability, Zone 2	0.0005	md

Table A.4 Reservoir properties and hydraulic fracture parameters for SPSA and CMA-ES optimizations in Chapter IV

Parameters	***Values***	***Unit***
Model dimensions	2220 x 2000 x 200	ft
Initial reservoir pressure	2950	psi
Reservoir temperature	150	F
Bulk Density	161	lbs/ft3
Bottom hole pressure	500	psi
Horizontal well length	2968	ft
Production Period	20	years
Matrix permeability	0.00015	md
Matrix porosity	0.06	100%
Natural fracture efficient permeability	0.0002	md
Natural fracture porosity	0.00005	100%
Hydraulic fracture conductivity	1	md-ft
Minimum hydraulic fracture spacing	100	ft
Hydraulic fracture height	200	ft

Hydraulic fracture half-length	250	ft
SRV permeability, Zone 1	0.05	md
SRV permeability, Zone 2	0.0005	md